

Large-Scale Multiple Testing of Composite Null Hypotheses Under Heteroskedasticity

Bowen Gang and Trambak Banerjee
Fudan University and University of Kansas

Abstract

Heteroskedasticity poses several methodological challenges in designing valid and powerful procedures for simultaneous testing of composite null hypotheses. In particular, the conventional practice of standardizing or re-scaling heteroskedastic test statistics in this setting may severely affect the power of the underlying multiple testing procedure. Additionally, when the inferential parameter of interest is correlated with the variance of the test statistic, methods that ignore this dependence may fail to control the type I error at the desired level. We propose a new Heteroskedasticity Adjusted Multiple Testing (HAMT) procedure that avoids data reduction by standardization, and directly incorporates the side information from the variances into the testing procedure. Our approach relies on an improved nonparametric empirical Bayes deconvolution estimator that offers a practical strategy for capturing the dependence between the inferential parameter of interest and the variance of the test statistic. We develop theory to show that HAMT is asymptotically valid and optimal for FDR control. Simulation results demonstrate that HAMT outperforms existing procedures with substantial power gain across many settings at the same FDR level. The method is illustrated on an application involving the detection of engaged users on a mobile game app.

Keywords: Composite null hypotheses; Deconvolution estimates; Empirical Bayes; False discovery rate; Heteroskedasticity; Multiple testing with covariates.

1 Introduction

Suppose $X_i, i = 1, \dots, m$, are independent summary statistics arising from the following random mixture model:

$$X_i = \mu_i + \sigma_i \epsilon_i, \epsilon_i \stackrel{i.i.d.}{\sim} \eta(\cdot), \quad (1)$$

$$\mu_i | \sigma_i \stackrel{ind.}{\sim} g_\mu(\cdot | \sigma_i), \sigma_i \stackrel{i.i.d.}{\sim} g_\sigma(\cdot), \quad (2)$$

where ϵ_i are i.i.d. 0 mean random variables with a known probability density function (PDF) $\eta(\cdot)$ and $g_\mu(\cdot | \sigma_i)$, $g_\sigma(\cdot)$ are, respectively, the PDFs of the unknown mixing distributions of μ given σ_i and σ_i . Model (1) incorporates, for instance, the setting where ϵ_i are central t -distributed random variables with $\nu > 2$ degrees of freedom, as well as the more common case of $X_i | \mu_i, \sigma_i \stackrel{ind.}{\sim} N(\mu_i, \sigma_i^2)$, which finds substantial use in large-scale inference problems (Efron, 2004, 2012, Efron and Tibshirani, 2007, Jin and Cai, 2007). Following Fu et al. (2022), Sun and McLain (2012), Weinstein et al. (2018), Xie et al. (2012), we assume that σ_i are known or can be well estimated from the data. Upon observing the pair (X_i, σ_i) , the goal is to simultaneously test the following m hypotheses:

$$H_{0,i} : \mu_i \in \mathcal{A} \quad \text{versus} \quad H_{1,i} : \mu_i \notin \mathcal{A}, \quad i = 1, \dots, m, \quad (3)$$

where \mathcal{A} represents the indifference region such that the researcher is indifferent to the effects in \mathcal{A} (Sun and McLain, 2012). Here $H_{0,i}$ represents a composite null hypothesis as opposed to a simple null hypothesis when \mathcal{A} is singleton.

Much of the focus of extant multiple testing methods is directed towards simultaneously testing simple null hypotheses against composite alternatives. A typical example arises in genome-wide association studies involving millions of single nucleotide polymorphisms (SNPs), where the primary goal is to discover SNPs that are statistically associated with a specific trait or disease of interest (Basu et al., 2018, Uffelmann et al., 2021). The simultaneous inference problem in these applications require testing m hypotheses of the form $H_{0,i} : \mu_i = 0$ vs $H_{1,i} : \mu_i \neq 0$ where μ_i is the unknown effect of SNP i on the disease response, such as cholesterol level. However, across numerous medical and social science applications it is important to detect if $\mu_i \notin \mathcal{A}$. For instance, Gu and Shen (2018), Pop-Eleches and Urquiola (2013) study the effect of attending a more selective school on the exam grade of high-school students in Romania. There the inferential objective is to identify schools with a positive effect on the average exam grade and it is desirable for the null hypothesis to include both zero and negative effects, i.e., to test a one-sided composite null hypothesis $H_{0,i} : \mu_i \in \mathcal{A}$ against the alternative $H_{1,i} : \mu_i \notin \mathcal{A}$, $i = 1, \dots, m$, where $\mathcal{A} = (-\infty, 0]$. In high-throughput gene sequencing studies, a fundamental task is to discover genes that exhibit differential expression levels that exceed a biologically relevant threshold μ_0 (Love et al., 2014). So, for each gene i a two-sided composite null hypothesis $H_{0,i} : \mu_i \in \mathcal{A}$ is tested against the alternative $H_{1,i} : \mu_i \notin \mathcal{A}$ where $\mathcal{A} = [-\mu_0, \mu_0]$.

The standard practice for simultaneously testing a large number of hypotheses involves constructing significance indices, such as p -values or local false discovery rate (Lfdr) statistics (Basu et al., 2018, Efron, 2012, Sun and Cai, 2007, Sun and McLain, 2012), for ranking the hypotheses and then estimating a threshold along the ranking for type I error control. However, for testing composite null hypotheses, procedures based on p -values are not as powerful since the p -values may fail to adapt to the potential asymmetry of the alternative about the null (Sun and Cai, 2007, Sun and McLain, 2012) and tend to concentrate near 1 under the null. The Lfdr statistic, on the contrary, adapts to such

asymmetry by incorporating information about the null as well as the alternative distribution of the test statistic. Given a summary statistic X_i of μ_i , the Lfdr statistic represents the posterior probability of a case being null and relies on the mixture density of X_i under the null and the alternative. When testing composite null hypotheses, this density is unknown in practical applications and must be estimated from the available data. The heteroskedasticity in the summary statistics raises two main challenges in estimating the mixture density.

Effect of heteroskedasticity on the inferential parameter of interest - In heteroskedastic settings, the parameter μ_i may be correlated with σ_i (Weinstein et al., 2018). For instance, in a restaurant rating app it is often the case that extremely good and extremely bad restaurants tend to receive a large number of reviews. Thus, if the goal is to identify restaurants within a certain rating range then both the mean (μ_i) and standard deviation (σ_i) of the ratings are related to the number of reviews. A key to constructing reliable estimate of the mixture density depends on a deconvolution step that learns the distribution of μ_i from the data and can effectively capture the dependence between μ_i and σ_i . However, existing approaches for empirical Bayes deconvolution, such as Efron (2016), Koener and Mizera (2014), assume independence between μ_i and σ_i , which is often violated in practice. In Section 3.3, we demonstrate via a numerical example that procedures for testing composite null hypotheses may incur power loss and even fail to control the FDR when their underlying deconvolution estimator ignores this dependence.

Power distortion due to standardization - The conventional approach to mitigate the impact of heteroskedasticity is to re-scale each X_i by σ_i and construct z -values $Z_i = X_i/\sigma_i$ so that the Lfdr statistics can be estimated using the homoskedastic Z_i 's. However, for two-sided composite null hypotheses standardization distorts the underlying scientific question (Sun and McLain, 2012) and, recently, Fu et al. (2022) demonstrate that such a data reduction step may severely affect the power of multiple testing procedures even in the case of simple null hypotheses. In Section 2.3, we present illustrative examples to demonstrate that standardization may lead to considerable power loss while testing one-sided composite null hypotheses as the power of testing procedures can vary substantially with σ_i .

In this article, we propose a new heteroskedasticity-adjusted multiple testing (HAMT) procedure for composite null hypotheses (Equation (3)). HAMT represents an effective strategy for incorporating the side-information in the standard deviations for simultaneous testing of composite nulls and it operates in two steps: in step (1) HAMT constructs a significance index for ranking the hypotheses and then in step (2) it estimates a threshold along the ranking for identifying interesting hypotheses. The significance index is a new Lfdr statistic that addresses the methodological challenges discussed earlier in dealing with heteroskedasticity. First, our Lfdr statistic utilizes the full data, namely the summary statistic and its standard deviation, thus avoiding standardization to z -values and the potential power distortion due to data reduction. Second, the construction of the Lfdr statistic relies on an

improved nonparametric empirical Bayes deconvolution estimator that provides a practical strategy for estimating $g_\mu(\cdot|\sigma_i)$ (Equation (2)) while incorporating its dependence on σ_i . Third, while conventional empirical Bayes deconvolution techniques, such as Efron (2016), involve maximizing the marginal likelihood of the data, HAMT relies on a density matching approach (Section 3) to learn $g_\mu(\cdot|\sigma_i)$, which ultimately yields a consistent estimate of the mixture density in the heteroskedastic setting. HAMT is designed for problems where the number of hypotheses being tested is large, which allows the deconvolution estimator to efficiently learn the latent structural relationship between μ_i and σ_i in the data. Our theoretical results (Section 4) show that for such large-scale problems, HAMT is valid for FDR control and is as powerful as the oracle procedure that has full knowledge of the underlying data generating process under our hierarchical model (Equations (1)–(2)). In our numerical experiments (sections 5 and D), we find that HAMT exhibits substantial power gains over existing methods across many settings while controlling FDR at the target level.

Our work is closely related to Sun and McLain (2012), Stephens (2017) and Gu and Shen (2018). Sun and McLain (2012) develop an FDR controlling procedure based on Lfdr statistics for testing composite null hypotheses under heteroskedasticity. However, HAMT differs on two important aspects. First, and in contrast to Sun and McLain (2012), we allow μ_i and σ_i to be dependent in our hierarchical model, which presents a challenging deconvolution problem for estimating the mixture density. Second, the kernel method developed in Sun and McLain (2012) for estimating this density is highly unstable (Fu et al., 2022). Here, we develop a nonparametric empirical Bayes deconvolution estimator which is scalable to large problems and provides a consistent estimate of the mixture density. In the terminology of Efron (2014), our deconvolution estimator is related to the g -modeling strategy for empirical Bayes estimation. While existing g -modeling approaches, such as Efron (2016), Koenker and Mizera (2014), ignore the dependence between μ_i and σ_i , we develop a simple yet effective technique for modeling such dependence while estimating the distribution of μ_i . Stephens (2017) develop a multiple testing procedure, ASH, for FDR control. Similar to HAMT, their approach relies on using the bivariate sequence (X_i, σ_i) instead of summarizing them to p - or z - values. The hierarchical model underlying ASH assumes that conditional on σ_i and for an unknown constant $c \geq 0$, the distribution of μ_i/σ_i^c is unimodal and posits it as a mixture of a point mass at 0 and a scale-mixture of zero-mean Gaussian distributions. Extensions to ASH allow mixtures of uniforms, half-uniforms and half-normals, among others, depending on the prior knowledge regarding the sign and symmetry of the distribution of μ_i 's. We note that there are two key differences between the hierarchical models underlying ASH and HAMT. First, ASH assumes that conditional on σ_i the distribution of μ_i/σ_i^c is independent of σ_i for some $c \geq 0$. In contrast, HAMT does not make such an assumption and provides a practical approach for estimating the unknown mixing density $g_\mu(\cdot|\sigma_i)$ that accounts for the dependence of μ_i on σ_i . Second, unlike ASH, HAMT does not require a unimodal assumption for the distribution of μ_i given σ_i . In particular, our theoretical analyses in Section 4 only requires that (i) $g_\mu(\cdot|\sigma)$ is supported on a compact interval, and (ii) has bounded

first and second order derivatives with respect to σ , for providing valid FDR control as the number of hypotheses $m \rightarrow \infty$. Recently, [Gu and Shen \(2018\)](#) propose a FDR controlling method for one-sided composite null hypotheses. Their approach is based on z -values and relies on the deconvolution estimate obtained from nonparametric maximum likelihood ([Kiefer and Wolfowitz, 1956](#), [Laird, 1978](#)) techniques to estimate the Lfdr. The illustrative examples in Section 2.3 show that such an approach based on standardization may lead to substantial power loss when μ_i and σ_i are correlated.

Since variance can be viewed as a covariate in multiple testing problems, our work is also connected to the rapidly expanding literature on multiple testing with generic covariates. Here, proposals for heteroskedasticity adjustment of multiple testing methods vary from using σ_i as a potential covariate for pre-ordering the hypotheses ([Cao et al., 2022](#), [G’Sell et al., 2016](#), [Lei and Fithian, 2016](#), [Li and Barber, 2017](#)) to grouping methods based on the magnitudes of σ_i ([Cai and Sun, 2009](#), [Efron, 2008](#), [Hu et al., 2010](#), [Liu et al., 2016](#)). However, such a pre-ordering or grouping based on σ_i may not always be informative since a larger σ_i does not necessarily imply a relatively higher or lower likelihood of rejecting the null hypothesis. More recently, several methods have been proposed that seek to directly use the covariate information along with the p -values to develop powerful testing procedures (see for example [Boca and Leek \(2018\)](#), [Chao and Fithian \(2021\)](#), [Ignatiadis and Huber \(2021\)](#), [Lei and Fithian \(2018\)](#), [Li and Barber \(2019\)](#), [Zhang et al. \(2019\)](#), [Zhang and Chen \(2022\)](#) and the references therein). While testing composite null hypotheses, the aforementioned testing procedures, however, can suffer from low power when the null p -values are overly conservative. Methods that estimate the Lfdr statistic utilizing test statistic X_i and additional covariates have also been developed (see for instance [Chao and Fithian \(2021\)](#), [Leung and Sun \(2021\)](#), [Scott et al. \(2015\)](#), [Tansey et al. \(2018\)](#)). In particular, [Scott et al. \(2015\)](#), [Tansey et al. \(2018\)](#) use the covariate information to estimate the null proportion in an empirical Bayes two-groups model while [Chao and Fithian \(2021\)](#) posit a Gaussian mixture model with K classes to model the conditional distribution of μ_i given the covariates, where only the class probabilities depend on the covariates. In contrast to these works, HAMT does not rely on any pre-ordering or grouping of the hypotheses based on the magnitude of σ_i . Instead, HAMT is based on a Lfdr statistic that directly characterizes the impact of heteroskedasticity on the mixture density of the test statistic. For estimating the Lfdr statistics, our approach utilizes an empirical Bayes deconvolution estimator that does not depend on any parametric representation of the distribution of μ_i conditional on σ_i .

In the following sections, we formally describe the multiple testing problem involving composite null hypotheses, present the oracle procedure, and then introduce the HAMT procedure and its asymptotic properties.

2 Multiple testing of composite null hypotheses

2.1 Problem formulation

Let $\theta_i = I(\mu_i \notin \mathcal{A})$ be an indicator function that gives the true state of the i th testing problem in Equation (3). For instance, if $\theta_i = 1$ then the alternative hypothesis $H_{1,i}$ is true. Let $\delta_i \in \{0, 1\}$ be the decision we make about hypothesis test i , with $\delta_i = 1$ being a decision to reject $H_{0,i}$. Denote the vector of all m decisions $\boldsymbol{\delta} = (\delta_1, \dots, \delta_m) \in \{0, 1\}^m$. A selection error, or false positive, occurs if we assert that μ_i is not in \mathcal{A} when it actually is. In large-scale multiple testing problems, false positive decisions are inevitable if we wish to discover interesting effects with a reasonable power. Instead of aiming to avoid any false positives, a practical goal is to keep the false discovery rate (FDR) (Benjamini and Hochberg, 1995) small, which is the expected proportion of false positives among all selections,

$$\text{FDR}(\boldsymbol{\delta}) = E \left[\frac{\sum_{i=1}^m (1 - \theta_i) \delta_i}{\max\{\sum_{i=1}^m \delta_i, 1\}} \right].$$

The power of a testing procedure is measured by the expected number of true positives (ETP) where,

$$\text{ETP}(\boldsymbol{\delta}) = E \left(\sum_{i=1}^m \theta_i \delta_i \right) = E \left(\sum_{i=1}^m I(\mu_i \notin \mathcal{A}) \delta_i \right).$$

Hence, the multiple testing problem in Equation (3) can be formulated as

$$\text{maximize}_{\boldsymbol{\delta}} \text{ETP}(\boldsymbol{\delta}) \text{ subject to } \text{FDR}(\boldsymbol{\delta}) \leq \alpha,$$

where $\alpha \in (0, 1)$ is a user-defined cap on the maximum acceptable FDR. A quantity that is closely related to the FDR is the marginal false discovery rate (mFDR) where,

$$\text{mFDR}(\boldsymbol{\delta}) = \frac{E\{\sum_{i=1}^m (1 - \theta_i) \delta_i\}}{E\{\sum_{i=1}^m \delta_i\}}.$$

Under certain first and second-order conditions on the number of rejections, the mFDR and the FDR are asymptotically equivalent (Basu et al., 2018, Genovese and Wasserman, 2002), and for theoretical convenience we will aim to control mFDR instead. Formally, we study the following problem for the rest of the article:

$$\text{maximize}_{\boldsymbol{\delta}} \text{ETP}(\boldsymbol{\delta}) \text{ subject to } \text{mFDR}(\boldsymbol{\delta}) \leq \alpha. \quad (4)$$

2.2 Oracle procedure

In this section we assume that the mixing densities $g_{\mu}(\cdot \mid \sigma)$ and $g_{\sigma}(\cdot)$ in Model (2) are known by the oracle and present the oracle procedure that solves Problem (4). There are two steps involved in

the derivation of the oracle procedure: the first step constructs the optimal ranking of hypotheses and the second step determines the best threshold along the ranking that satisfies the mFDR constraint in Problem (4).

To rank the m hypotheses, consider the oracle conditional local FDR (Clfdr) statistic which is defined as,

$$T_i^{\text{OR}} = T^{\text{OR}}(x_i, \sigma_i) = P(\mu_i \in \mathcal{A} | x_i, \sigma_i) = \frac{f_0(x_i | \sigma_i)}{f(x_i | \sigma_i)}, \quad (5)$$

where

$$f_0(x | \sigma) = \int_{\mu \in \mathcal{A}} \eta_\sigma(x - \mu) g_\mu(\mu | \sigma) d\mu \text{ and } f(x | \sigma) = \int_{\mathbb{R}} \eta_\sigma(x - \mu) g_\mu(\mu | \sigma) d\mu. \quad (6)$$

In Equation (6), $f(x | \sigma)$ denotes the marginal density of X given σ under Model (1)–(2) and $\eta_\sigma(x - \mu) = \sigma^{-1} \eta\{(x - \mu)/\sigma\}$ is the density of X_i conditional on (μ_i, σ_i) . Next, to derive the best threshold, suppose $Q(t)$ denotes the mFDR level of the testing procedure $\delta^{\text{OR}}(t) = \{I(T_i^{\text{OR}} \leq t) : 1 \leq i \leq m\}$ for some $t \in (0, 1)$. We propose the following oracle procedure for Problem (4),

$$\delta^{\text{OR}}(t^*) = \{I(T_i^{\text{OR}} < t^*) : 1 \leq i \leq m\}, \quad (7)$$

where $t^* = \sup\{t \in (0, 1) : Q(t) \leq \alpha\}$.

Denote $\mathbf{X} = (X_1, \dots, X_m)$ and $\boldsymbol{\sigma} = (\sigma_1, \dots, \sigma_m)$. In Theorem 1 we show that $\delta^{\text{OR}}(t^*)$ has the highest power among all procedures based on $(\mathbf{X}, \boldsymbol{\sigma})$ that control the mFDR at level α .

Theorem 1. *Consider Model (1)–(2). The oracle procedure $\delta^{\text{OR}}(t^*)$ in Equation (7) controls mFDR at level α . Additionally if δ is any other procedure based on $(\mathbf{X}, \boldsymbol{\sigma})$ that controls mFDR at level α then we have $ETP\{\delta^{\text{OR}}(t^*)\} \geq ETP(\delta)$.*

Theorem 1 establishes that the oracle procedure $\delta^{\text{OR}}(t^*)$ is valid and optimal for mFDR control. However, $\delta^{\text{OR}}(t^*)$ is not implementable in practice since both T_i^{OR} and t^* are unknown in practical applications. In Section 3 we describe the proposed HAMT procedure that relies on a nonparametric empirical Bayes deconvolution estimator of $g_\mu(\cdot | \sigma_i)$ to construct a data-driven estimate of T_i^{OR} and uses a step-wise procedure to estimate t^* .

2.3 Power loss due to standardization: illustrative examples

While $\delta^{\text{OR}}(t^*)$ is the optimal solution to Problem (4) based on $(\mathbf{X}, \boldsymbol{\sigma})$, a plausible approach for solving Problem (4) is to construct z -values $Z_i = X_i/\sigma_i$ and then reject the null hypothesis for suitably small values of Z_i^{OR} where $Z_i^{\text{OR}} = P(\mu_i \in \mathcal{A} | z_i)$. In fact, Sun and Cai (2007) show that this approach is the most powerful z -value method. The apparent advantage of this data reduction step is that it transforms the heteroskedastic multiple testing problem to a homoskedastic one, and

enables a like-for-like comparison of the m study units under consideration. However, in the case of two-sided composite null hypothesis, such a standardization may distort the underlying scientific question (Sun and McLain, 2012). Moreover, Fu et al. (2022) demonstrate that data reduction via standardization could lead to power loss for multiple testing procedures even in the case of simple null hypotheses. In this section we consider two illustrative examples to demonstrate that power loss due to standardization can be substantial while testing one-sided composite null hypotheses.

Example 1. Suppose data are generated from Model (1)–(2) with $X_i \mid \mu_i, \sigma_i \stackrel{ind.}{\sim} N(\mu_i, \sigma_i^2)$, $\sigma_i \stackrel{i.i.d.}{\sim} Unif(0.5, 4)$ and $\mu_i \mid \sigma_i \stackrel{ind.}{\sim} 0.9\delta_0(\cdot) + 0.1\delta_{\sigma_i^{1.5}}(\cdot)$, where $\delta_a(\cdot)$ is a Dirac delta function indicating a point mass at a . In this example σ_i controls the magnitude of the non-zero μ_i and we are interested in Problem (3) with $\mathcal{A} = (-\infty, 0]$. We first consider the oracle procedure based on the z -values $\mathbf{Z} = (Z_1, \dots, Z_m)$. In Section A we show that this oracle procedure is a thresholding rule of the form $\delta^{\text{ZOR}}(t_z) = \{I(Z_i > t_z) : 1 \leq i \leq m\}$ where $t_z = 3.273$ at $\alpha = 0.1$. Next, recall from Equation (7) that the oracle procedure $\delta^{\text{OR}}(t^*)$ based on $(\mathbf{X}, \boldsymbol{\sigma})$ is of the form $\{I(T_i^{\text{OR}} < t^*) : 1 \leq i \leq m\}$. This is equivalent to a thresholding rule $\{I(Z_i > \lambda_{\sigma_i}(t^*)) : 1 \leq i \leq m\}$ (details provided in Section A), where

$$\lambda_{\sigma}(t) = \frac{1}{\sqrt{\sigma}} \left[-\log \left\{ \frac{0.1t}{(1-t)0.9} \right\} + 0.5\sigma \right],$$

and $t^* = 0.177$ at $\alpha = 0.1$.

While both δ^{ZOR} and δ^{OR} control the mFDR exactly at α , their powers are substantially different in this example: power of $\delta^{\text{ZOR}}(t_z)$ is 0.0432 and that of δ^{OR} is 0.0611. To further examine the power gain of $\delta^{\text{OR}}(t^*)$, we consider the left panel of Figure 1 that plots the rejection regions of $\delta^{\text{OR}}(t^*)$ and $\delta^{\text{ZOR}}(t_z)$ as a function of Z_i and σ_i . In the red shaded region $\delta^{\text{ZOR}}(t_z)$ rejects while $\delta^{\text{OR}}(t^*)$ does not, in the blue region $\delta^{\text{OR}}(t^*)$ rejects while $\delta^{\text{ZOR}}(t_z)$ does not and both procedures reject in the white region. Finally, in the gray shaded region neither procedures reject. The black dots represent instances where the null hypothesis is false and fall within the three rejection regions. While it is clear that a vast majority of the non-null cases appear in the white region, approximately 64%, the blue region captures relatively more non-null cases than the red region, 30% versus 6%. Thus, $\delta^{\text{OR}}(t^*)$ rejects an overall higher percentage of the non-null cases than $\delta^{\text{ZOR}}(t_z)$, which explains the power gain of the former over the latter.

Example 2. Unlike the previous setting, in this example σ_i controls the sparsity as well as the magnitude of the non-zero μ_i . Data are generated from Model (1)–(2) with $X_i \mid \mu_i, \sigma_i \stackrel{ind.}{\sim} N(\mu_i, \sigma_i^2)$, $\sigma_i \stackrel{i.i.d.}{\sim} Unif(0.5, 4)$ and $\mu_i \mid \sigma_i \stackrel{ind.}{\sim} \delta_0(\cdot)I\{\sigma_i \leq 3.65\} + \delta_{\sigma_i^{1.5}}(\cdot)I\{\sigma_i > 3.65\}$, where $P(\sigma_i \leq 3.65) = 0.9$. We are interested in Problem (3) with $\mathcal{A} = (-\infty, 0]$. The oracle procedure based on \mathbf{Z} is of the form $\delta^{\text{ZOR}}(t_z) = \{I(Z_i > t_z) : 1 \leq i \leq m\}$ where $t_z = 4.124$ at $\alpha = 0.1$ with power 0.0015. In contrast, $\delta^{\text{OR}}(t^*)$ in this example simply observes if $\sigma_i > 3.65$ to detect if $H_{0,i}$ is false and thus, provides a perfect classification rule with FDR equal to 0 and power equal to 1. The stark contrast

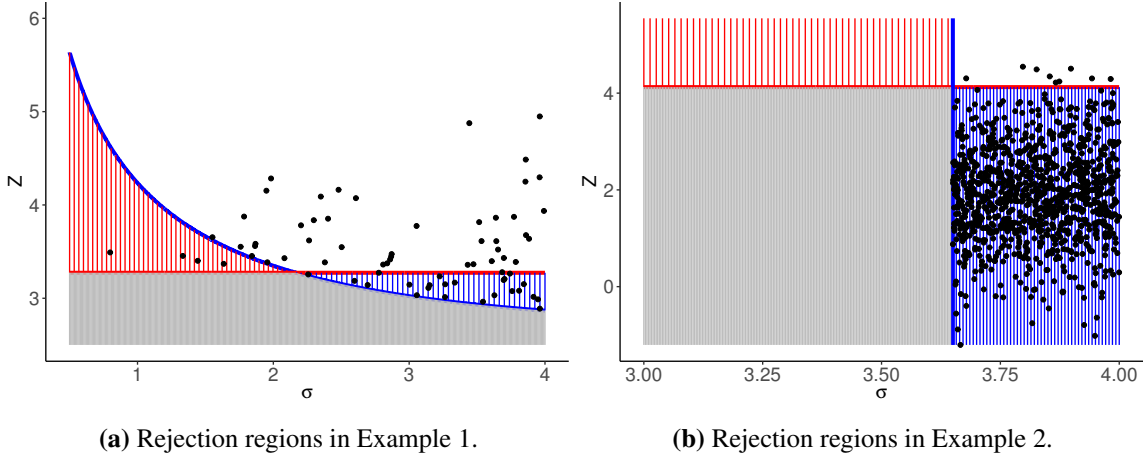


Figure 1: In the red shaded region $\delta^{\text{ZOR}}(t_z)$ rejects while $\delta^{\text{OR}}(t^*)$ does not, in the blue region $\delta^{\text{OR}}(t^*)$ rejects while $\delta^{\text{ZOR}}(t_z)$ does not and both procedures reject in the white region. Finally, in the gray shaded region neither procedures reject. The black dots represent instances where the null hypothesis is false and fall within the three rejection regions.

in the power of these two procedures is further elucidated in the right panel of Figure 1. Here, the rejection regions continue to have the same interpretation as in the left panel. However, the blue region now captures almost 99% of all the non-null cases that fall within the three regions while the white region only accounts for the remaining 1%. Moreover, the red region does not capture any non-null case, thus explaining the substantially low power of $\delta^{\text{ZOR}}(t_z)$ in this setting.

The preceding examples illustrate that data reduction via standardization may lead to power loss even when testing one-sided composite null hypotheses. While standardization is a natural pre-processing step for testing heteroskedastic units, Examples 1 and 2 demonstrate that such a step suppresses the information contained in the standard deviations that can boost the power of these tests. Our numerical experiments in Section 5.2 and Section D of the supplement corroborate this observation where we find that z -value procedures are, in general, not as powerful as the proposed HAMT procedure which is based on (\mathbf{X}, σ) .

3 Heteroskedasticity adjusted multiple testing procedure for composite null hypotheses

3.1 Improved empirical Bayes deconvolution

This section develops a data-driven procedure to mimic the oracle. We discuss the estimation of T_i^{OR} and t^* , and present the HAMT procedure in Definition 2. Our approach for estimating T_i^{OR} involves constructing a nonparametric empirical Bayes deconvolution estimate of the unknown mixing density $g_\mu(\cdot | \sigma_i)$. While there are several popular approaches to estimating an unknown mixing density, we

demonstrate in Section 3.3 that existing methods that fail to account for the dependence between μ_i and σ_i can suffer from power loss and may not even provide FDR control. Here we present a practical approach for estimating $g_\mu(\cdot | \sigma_i)$ that effectively accounts for this dependence.

Suppose $g_\mu(\cdot | \sigma_i)$ is continuous in σ_i . We first approximate the parameter space of μ_i using a discrete equispaced grid $\mathcal{T} = \{u_1, \dots, u_S\}$ of size S . Then, the conditional prior density $g_\mu(\cdot | \sigma_i)$ can be approximated by a mixture of point masses as follows:

$$g_\mu(\cdot | \sigma_i) \approx \sum_{j=1}^S g_j(\sigma_i) \delta_{u_j}(\cdot),$$

where $\delta_{u_j}(\cdot)$ is the point mass at u_j and $g_j(\sigma_i) = g_\mu(u_j | \sigma_i)$ is the prior probability mass on u_j conditional on σ_i . A formal statement justifying this approximation is presented in Lemma 1 in the supplement. We view $g_j(\sigma_i)$ as a continuous function of σ_i and approximate it as a linear combination of K basis functions as follows:

$$g_j(\sigma_i) \approx \sum_{k=1}^K w_{jk} q_k(\sigma_i) = \mathbf{w}_j^T \mathbf{q}(\sigma_i). \quad (8)$$

In Equation (8), \mathbf{w}_j is a K -dimensional vector of unknown weights and $\mathbf{q}(\sigma_i)$ is a known vector of basis functions that depend on σ_i . We discuss the choice of these basis functions in Section 5.1. In this discrete setting, and using Equation (8), the quantities in Equation (6) have the following representation:

$$\tilde{f}_0(x | \sigma_i) = \sum_{j: u_j \in \mathcal{A}} \eta_{\sigma_i}(x - u_j) \mathbf{w}_j^T \mathbf{q}(\sigma_i), \quad \tilde{f}(x | \sigma_i) = \sum_{j=1}^S \eta_{\sigma_i}(x - u_j) \mathbf{w}_j^T \mathbf{q}(\sigma_i).$$

Our goal is to estimate the K -dimensional vectors $\{\mathbf{w}_1, \dots, \mathbf{w}_S\}$ such that (i) $\sum_{j=1}^S \mathbf{w}_j^T \mathbf{q}(\sigma_i) = 1$ for $i = 1, \dots, m$, and (ii) $\mathbf{w}_j^T \mathbf{q}(\sigma_i) \geq 0$ for $j = 1, \dots, S$, $i = 1, \dots, m$. A standard approach involves maximizing the marginal log-likelihood of the data with respect to the \mathbf{w}_j s under the above two constraints as follows:

$$\begin{aligned} & \min_{\{\mathbf{w}_1, \dots, \mathbf{w}_S\} \in \mathbb{R}^K} - \sum_{i=1}^m \log \sum_{j=1}^S \eta_{\sigma_i}(x_i - u_j) \mathbf{w}_j^T \mathbf{q}(\sigma_i) \\ & \text{subject to: } \sum_{j=1}^S \mathbf{w}_j^T \mathbf{q}(\sigma_i) = 1 \text{ for } i = 1, \dots, m. \\ & \mathbf{w}_j^T \mathbf{q}(\sigma_i) \geq 0 \text{ for } j = 1, \dots, S \text{ and } i = 1, \dots, m. \end{aligned} \quad (9)$$

Equation (9) is a convex optimization problem that can be solved, relatively efficiently, using solvers, such as MOSEK (MOSEK, 2019). We provide those details in Section C of the supplement. In this article, however, we take a different approach and estimate \mathbf{w}_j s using a density matching technique, which involves minimizing the average squared error loss between $\tilde{f}(x_i|\sigma_i)$ and a pilot estimate of the true marginal density $f(x_i | \sigma_i)$ with respect to the \mathbf{w}_j s. We first describe our approach and then discuss its advantage over Problem (9).

If $f(x_i|\sigma_i)$ were known, the proposed density matching technique would involve the following minimization problem with respect to the \mathbf{w}_j s:

$$\begin{aligned} & \min_{\{\mathbf{w}_1, \dots, \mathbf{w}_S\} \in \mathbb{R}^K} \frac{1}{2m} \sum_{i=1}^m \left\{ f(x_i | \sigma_i) - \sum_{j=1}^S \eta_{\sigma_i}(x_i - u_j) \mathbf{w}_j^T \mathbf{q}(\sigma_i) \right\}^2 \\ & \text{subject to: } \sum_{j=1}^S \mathbf{w}_j^T \mathbf{q}(\sigma_i) = 1 \text{ for } i = 1, \dots, m. \\ & \mathbf{w}_j^T \mathbf{q}(\sigma_i) \geq 0 \text{ for } j = 1, \dots, S \text{ and } i = 1, \dots, m. \end{aligned} \quad (10)$$

However, $f(x_i | \sigma_i)$ s in Problem (10) are not known in practice and estimating them directly from the data is difficult as we only have one pair of observation (X_i, σ_i) for estimating each density. Recently, Fu et al. (2022) consider a heteroskedasticity adjusted bivariate kernel density estimator $\hat{\varphi}^m(x, \sigma_i)$ for $f(x | \sigma_i)$ where

$$\hat{\varphi}^m(x, \sigma_i) = \sum_{j=1}^m \frac{\phi_{h_\sigma}(\sigma_i - \sigma_j)}{\sum_{k=1}^m \phi_{h_\sigma}(\sigma_i - \sigma_k)} \phi_{h_{xj}}(x - x_j). \quad (11)$$

In Equation (11), $\phi_\sigma(\cdot)$ is the density of a Gaussian random variable with mean 0 and standard deviation σ , $h_{xj} = h_x \sigma_j$ and $\mathbf{h} = (h_x, h_\sigma)$ is a pair of bandwidths. The weights $\phi_{h_\sigma}(\sigma_i - \sigma_j) / \sum_{k=1}^m \phi_{h_\sigma}(\sigma_i - \sigma_k)$ are designed to borrow strength from observations with variability close to σ_i , while placing little weight on points where σ_i and σ_j are far apart. The variable bandwidth h_{xj} adjusts for the heteroskedasticity in the data by inducing flatter kernels for data points that are observed with a higher variance. Furthermore, Fu et al. (2022) show that $\hat{\varphi}^m(x, \sigma_i)$ is a consistent estimator of $f(x | \sigma_i)$ in the sense that $E \int \{\hat{\varphi}^m(x, \sigma_i) - f(x | \sigma_i)\}^2 dx \rightarrow 0$ as $m \rightarrow \infty$ for all $\sigma_i > 0$. In our analysis, we solve Problem (10) with a jackknifed version $\hat{\varphi}_{(-i)}^m(x_i, \sigma_i)$ of $\hat{\varphi}^m(x_i, \sigma_i)$ as a pilot estimate of $f(x_i | \sigma_i)$, where

$$\hat{\varphi}_{(-i)}^m(x_i, \sigma_i) = \sum_{j \neq i=1}^m \frac{\phi_{h_\sigma}(\sigma_i - \sigma_j)}{\sum_{k \neq i=1}^m \phi_{h_\sigma}(\sigma_i - \sigma_k)} \phi_{h_{xj}}(x_i - x_j). \quad (12)$$

Denote $\hat{\varphi}^m = [\hat{\varphi}_{(-1)}^m(x_1, \sigma_1), \dots, \hat{\varphi}_{(-m)}^m(x_m, \sigma_m)]$, $\mathbf{a}_{ij} = \eta_{\sigma_i}(x_i - u_j) \mathbf{q}(\sigma_i)$, $\mathbf{a}_i = (\mathbf{a}_{i1}^T, \dots, \mathbf{a}_{iS}^T)^T$ and $A = (\mathbf{a}_1, \dots, \mathbf{a}_m)^T$. Additionally, let $C = [\mathbf{1}_S \otimes \mathbf{q}(\sigma_1) \dots \mathbf{1}_S \otimes \mathbf{q}(\sigma_m)]^T$ where \otimes denotes

the usual Kronecker product of two matrices, and denote \mathbf{c}_r as an r -dimensional vector with all entries equal to the scalar $c \in \mathbb{R}$. Finally, for $s = 1, \dots, S$, let B_s denote a $m \times KS$ matrix whose entries are 0 except for the $\{K(s-1) + 1\}$ th column which equals $[\mathbf{q}(\sigma_1), \dots, \mathbf{q}(\sigma_m)]^T$ and let $B = [B_1^T \dots B_S^T]^T$. Problem (10), with $f(x_i|\sigma_i)$ replaced by $\hat{\varphi}_{(-i)}^m(x_i, \sigma_i)$, is then equivalent to the following convex optimization problem with respect to $\mathcal{W} = (\mathbf{w}_1^T, \dots, \mathbf{w}_S^T)^T$:

$$\min_{\mathcal{W} \in \mathbb{R}^{KS}} \frac{1}{2m} \left\| \hat{\varphi}^m - A\mathcal{W} \right\|_2^2 \quad \text{subject to } B\mathcal{W} \succeq \mathbf{0}_{Sm}, \quad C\mathcal{W} = \mathbf{1}_m. \quad (13)$$

The density matching approach (Problem (13)) to estimating \mathcal{W} has a distinct advantage over the one that estimates \mathcal{W} by maximizing the marginal log-likelihood of the data (Problem (9)). When the distribution of μ depends on σ_i , Problem (13) is a relatively superior strategy for learning $g_\mu(\mu|\sigma_i)$ than maximizing the marginal log-likelihood since the extra information encoded in σ can be better exploited by the bivariate kernel density estimator $\hat{\varphi}_{(-i)}^m(x_i, \sigma_i)$ (Equation (12)) of $f(x_i | \sigma_i)$. This intuition is supported by the numerical studies in sections 5.2 and D where, across many settings, the proposed procedure HAMT, that relies on the solution $\hat{\mathcal{W}}_m = (\hat{\mathbf{w}}_{1,m}, \dots, \hat{\mathbf{w}}_{S,m})$ from Problem (13), demonstrates substantially higher power at the same FDR level than the competing procedure NPMLE B, which uses Problem (9) to learn $g_\mu(\mu|\sigma_i)$. Furthermore, in Proposition 1 (Section 4) we show that $\hat{\mathcal{W}}_m$ yields a consistent estimator of $f(x_i|\sigma_i)$, which plays an important role in establishing the validity and optimality of the data-driven HAMT procedure. Parallel results establishing the validity of NPMLE B is, to the best of our knowledge, still unknown at the time of writing this article. A recent development in this direction is by Chen (2024) who model the distribution of μ given σ_i as a flexible location-scale family and show that with high probability the average squared Hellinger distance between the estimated and the true marginal densities is small. However, their methodological development does not cover the problem of multiple testing. Much research is needed to fully comprehend the conditions under which NPMLE B can guarantee asymptotic FDR control and how the hyper-parameters S and K impact its power. In Section E.2 of the supplement we provide additional insights on when NPMLE B can be expected to outperform HAMT in power at the same FDR level.

In the next section, we present our data-driven HAMT procedure that relies on the solution $\hat{\mathcal{W}}_m$ to Problem (13). Section 5.1 provides the recommended choices for \mathcal{T} , S and K in the context of HAMT while Section C in the supplement includes the implementation details for solving Problem (13).

3.2 Proposed HAMT procedure

We first present the estimator of the oracle Clfdr statistic T_i^{OR} in Definition 1.

Definition 1. Let $\hat{\mathcal{W}}_m = (\hat{\mathbf{w}}_{1,m}, \dots, \hat{\mathbf{w}}_{S,m})$ be the solution to Problem (13). The data-driven Clfdr

statistic is given by

$$\hat{T}_{i,m} = \frac{\hat{f}_0^m(x_i | \sigma_i)}{\hat{f}^m(x_i | \sigma_i)}, \quad \text{where}$$

$$\hat{f}_0^m(x | \sigma_i) = \sum_{j:u_j \in \mathcal{A}} \eta_{\sigma_i}(x - u_j) \hat{\mathbf{w}}_{j,m}^T \mathbf{q}(\sigma_i), \quad \hat{f}^m(x | \sigma_i) = \sum_{j=1}^S \eta_{\sigma_i}(x - u_j) \hat{\mathbf{w}}_{j,m}^T \mathbf{q}(\sigma_i).$$

Next, in Definition 2 we present the proposed HAMT procedure that relies on the estimate $\hat{T}_{i,m}$ and uses a step-wise procedure from Sun and McLain (2012) to estimate t^* .

Definition 2. (HAMT procedure) Denote $\hat{T}_{(1),m} \leq \dots \leq \hat{T}_{(m),m}$ the sorted Clfdr statistics and $H_{(1)}, \dots, H_{(m)}$ the corresponding hypotheses. Suppose

$$r = \max \left\{ j : \frac{1}{j} \sum_{i=1}^j \hat{T}_{(i),m} \leq \alpha \right\}.$$

Then, the HAMT procedure rejects the ordered hypotheses $H_{(1)}, \dots, H_{(r)}$. Furthermore, in comparison to the oracle procedure $\delta^{\text{OR}}(t^*)$ in Equation (7), HAMT has the following form:

$$\delta^{\text{HAMT}}(\hat{t}_m^*) = \{I(\hat{T}_{i,m} < \hat{t}_m^*) : 1 \leq i \leq m\}, \quad \text{where } \hat{t}_m^* = \hat{T}_{(r),m}.$$

In Definition 2, the estimate \hat{t}_m^* of t^* is based on the intuition that when the first j ordered hypotheses are rejected then a good estimate of the false discovery proportion is given by the moving average $(1/j) \sum_{i=1}^j \hat{T}_{(i),m}$ and the condition $(1/j) \sum_{i=1}^j \hat{T}_{(i),m} \leq \alpha$ then helps fulfill the FDR constraint. In Section 4 we show that for large m , $\hat{T}_{i,m}$ is asymptotically close to T_i^{OR} uniformly in i , and the HAMT procedure in Definition 2 is a good approximation to the oracle procedure $\delta^{\text{OR}}(t^*)$.

3.3 Effect of ignoring the dependence between μ_i and σ_i

Here, we consider a numerical example to illustrate the effect on the power and validity of multiple testing procedures if the underlying deconvolution estimator for constructing the Clfdr statistics ignores the dependence between μ_i and σ_i .

We fix $m = 10^4$ and, for $i = 1, \dots, m$, sample X_i independently from $N(\mu_i, \sigma_i^2)$ with $\mu_i = 3\sigma_i$ and $\sigma_i \stackrel{i.i.d.}{\sim} \text{Unif}(0.5, 2)$. The goal is to test $H_{0,i} : \mu_i \in \mathcal{A}$ vs $H_{1,i} : \mu_i \notin \mathcal{A}$ where $\mathcal{A} = (-\infty, 4]$ and $\alpha = 0.1$. The following three testing procedures are evaluated in this example: the procedure that relies on the deconvolution estimate obtained from nonparametric maximum likelihood (Kiefer and Wolfowitz, 1956, Koenker and Gu, 2017, Laird, 1978) (NPMLE) techniques to estimate the Clfdr statistic, the procedure that uses the deconvolution estimate from Efron (2016) (DECONV) to estimate T_i^{OR} and the HAMT procedure from Definition 2. While these procedures employ different methods for estimating T_i^{OR} , they all rely on Definition 2 to estimate the threshold t^* .

The first row of Figure 2 highlights in red the hypotheses that were rejected by the three procedures. Here the dotted horizontal line is $\sigma = 4/3$ and represents the oracle decision rule which rejects any hypothesis above that line. The rightmost panel presents the hypotheses that were rejected by HAMT and appears to correctly discover a substantially larger proportion of the non-null cases than NPMLE and DECONV while safeguarding, at the same time, the number of false discoveries. For instance, across 200 repetitions of this multiple testing problem the average false discovery proportions for NPMLE, DECONV and HAMT are, respectively, 0.157, 0.186 and 0.010 while their average proportion of true discoveries are 0.142, 0.231 and 0.845. The relatively poorer performance

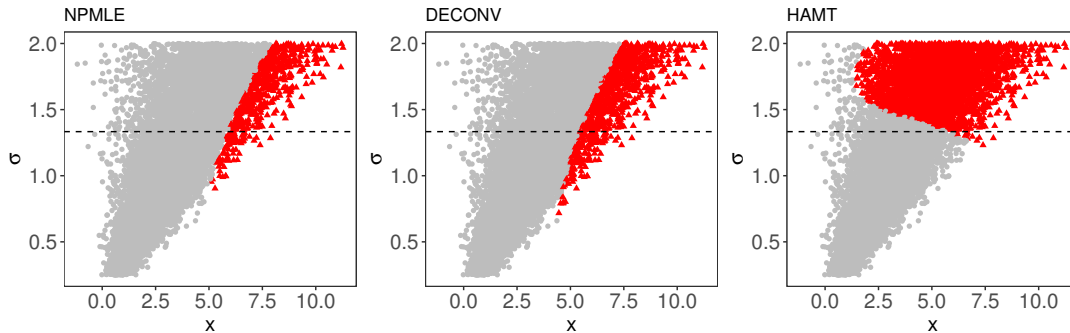


Figure 2: We test $H_{0,i} : \mu_i \leq 4$ vs $H_{1,i} : \mu_i > 4$, $i = 1, \dots, m$, where $X_i \stackrel{ind}{\sim} N(\mu_i, \sigma_i^2)$, $\mu_i = 3\sigma_i$, $\sigma_i \stackrel{i.i.d.}{\sim} \text{Unif}(0.5, 2)$ and $m = 10,000$. Across the three panels, in red are the hypotheses that were rejected by the testing procedures at $\alpha = 0.1$. The dotted horizontal line is the oracle decision rule which rejects any hypothesis above that line. The left and center panels depict testing procedures that rely, respectively, on NPMLE's and DECONV's deconvolution estimates. The rightmost panel presents the HAMT procedure.

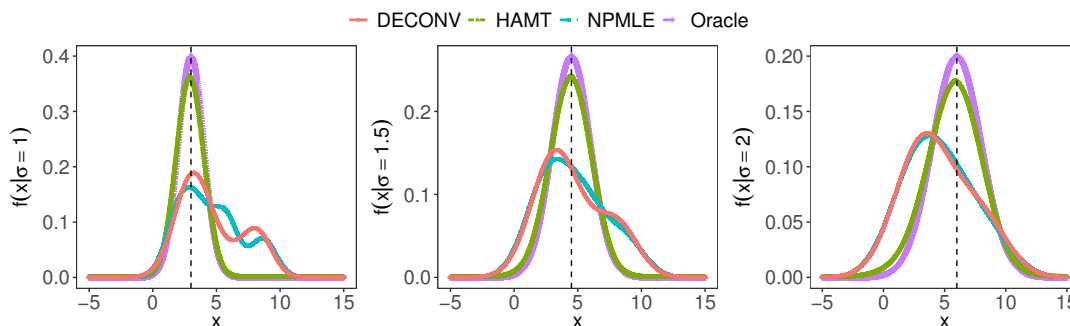


Figure 3: The oracle marginal density $f(x | \sigma)$ in green and the estimated marginal densities from the deconvolution estimates of NPMLE, DECONV and HAMT for $\sigma \in \{1, 1.5, 2\}$. The dotted vertical line represents the mean of the distribution of X given σ .

of NPMLE and DECONV in this example is related to the fact that the underlying deconvolution estimator for both these procedures ignore the dependence between μ_i and σ_i . To see that, we present the estimate of $f(\cdot | \sigma)$ for $\sigma \in \{1, 1.5, 2\}$ in Figure 3. Across the three panels, the deconvolution estimates from NPMLE and DECONV result in marginal density estimates that are substantially different from the ground truth. The deconvolution estimator underlying the HAMT procedure, on

the other hand, seems to generate marginal density estimates that are relatively closer to $f(\cdot | \sigma)$. In Section 4 we present formal theories supporting this intuition and establish that $\hat{f}_0^m(\cdot | \sigma_i)$ and $\hat{f}^m(\cdot | \sigma_i)$ in Definition 1 are, in fact, consistent estimators of $f_0(\cdot | \sigma_i)$ and $f(\cdot | \sigma_i)$, respectively, as $m \rightarrow \infty$.

4 Theory

In this section we study the asymptotic properties of HAMT under the setting where the grid size $S = S(m)$ and the number of bases $K = K(m)$ vary with m . For two real sequences a_m, b_m , we will use $a_m \asymp b_m$ to mean that there exists constants $c_2 \geq c_1 > 0$ such that $c_1 b_m \leq a_m \leq c_2 b_m$ for large m . The following regularity conditions are needed in our technical analysis.

- (A1) The density $g_\mu(\cdot | \sigma)$ is supported on a compact interval $[-M, M]$ for some $M < \infty$ and has bounded first and second derivatives with respect to σ for all $\mu \in [-M, M]$.
- (A2) The density $g_\sigma(\cdot)$ satisfies $0 < C_1 < g_\sigma(\sigma) < C_2 < \infty$ and $|g'_\sigma(\sigma)| < C_3$ for some fixed constants C_1, C_2 and C_3 on $\text{supp}(g_\sigma)$ where $\text{supp}(g_\sigma) \subset [M_1, M_2]$, for some $M_2 < \infty$ and $M_1 > 0$.
- (A3) The bandwidths (h_x, h_σ) satisfy $h_x \asymp m^{-\nu_x}$, $h_\sigma \asymp m^{-\nu_\sigma}$ where ν_x and ν_σ are small positive constants such that $0 < \nu_\sigma + \nu_x < 1$.
- (A4) The density $\eta(\cdot)$ is smooth.

Assumption (A1) on the first and second derivatives of $g_\mu(\cdot | \sigma)$ with respect to σ is a necessary condition in our proofs for information pooling across the heteroskedastic units and controlling the bias of pilot estimate. The compactness of the supports of $g_\mu(\cdot | \sigma)$ and $g_\sigma(\cdot)$ in Assumptions (A1) and (A2) are standard regularity conditions for empirical Bayes deconvolution problems (see for example [Dicker and Zhao \(2016\)](#)) and are satisfied in most practical scenarios where the true mean μ often represents a score. The boundedness of $g_\sigma(\cdot)$ in (A2) is needed for controlling the variance of the pilot estimate. Assumption (A3) is satisfied by common choices of bandwidths in [Silverman \(1986\)](#), [Wand and Jones \(1994\)](#). Assumption (A4) holds for typical error distributions such as Gaussian, T, and Laplace distributions.

Proposition 1 formally establishes the asymptotic consistency of $\hat{f}_0^m(\cdot | \sigma)$ and $\hat{f}^m(\cdot | \sigma)$ as $m \rightarrow \infty$.

Proposition 1. *Consider Model (1)–(2) and suppose assumptions (A1)–(A4) hold. Then as $m, S(m), K(m) \rightarrow \infty$ and $\sigma \sim g_\sigma$, we have,*

$$\begin{aligned} E\|\hat{f}^m(\cdot | \sigma) - f(\cdot | \sigma)\|^2 &= E \int \{\hat{f}^m(x | \sigma) - f(x | \sigma)\}^2 dx \rightarrow 0 \text{ and} \\ E\|\hat{f}_0^m(\cdot | \sigma) - f_0^m(\cdot | \sigma)\|^2 &= E \int \{\hat{f}_0^m(x | \sigma) - f_0^m(x | \sigma)\}^2 dx \rightarrow 0, \end{aligned}$$

where the expectation is taken over (\mathbf{X}, σ) and σ .

While Proposition 1 does not place any restrictions on the rates at which $K(m)$ and $S(m) \rightarrow \infty$, the sizes of $K(m)$ and $S(m)$ do affect the quality of $\hat{f}_0^m(\cdot|\sigma)$ and $\hat{f}^m(\cdot|\sigma)$ for large m . To see that, first note that since $\hat{f}^m(\cdot|\sigma)$ is approximating $\hat{\varphi}^m(\cdot, \sigma)$, the order of $E\|\hat{f}^m(\cdot|\sigma) - f(\cdot|\sigma)\|^2$ is upper bounded by the order of $E\|\hat{\varphi}^m(\cdot, \sigma) - f(\cdot|\sigma)\|^2$. It was shown in Wand and Jones (1994) that when $h_x \asymp m^{-1/6}$ and $h_\sigma \asymp m^{-1/6}$, the optimal rate at which $E\|\hat{\varphi}^m(\cdot, \sigma) - f(\cdot|\sigma)\|^2 \rightarrow 0$ is $O(m^{-2/3})$. To achieve this rate in our context, suppose, for instance, that $\eta(\cdot)$ is the density of a standard Gaussian random variable. Then, it is sufficient for $S(m) \asymp m^{1/3}\sqrt{\log m}$. This is formally established in Remark 1 in the supplement. Moreover, on the appropriate choice of the number of basis functions $K(m)$ in this setting, Remark 2 (in Section B.2 of the supplement) shows that if $g_j(\cdot) = \sum_{k=1}^{\infty} w_{jk}q_k(\cdot)$ and $\mathbf{w}_j = \{w_{jk} : k = 1, 2, \dots, \}$ belong to the Sobolev ellipsoid $\Theta(\gamma, c)$ with order $\gamma > 0$ and radius $c < \infty$ for $j = 1, \dots, S(m)$, then $K(m) \asymp m^{1/(2\gamma)}(\log m)^{1/(4\gamma)}$. Thus, while larger $K(m)$, $S(m)$ will not improve the quality of $\hat{f}^m(\cdot|\sigma)$, smaller $K(m)$, $S(m)$ may result in a slower convergence rate of $E\|\hat{f}^m(\cdot|\sigma) - f(\cdot|\sigma)\|^2$ to 0. In Section 5.1 we provide recommendations on the practical choices of $S(m)$ and $K(m)$ that work well in our numerical experiments and real data analyses.

A consequence of Proposition 1 is Corollary 1 which establishes that the data-driven Clfdr statistic $\hat{T}_{i,m}$ in Definition 2 converges in probability to its oracle counterpart as $m \rightarrow \infty$.

corollary 1. *Under the conditions of Proposition 1 and uniformly in i , $\hat{T}_{i,m} \rightarrow T_i^{\text{OR}}$ in probability as $m \rightarrow \infty$.*

Next, we state the main theorem of this section which is related to the asymptotic performance of HAMT as $m \rightarrow \infty$.

Theorem 2. *Consider Model (1)–(2). Under assumptions (A1) – (A4) and as $m \rightarrow \infty$, we have (i) the $m\text{FDR}$ and FDR of $\delta^{\text{HAMT}}(\hat{t}_m)$ are controlled at level $\alpha + o(1)$, and (ii) $\text{ETP}\{\delta^{\text{HAMT}}(\hat{t}_m)\}/\text{ETP}\{\delta^{\text{OR}}(t^*)\} = 1 + o(1)$.*

Together with Theorem 1, Theorem 2 establishes that the proposed HAMT procedure is asymptotically valid for FDR control and attains the performance of the oracle procedure as $m \rightarrow \infty$.

5 Numerical experiments

5.1 Recommended choices of \mathcal{T} , S , K and $q(\sigma_i)$

While Section 4 provides guidance on the asymptotic choices of the grid size $S(m)$ and the number of basis functions $K(m)$, in our implementation we fix $S = 50$ and $K = 10$, which work well in all of our numerical and real data examples. For the grid support \mathcal{T} , HAMT uses S equispaced

points in $[X_{(1)}, X_{(m)}]$ where $X_{(1)} = \min\{X_1, \dots, X_m\}$ and $X_{(m)} = \max\{X_1, \dots, X_m\}$. Next, for the basis functions $\mathbf{q}(\sigma_i) = (q_{1,i}, \dots, q_{K,i})$ in Equation (8) we use the cosine basis $q_{k,i} = 0.5\{1 + \cos(k\sigma_i)\}$. Since we assume the dependence of $g_{\mu}(\cdot|\sigma)$ on σ is continuous, the number of cosine basis functions used in Equation (8) can be interpreted as the user’s belief about the smoothness of such dependence. Lastly, the pilot estimator $\hat{\varphi}_{(-i)}^m(x_i, \sigma_i)$ in Equation (12) is borrowed from [Fu et al. \(2022\)](#) and depends on a pair of bandwidths $\mathbf{h} = (h_x, h_\sigma)$. We follow the author’s recommendation in choosing these bandwidths which rely on Silverman’s rule of thumb ([Silverman, 1986](#)). Additional details related to the implementation of HAMT are provided in Section C of the supplement. The R code for reproducing all numerical results in the paper is available at https://github.com/trambakbanerjee/HAMT_paper.

5.2 Experiments involving one-sided composite null hypotheses

In this section we assess the numerical performance of HAMT for one-sided composite null hypotheses. Specifically, we test $m = 10^4$ hypotheses of the form $H_{0i} : \mu_i \in \mathcal{A}$ vs $H_{1i} : \mu_i \notin \mathcal{A}$ where $\mathcal{A} = (-\infty, \mu_0]$. We consider eleven competing testing procedures of which four are p -value based methods and seven rely on an Lfdr estimate for ranking the hypotheses. The four p -value procedures are: **BH** - the Benjamini-Hochberg procedure from [Benjamini et al. \(2006\)](#) which is designed to overcome the conservativeness of the original [Benjamini and Hochberg \(1995\)](#) procedure by including a correction in size, **AdaPTGMM** - the procedure from [Chao and Fithian \(2021\)](#) that uses σ as an additional covariate, **CAMT** - the method from [Zhang and Chen \(2022\)](#) and **IHW** - the procedure from [Ignatiadis and Huber \(2021\)](#). Along with **AdaPTGMM**, both **CAMT** and **IHW** are designed to exploit the side information in σ for testing the m hypotheses. The remaining seven methods are the following Lfdr based procedures: **OR** - the oracle procedure from Equation (7), **DECONV** - this procedure ignores the dependence between μ_i and σ_i , uses the empirical Bayes deconvolution method from [Efron \(2016\)](#) to estimate T_i^{OR} and then relies on Definition 2 to estimate the threshold t^* , **NPMLE B** - this method is similar to HAMT where $g_j(\sigma_i) = \mathbf{w}_j^T \mathbf{q}(\sigma_i)$ but we estimate the \mathbf{w}_j ’s by solving Problem (9), **GS 1** - the testing procedure from [Gu and Shen \(2018\)](#) that is based on the standardized statistic $Z_i = (X_i - \mu_0)/\sigma_i$ and relies on the deconvolution estimate obtained from non-parametric maximum likelihood estimation to construct the Lfdr, **GS 2** - another procedure from [Gu and Shen \(2018\)](#) that allows for the possibility that in some applications, there might be a non-trivial probability mass at μ_0 which may lead to poor FDR control if not accounted for while estimating the marginal density of Z_i , **ASH** - the method from [Stephens \(2017\)](#) with $c = 0$ and **ASH 1** - the same method from [Stephens \(2017\)](#) but with $c = 1$. Section C of the supplement includes more details related to the implementation of **NPMLE B**, **ASH** and **ASH 1**.

The aforementioned procedures are evaluated on five different simulation settings with α fixed at 0.1. For each simulation setting, the data are generated from Model (1)-(2) with $\epsilon_i \stackrel{i.i.d.}{\sim} N(0, 1)$,

and the average false discovery proportion $\text{FDP}(\delta) = \sum_{i=1}^m \{(1 - \theta_i)\delta_i\} / \max(\sum_{i=1}^m \delta_i, 1)$ and the average proportion of true positives discovered $\text{PTP}(\delta) = \sum_{i=1}^m \theta_i \delta_i / \max(\sum_{i=1}^m \theta_i, 1)$ across 200 Monte-Carlo (MC) repetitions are reported.

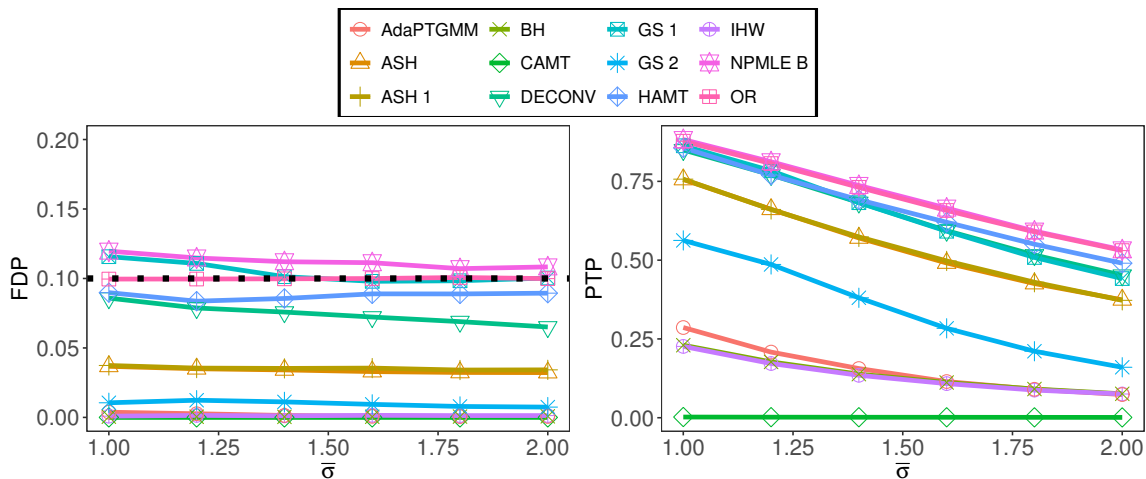


Figure 4: Setting 1 - $\sigma_i \stackrel{i.i.d.}{\sim} \text{Unif}(0.5, \bar{\sigma})$, $\mu_i = 0$ with probability 0.9 and $\mu_i \stackrel{i.i.d.}{\sim} N(3, 1)$ with probability 0.1. Here $\mathcal{A} = (-\infty, 2]$. For ASH and ASH 1, `mixcompdist = "normal"`.

In the first setting (μ_i, σ_i) are independent. We sample $\sigma_i \stackrel{i.i.d.}{\sim} \text{Unif}(0.5, \bar{\sigma})$ and let $\mu_i = 0$ with probability 0.9 and $\mu_i \stackrel{i.i.d.}{\sim} N(3, 1)$ with probability 0.1. We vary $\bar{\sigma} \in \{1, 1.2, 1.4, 1.6, 1.8, 2\}$ and take $\mu_0 = 2$. Figure 4 reports the average FDP and PTP for the competing procedures in this setting. We observe that the four p -value methods are the most conservative with CAMT exhibiting the least power. The procedure GS 2 closely follows the p -value methods in FDR control but exhibits substantially better power. The remaining methods have an overall similar performance in this setting although GS1 and NPMLE B marginally fail to control the FDR level at 10% for small values of $\bar{\sigma}$.

The second setting represents a scenario where μ_i and σ_i are correlated and have discrete distributions. Setting 2 is presented in Figure 5 where σ_i can take three values $\{0.5, 1, 2\}$ with equal probabilities. Conditional on σ_i , $\mu_i = 0$ with probability 0.9 or $\mu_i = \bar{\sigma}\sigma_i$ with probability 0.1. We set $\mu_0 = 2$ and find that all methods control the FDR level in Figure 5. Among the data-driven procedures, HAMT has the highest power and is closely followed by NPMLE B, GS 1 and ASH 1. DECONV, which completely ignores the dependence between μ_i and σ_i , exhibits a substantially lower power than HAMT in this setting.

For Setting 3, $\sigma_i \stackrel{i.i.d.}{\sim} \text{Unif}(0.5, \bar{\sigma})$ and conditional on σ_i , $\mu_i \stackrel{i.i.d.}{\sim} 0.9N(-\sigma_i, 0.5) + 0.1\delta_{(2\sigma_i^2)}$, where $\delta_{(a)}$ represents a point mass at a . Setting 3 is presented in Figure 6 where $\mu_0 = 1$. We find that GS 1 fails to control the FDR level at 10% while ASH and DECONV control the FDR at all values of $\bar{\sigma}$, except the first two where the latter exhibits an FDR value bigger than 0.2 at $\bar{\sigma} = 1$. HAMT effectively captures the dependence between μ_i and σ_i and is, by far, the best testing procedure in this setting along with NPMLE B.

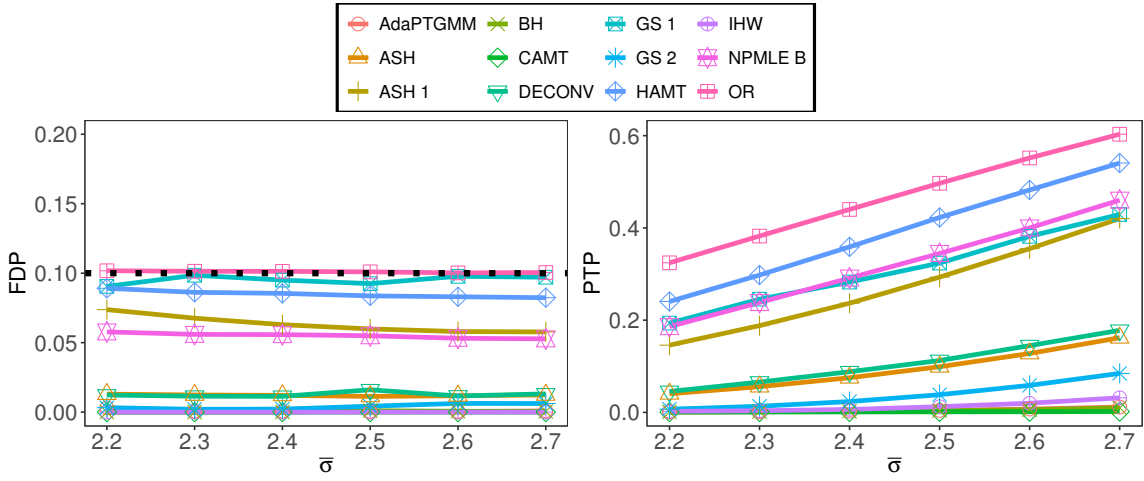


Figure 5: Setting 2 - $\sigma_i \stackrel{i.i.d.}{\sim} (1/3)I_{(0.5)} + (1/3)I_{(1)} + (1/3)I_{(2)}$ and conditional on $\sigma_i, \mu_i = 0$ with probability 0.9 or $\mu_i = \bar{\sigma}\sigma_i$ with probability 0.1. Here $\mathcal{A} = (-\infty, 2]$. For ASH and ASH 1, `mixcompdist = "+uniform"`.

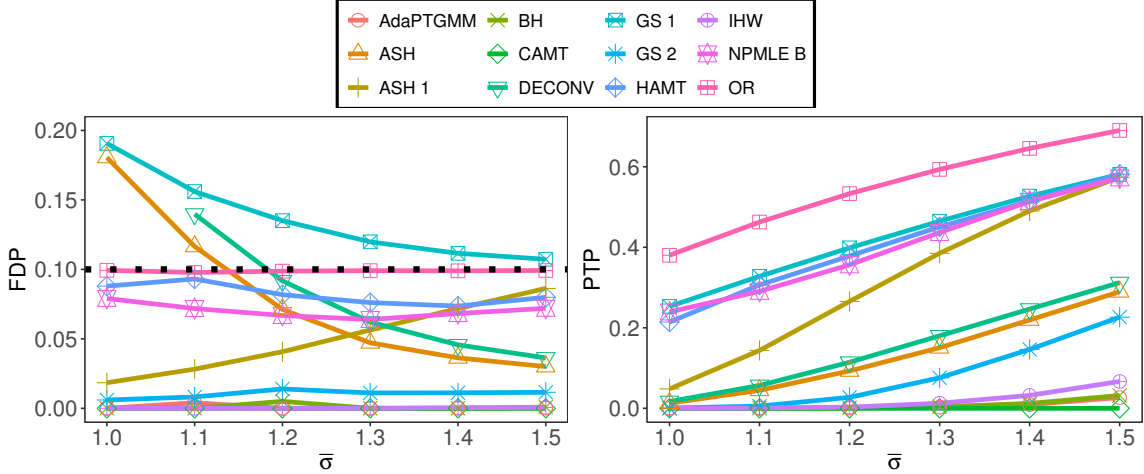


Figure 6: Setting 3: $\sigma_i \stackrel{i.i.d.}{\sim} \text{Unif}(0.5, \bar{\sigma})$ and conditional on $\sigma_i, \mu_i \stackrel{i.i.d.}{\sim} 0.9N(-\sigma_i, 0.5) + 0.1\delta_{(2\sigma_i^2)}$, where $\delta_{(a)}$ represents a point mass at a . Here $\mathcal{A} = (-\infty, 1]$. For ASH and ASH 1, `mixcompdist = "+uniform"`. At $\bar{\sigma} = 1$, DECONV exhibits an FDR bigger than 0.2.

The remaining two settings present scenarios where HAMT provides a substantial improvement over all competing methods, both in terms of FDR control and power. In the fourth setting, $\sigma_i \stackrel{i.i.d.}{\sim} 0.9\text{Unif}(0.5, 1) + 0.1\text{Unif}(1, u)$, $\mu_i = 0$, if $\sigma_i \leq 1$ and $2/\sigma_i$, otherwise. Thus, in this setting σ_i controls both the sparsity level of μ_i and the distribution of its non-zero effects. The performance of the competing methods is presented in Figure 7 where $\mu_0 = 1$. The oracle procedure (OR) in this setting perfectly classifies each μ_i as satisfying $\mu_i \leq \mu_0$ or $\mu_i > \mu_0$ simply by observing if $\sigma_i \leq 1$ or $\sigma_i > 1$ and $2/\sigma_i > \mu_0$. Thus in Figure 7, OR has FDP equal to 0 and PTP equal to 1 for all $\bar{\sigma}$. While, all other methods control the FDR at 10%, HAMT exhibits a substantially higher power in this setting for all values of $\bar{\sigma}$.

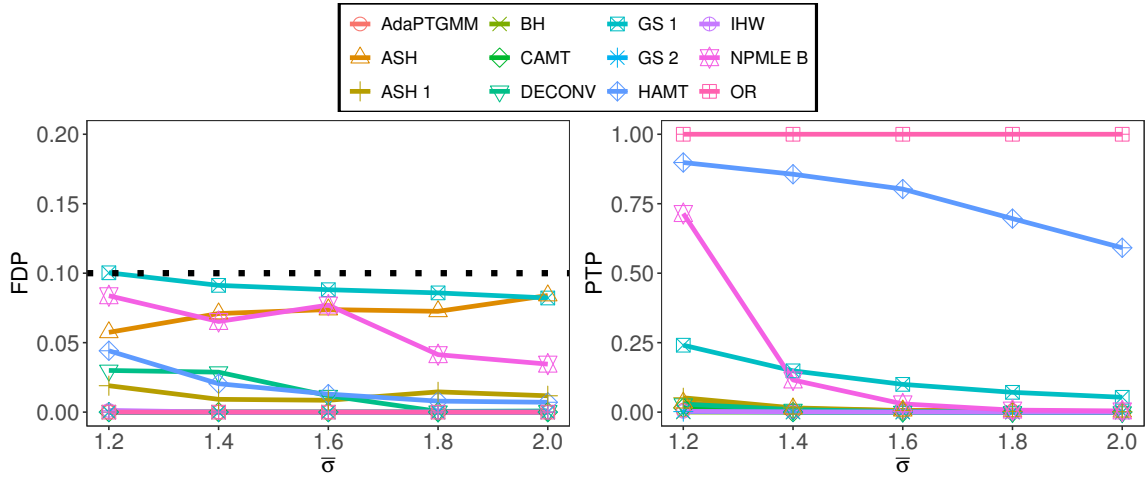


Figure 7: Setting 4 - $\sigma_i \stackrel{i.i.d.}{\sim} 0.9\text{Unif}(0.5, 1) + 0.1\text{Unif}(1, \bar{\sigma})$ and $\mu_i = 0$, if $\sigma_i \leq 1$ and $2/\sigma_i$, otherwise. Here $\mathcal{A} = (-\infty, 1]$. For ASH and ASH 1, `mixcompdist = "halfuniform"`.

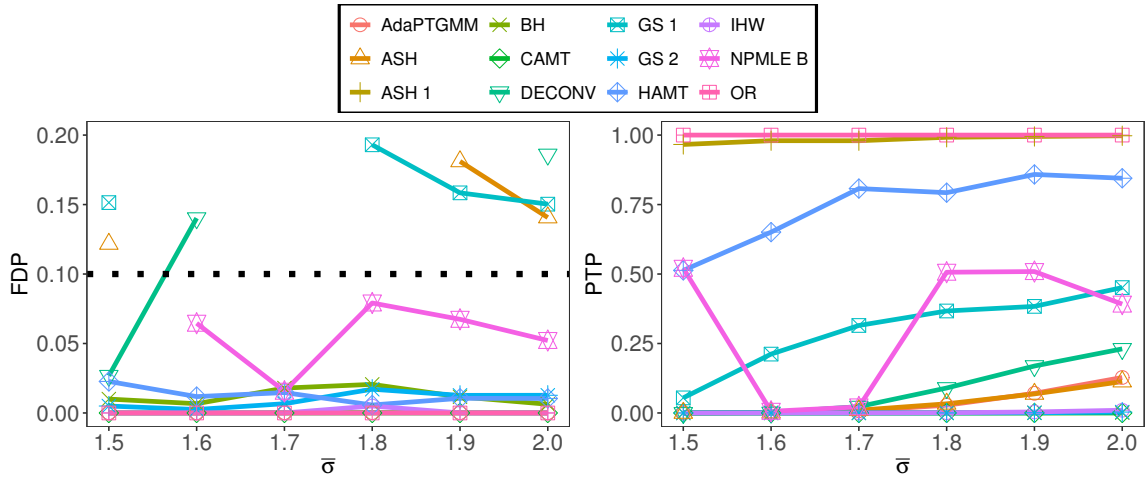


Figure 8: Setting 5 - $\sigma_i \stackrel{i.i.d.}{\sim} \text{Unif}(0.25, \bar{\sigma})$ and conditional on σ_i , $\mu_i = 3\sigma_i$. Here $\mathcal{A} = (-\infty, 4]$. For ASH and ASH 1, `mixcompdist = "+uniform"`.

In the fifth setting, we allow μ_i and σ_i to be perfectly correlated. Specifically, $\sigma_i \stackrel{i.i.d.}{\sim} \text{Unif}(0.25, u)$, $\mu_i = 3\sigma_i$ and $\mu_0 = 4$. In Figure 8, several methods fail to control the FDR at 10% and for some values of $\bar{\sigma}$, they exhibit FDP values bigger than 0.2. The left panel of Figure 8 excludes those values of $\bar{\sigma}$ for such methods. NPMLE B, in particular, exhibits a relatively high MC error in its FDP distribution for the first three values of $\bar{\sigma}$ and so for each $\bar{\sigma}$ we report its median FDP and PTP across the 200 MC repetitions. The oracle procedure in this setting simply observes if $3\sigma_i > \mu_0$ for rejecting the null hypothesis and its data-driven counterpart, HAMT, has the highest power among all other testing procedures considered here.

Overall, the aforementioned simulation experiments reveal that the p -value procedures considered here are considerably more conservative than their Lfdr counterparts, while the Lfdr methods that ignore the dependence between μ_i and σ_i may even fail to control the FDR at the desired level.

In contrast, HAMT, which relies on an improved deconvolution estimator for constructing the Clfdr statistic, provides an alternative multiple testing procedure that is often more powerful than competing methods, such as ASH, ASH 1, at the same FDR level. In Section D of the supplement we present more simulation studies to assess the numerical performance of HAMT in settings involving (i) two-sided composite nulls, (ii) non-Gaussian likelihoods and (iii) unknown σ and Section E includes an additional discussion on the empirical performances of HAMT, NPMLE B and ASH reported here. A real data application is presented in Section F.

6 Discussion

Heteroskedasticity presents a challenging setting for designing valid and powerful multiple testing procedures. For testing composite null hypotheses, we show that the conventional practice of standardizing heteroskedastic test statistics may severely affect the power of the underlying testing procedure. Additionally, when the inferential parameter of interest is correlated with the variance of the test statistic, existing methods that ignore this dependence may fail to control the type I error at the desired level. In this article, we propose HAMT which is a general framework for simultaneously testing composite null hypotheses under heteroskedasticity. HAMT avoids data reduction by standardization and directly incorporates the side information from the variances into the testing procedure. It ranks the hypotheses using Clfdr statistics that rely on a carefully designed deconvolution estimator that captures the dependence between μ_i and σ_i . Our asymptotic analysis establishes that HAMT is valid and optimal for FDR control. In the numerical experiments, HAMT demonstrates substantial power gain against competing methods, particularly in the settings where μ_i and σ_i are correlated.

We conclude this article with a brief discussion on the limitations of HAMT and potential areas for future research. *First*, it is of tremendous interest to develop powerful and valid multiple testing procedures that can pool side information from several covariate sequences (see for example [Chao and Fithian \(2021\)](#), [Zhang and Chen \(2022\)](#) and the references therein). In the context of testing composite null hypotheses, HAMT can handle just one such sequence given by the σ_i 's and it is desirable to develop methods that can incorporate other side information, such as a grouping structure, in addition to heteroskedasticity. Given a p -dimensional side information vector $\mathbf{Y}_i \in \mathbb{R}^p$ for hypothesis i , the hierarchical Model (1)–(2) may be modified as follows:

$$X_i = \mu_i + \sigma_i \epsilon_i, \quad \epsilon_i \stackrel{i.i.d.}{\sim} \eta(\cdot), \quad \mu_i \mid (\sigma_i, \mathbf{y}_i) \stackrel{ind.}{\sim} g_\mu(\cdot \mid \sigma_i, \mathbf{y}_i), \quad (\sigma_i, \mathbf{Y}_i) \stackrel{i.i.d.}{\sim} g_{\sigma, \mathbf{y}}(\cdot),$$

where $g_\mu(\cdot \mid \sigma_i, \mathbf{y}_i)$ and $g_{\sigma, \mathbf{y}}(\cdot)$ are, respectively, the probability density functions of the unknown mixing distributions of μ given (σ_i, \mathbf{y}_i) and (σ_i, \mathbf{Y}_i) . A major methodological challenge towards extending HAMT in this direction will be to develop a reliable deconvolution estimator of $g_\mu(\cdot \mid$

σ_i, \mathbf{y}_i) for constructing the Clfdr statistic. This is especially important because for $p \geq 3$, the bivariate kernel density estimator of Fu et al. (2022) may no longer provide a stable pilot estimate of the marginal density $f(x_i|\sigma_i, \mathbf{y}_i)$. *Second*, our testing framework assumes that σ_i are known and while numerical experiments in Section D.3 of the supplement show that using sample variances HAMT still controls the FDR level, it would be of great interest to further study the impact of estimating σ_i on the power and validity of multiple testing procedures. In particular, the bandwidths (h_{x_j}, h_σ) used in the pilot density estimator $\hat{\varphi}^m(\cdot, \sigma_i)$ depend on σ_i and play an important role in establishing the consistency of $\hat{f}^m(\cdot|\sigma_i)$. When σ_i are unknown, a natural alternative is to simply use the sample variance to determine the bandwidths but the corresponding density estimator may be highly unstable at the tails under such a choice, especially when the number of replicates available for each hypothesis is relatively small. Another strategy is to use variance estimates from empirical Bayes methods, such as those proposed in Banerjee et al. (2023), Lu and Stephens (2019), however much research is needed to understand the theoretical properties of the resulting pilot density estimator. *Finally*, while HAMT is guaranteed to provide asymptotic FDR control, it will be of interest to modify HAMT so that it can provably control FDR in finite samples, particularly when additional covariate sequences \mathbf{Y}_i are available. Promising ideas in this direction include the construction of knockoffs or mirror sequences as done in Barber and Candès (2015), Leung and Sun (2021), or the use of conformal techniques as pursued in Bates et al. (2021), Guan and Tibshirani (2022).

Acknowledgement

B. Gang’s research was supported by National Natural Science Foundation of China grant 12201123. T. Banerjee was partially supported by the University of Kansas General Research Fund allocation #2302216.

Supplement to “Large-Scale Multiple Testing of Composite Null Hypotheses Under Heteroskedasticity”

This supplement is organized as follows: the calculations for Examples 1 and 2 in Section 2.3 are presented in Section A. The proofs of all other theoretical results in the paper are presented in Section B. Further details related to the implementation of HAMT, NPMLE B, ASH and ASH 1 are available in Section C and additional numerical experiments are provided in Section D. Section E includes more discussion on the empirical performances of the various methods considered in this article. A real data application is discussed in Section F.

A Calculations for Section 2.3

Example 1 - we first consider the oracle rule based on the standardized statistic $Z_i = X_i/\sigma_i$. The marginal density function of Z_i under the alternative is

$$f_a(z) = \int_{0.5}^4 \frac{1}{3.5\sqrt{2\pi}} \exp\left\{-\frac{(z - \sqrt{\sigma})^2}{2}\right\} d\sigma,$$

and the distribution function of Z_i under the alternative is

$$F_a(t) = P(Z < t) = \int_{-\infty}^t f_a(z) dz = \int_{0.5}^4 \frac{1}{3.5} \Phi(t - \sqrt{\sigma}) d\sigma,$$

where Φ is the distribution function of $N(0, 1)$. Then, using the definition of mFDR, it is not hard to see that the oracle procedure based on $\mathbf{Z} = (Z_1, \dots, Z_m)$ is of the form $\delta^{\text{ZOR}}(t_z) = \{I(Z_i > t_z) : 1 \leq i \leq m\}$ where,

$$t_z = \inf \left\{ t > 0 : \frac{0.9\{1 - \Phi(t)\}}{0.9\{1 - \Phi(t)\} + 0.1\{1 - F_a(t)\}} \leq \alpha \right\}.$$

When $\alpha = 0.1$, the above display can be solved numerically for t to get $t_z = 3.273$ and the power of $\delta^{\text{ZOR}}(t_z)$ is $1 - F_a(t_z) = 0.0432$.

Next, consider the oracle rule $\delta^{\text{OR}}(t^*)$. Recall that $\delta^{\text{OR}}(t^*)$ is of the form $\{I(T_i^{\text{OR}} < t^*) : 1 \leq i \leq m\}$. Using the definition of Clfdr in Equation (5), it is straightforward to show that this rule is equivalent to $\{I(Z_i > \lambda_\sigma(t^*)) : 1 \leq i \leq m\}$, where

$$\lambda_\sigma(t) = \frac{-\log\left(\frac{0.1t}{0.9(1-t)}\right) + \frac{1}{2}\sigma}{\sqrt{\sigma}},$$

and

$$t^* = \sup \left[t \in [0, 1] : \frac{0.9 \int (1 - \Phi\{\lambda_\sigma(t)\}) d\sigma}{0.9 \int (1 - \Phi\{\lambda_\sigma(t)\}) d\sigma + 0.1 \int (1 - \Phi\{\lambda_\sigma(t) - \sqrt{\sigma}\}) d\sigma} \leq \alpha \right].$$

When $\alpha = 0.1$, the above display can be solved numerically to get $t^* = 0.177$ and the power of $\delta^{\text{OR}}(t^*)$ is given by $(1/3.5) \int (1 - \Phi\{\lambda_\sigma(t^*) - \sqrt{\sigma}\}) d\sigma = 0.0611$. ■

Example 2 - for the oracle rule based on Z_i , the calculations from Example 1 give $t_z = 4.124$ at $\alpha = 0.1$ and the power of $\delta^{\text{ZOR}}(t_z) = 0.0015$. Now, consider the oracle rule based on T_i^{OR} . Note that $T_i^{\text{OR}} = 1$ if $\sigma_i \leq 3.65$ and 0 otherwise. So, T_i^{OR} perfectly classifies each case as being null or non-null based on (X_i, σ_i) . Consequently, the power of this procedure is 1 while the FDR is 0.

B Proofs

B.1 Proof of Theorem 1

We divide the proof into two parts. In Part (a), we establish two properties of the testing rule $\delta^{\text{OR}}(t) = \{I(T_i^{\text{OR}} < t) : 1 \leq i \leq m\}$ for an arbitrary $0 < t < 1$. In Part (b) we show that the oracle rule $\delta^{\text{OR}}(t^*)$ attains the mFDR level exactly and is optimal amongst all mFDR procedures at level α .

Part (a). Denote $\alpha(t)$ the mFDR level of $\delta^{\text{OR}}(t)$. We shall show that (i) $\alpha(t) < t$ for all $0 < t < 1$ and that (ii) $\alpha(t)$ is nondecreasing in t .

First, note that $E \left\{ \sum_{i=1}^m (1 - \theta_i) \delta_i^{\text{OR}}(t) \right\} = E_{\mathbf{X}, \sigma} \left\{ \sum_{i=1}^m T_i^{\text{OR}} \delta_i^{\text{OR}}(t) \right\}$. Then, according to the definition of $\alpha(t)$, we have

$$E_{\mathbf{X}, \sigma} \left\{ \sum_{i=1}^m \{T_i^{\text{OR}} - \alpha(t)\} I(T_i^{\text{OR}} \leq t) \right\} = 0. \quad (14)$$

We claim that $\alpha(t) < t$. Otherwise if $\alpha(t) \geq t$, then we must have $T_i^{\text{OR}} < t \leq \alpha(t)$. It follows that the LHS must be negative, contradicting (14).

Next we show (ii), i.e, $\alpha(t)$ is nondecreasing in t . Let $\alpha(t_j) = \alpha_j$. We claim that if $t_1 < t_2$, then we must have $\alpha_1 \leq \alpha_2$. We argue by contradiction. Suppose that $t_1 < t_2$ but $\alpha_1 > \alpha_2$. Then

$$\begin{aligned} (T_i^{\text{OR}} - \alpha_2) I(T_i^{\text{OR}} < t_2) &= (T_i^{\text{OR}} - \alpha_1) I(T_i^{\text{OR}} < t_1) + (\alpha_1 - \alpha_2) I(T_i^{\text{OR}} < t_1) \\ &\quad + (T_i^{\text{OR}} - \alpha_2) I(t_1 \leq T_i^{\text{OR}} < t_2) \\ &\geq (T_i^{\text{OR}} - \alpha_1) I(T_i^{\text{OR}} < t_1) + (\alpha_1 - \alpha_2) I(T_i^{\text{OR}} < t_1) \\ &\quad + (T_i^{\text{OR}} - \alpha_1) I(t_1 \leq T_i^{\text{OR}} < t_2). \end{aligned}$$

It follows that $E \left\{ \sum_{i=1}^m (T_i^{\text{OR}} - \alpha_2) I(T_i^{\text{OR}} < t_2) \right\} > 0$ since $E \left\{ \sum_{i=1}^m (T_i^{\text{OR}} - \alpha_1) I(T_i^{\text{OR}} < t_1) \right\} = 0$ according to (14), $\alpha_1 > \alpha_2$ and $T_i^{\text{OR}} \geq t_1 > \alpha_1$. However, this contradicts Equation (14) and so we must have $\alpha_1 < \alpha_2$.

Part (b). Let $\bar{\alpha} = \alpha(1)$. In Part (a), we showed that $\alpha(t)$ is non-decreasing in t . It follows that for all $\alpha < \bar{\alpha}$, there exists a t^* such that $t^* = \sup\{t : \alpha(t^*) = \alpha\}$. By definition, t^* is the oracle threshold. Consider an arbitrary decision rule $\delta = (\delta_1, \dots, \delta_m) \in \{0, 1\}^m$ such that $\text{mFDR}(\delta) \leq \alpha$. We have $\mathbb{E} \left\{ \sum_{i=1}^m (T_i^{\text{OR}} - \alpha) \delta_i^{\text{OR}}(t^*) \right\} = 0$ and $E \left\{ \sum_{i=1}^m (T_i^{\text{OR}} - \alpha) \delta_i \right\} \leq 0$. Hence

$$E \left[\sum_{i=1}^m \{ \delta_i^{\text{OR}}(t^*) - \delta_i \} (T_i^{\text{OR}} - \alpha) \right] \geq 0. \quad (15)$$

Consider the transformation $h(x) = (x - \alpha)/(1 - x)$. Note that since $h(x)$ is monotone, we can rewrite $\delta_i^{\text{OR}}(t^*) = I \left[\{ (T_i^{\text{OR}} - \alpha)/(1 - T_i^{\text{OR}}) \} < \lambda \right]$, where $\lambda = (t^* - \alpha)/(1 - t^*)$. In Part (a) we have shown that $\alpha < t^* < 1$, which implies that $\lambda > 0$. Hence

$$E \left[\sum_{i=1}^m \{ \delta_i^{\text{OR}}(t^*) - \delta_i \} \{ (T_i^{\text{OR}} - \alpha) - \lambda(1 - T_i^{\text{OR}}) \} \right] \leq 0. \quad (16)$$

To see this, consider the terms where $\delta_i^{\text{OR}}(t^*) - \delta_i \neq 0$. Then we have two cases: (i) $\delta_i^{\text{OR}}(t^*) > \delta_i$ or (ii) $\delta_i^{\text{OR}}(t^*) < \delta_i$. In case (i), $\delta_i^{\text{OR}}(t^*) = 1$, implying that $\{ (T_i^{\text{OR}} - \alpha)/(1 - T_i^{\text{OR}}) \} < \lambda$. In case (ii), $\delta_i^{\text{OR}}(t^*) = 0$, implying that $\{ (T_i^{\text{OR}} - \alpha)/(1 - T_i^{\text{OR}}) \} \geq \lambda$. Therefore, we always have $\{ \delta_i^{\text{OR}}(t^*) - \delta_i \} \{ (T_i^{\text{OR}} - \alpha) - \lambda(1 - T_i^{\text{OR}}) \} \leq 0$. Summing over the m terms and taking the expectation yield (16).

Now, combining (15) and (16), we obtain

$$0 \leq E \left[\sum_{i=1}^m \{ \delta_i^{\text{OR}}(t^*) - \delta_i \} (T_i^{\text{OR}} - \alpha) \right] \leq \lambda E \left[\sum_{i=1}^m \{ \delta_i^{\text{OR}}(t^*) - \delta_i \} (T_i^{\text{OR}} - \alpha) \right].$$

Since $\lambda > 0$, it follows that $E \left[\sum_{i=1}^m \{ \delta_i^{\text{OR}}(t^*) - \delta_i \} (T_i^{\text{OR}} - \alpha) \right] > 0$. Finally, we apply the definition of ETP to conclude that $\text{ETP}\{\delta^{\text{OR}}(t^*)\} \geq \text{ETP}(\delta)$ for all $\delta \in \{0, 1\}^m$ such that $\text{mFDR}(\delta) \leq \alpha$. ■

B.2 Proof of Proposition 1

We first state two useful lemmata where $\delta_u(\cdot)$ denotes a point mass at u

Lemma 1. Let $\eta_\sigma(\cdot)$ be the density function of $\sigma\gamma$ where $\gamma \sim \eta(\cdot)$ and suppose assumption (A4) holds. For any g with support $\text{supp}(g) \subset [-M, M]$, and any $\epsilon > 0$, $\tau > 0$, with S large enough (depending on M, ϵ, τ only), there exists $g' \in \{ \sum_{j=1}^S \theta_j \delta_{u_j}(\cdot) \mid \sum_{j=1}^S \theta_j = 1, \theta_j \geq 0 \forall j \}$ with $u_j = -M + 2M(j-1)/(S-1)$ such that $|g * \eta_\tau(x) - g' * \eta_\tau(x)|^2 < \epsilon$ for all x .

Lemma 2. Suppose $\hat{f}(x|\sigma) = \hat{g} * \eta_\sigma(x)$ and $f(x|\sigma) = g * \eta_\sigma(x)$, where η_σ is as defined in Lemma 1 and satisfies the assumptions therein. Then $E_{\mathbf{x},\sigma} E_{x,\sigma} |\hat{f}(x|\sigma) - f(x|\sigma)|^2 \rightarrow 0$ implies $E_\tau E_{\mathbf{x},\sigma} \|\hat{g} * \eta_\tau - g * \eta_\tau\|_2^2 \rightarrow 0$. Here $E_{\mathbf{x},\sigma}$ is taken with respect to the data used to construct \hat{f} and \hat{g} , $E_{x,\sigma}$ is taken with respect to the input for \hat{f} and f , E_τ is taken with respect to $\tau \sim g_\sigma(\cdot)$.

Let $\tilde{f}(x_i|\sigma_i)$ be any bounded estimator of $f(x_i|\sigma_i)$. We begin by establishing

$$\frac{1}{m} \sum_{i=1}^m \{\tilde{f}(x_i|\sigma_i) - \hat{\varphi}_{(-i)}^m(x_i, \sigma_i)\}^2 \xrightarrow{p} \frac{1}{m} \sum_{i=1}^m \{\tilde{f}(x_i|\sigma_i) - f(x_i|\sigma_i)\}^2. \quad (17)$$

Note that

$$\begin{aligned} & \frac{1}{m} \sum_{i=1}^m \{\tilde{f}(x_i|\sigma_i) - f(x_i|\sigma_i)\}^2 \\ &= \frac{1}{m} \sum_{i=1}^m \{\tilde{f}(x_i|\sigma_i) - \hat{\varphi}_{(-i)}^m(x_i, \sigma_i) + \hat{\varphi}_{(-i)}^m(x_i, \sigma_i) - f(x_i|\sigma_i)\}^2 \\ &= \frac{1}{m} \sum_{i=1}^m \{\tilde{f}(x_i|\sigma_i) - \hat{\varphi}_{(-i)}^m(x_i, \sigma_i)\}^2 + \frac{2}{m} \sum_{i=1}^m \{\tilde{f}(x_i|\sigma_i) - \hat{\varphi}_{(-i)}^m(x_i, \sigma_i)\} \{\hat{\varphi}_{(-i)}^m(x_i, \sigma_i) - f(x_i|\sigma_i)\} \\ &+ \frac{1}{m} \sum_{i=1}^m \{\hat{\varphi}_{(-i)}^m(x_i, \sigma_i) - f(x_i|\sigma_i)\}^2 \end{aligned}$$

Hence, to prove Equation (17), we only need to establish

$$\frac{2}{m} \sum_{i=1}^m \{\tilde{f}(x_i|\sigma_i) - \hat{\varphi}_{(-i)}^m(x_i, \sigma_i)\} \{\hat{\varphi}_{(-i)}^m(x_i, \sigma_i) - f(x_i|\sigma_i)\} \xrightarrow{p} 0, \quad (18)$$

and

$$\frac{1}{m} \sum_{i=1}^m \{\hat{\varphi}_{(-i)}^m(x_i, \sigma_i) - f(x_i|\sigma_i)\}^2 \xrightarrow{p} 0. \quad (19)$$

Since by Assumption (A2) $\text{supp}(g_\sigma) \in [M_1, M_2]$ for some fixed $M_1 > 0, M_2 < \infty$, $f(x_i|\sigma_i) = \int g_\mu(\mu) \phi_\sigma(x_i - \mu) d\mu$ is bounded by some fixed constant $C > 0$. By capping \tilde{f} and $\hat{\varphi}_{(-i)}^m$ at C we assume, without loss of generality, that $|\tilde{f}(x_i|\sigma_i) - \hat{\varphi}_{(-i)}^m(x_i, \sigma_i)| \leq C$. Hence, Equation (18) is implied by

$$\frac{1}{m} \sum_{i=1}^m |\hat{\varphi}_{(-i)}^m(x_i, \sigma_i) - f(x_i|\sigma_i)| \xrightarrow{p} 0. \quad (20)$$

To prove equations (17) and (20) we borrow relevant results from the theory of kernel regression. Recall that for the following regression model

$$Y_i = m(\sigma_i) + \epsilon_i,$$

the Nadaraya-Watson kernel estimator, upon observing $\{(\sigma_i, Y_i)\}_{i=1}^m$, is defined as

$$\hat{m}(\sigma) = \sum_{j=1}^m \frac{\phi_{h_\sigma}(\sigma - \sigma_j)}{\sum_{k=1}^m \phi_{h_\sigma}(\sigma - \sigma_k)} Y_j. \quad (21)$$

It is well known that (Theorem 5.44 in Wasserman (2006)) the estimator in Equation (21) satisfies

$$E\{\hat{m}(\sigma) - m(\sigma)\} \asymp h_\sigma^2 \left(m''(\sigma) + 2 \frac{m'(\sigma)g'_\sigma(\sigma)}{g_\sigma(\sigma)} \right), \quad (22)$$

and

$$\text{Var}\{\hat{m}(\sigma)\} \asymp \frac{\gamma^2}{mh_\sigma} \{g_\sigma(\sigma)\}^{-1},$$

where γ^2 is an upper bound on the variance of ϵ_i . To use this result, for a given (x, σ) we simply take

$$m(\sigma_j) = E\{\phi_{h_x\sigma_j}(x - x_j)\}, \quad \text{and} \quad \epsilon_i = \phi_{h_x\sigma_j}(x - x_j) - E\{\phi_{h_x\sigma_j}(x - x_j)\},$$

where the expectation above is taken with respect to x_j under the conditional density function $f(x|\sigma_j) := \int \eta_{\sigma_j}(x - \mu)g_\mu(\mu|\sigma_j)d\mu$ and η_{σ_j} is the density function of $\sigma_j\epsilon_j$. Note that $m(\sigma_j)$ can be viewed as the density function of $\mu + \sigma_j\epsilon'_1 + h_x\sigma_j\epsilon'_2$ evaluated at x , where $\mu \sim g_\mu(\cdot|\sigma_j)$, $\epsilon'_1 \sim \eta(\cdot)$ and $\epsilon'_2 \sim N(0, 1)$ and ϵ'_1, ϵ'_2 are independent. Since by Assumption (A1) $|\frac{\partial}{\partial\sigma}g_\mu(\mu|\sigma)|$ and $|\frac{\partial^2}{\partial\sigma^2}g_\mu(\mu|\sigma)|$ are bounded for all μ , and $\eta(\cdot)$ is smooth by Assumption (A4), some elementary calculation shows $|m'(\sigma)| < C'$ and $|m''(\sigma)| < C''$ for some constants C' and C'' . Furthermore, by Assumption (A2) we have $|g'_\sigma(\sigma)| \leq C_3$ and $g_\sigma(\sigma) > C_1 > 0$ on $\text{supp}(g_\sigma)$. So the RHS of Equation (22) has order h_σ^2 .

Next, observe that the density function of $\sigma_j\epsilon'_1$ evaluated at x is $\eta_{\sigma_j}(x)$ and the density function of $\sigma_j\epsilon'_1 + h_x\sigma_j\epsilon'_2$ evaluated at x is $\int \eta_{\sigma_j}(x - \epsilon)\phi_{h_x\sigma_j}(\epsilon)dx$. Some elementary calculation shows (page 20 of Wand and Jones (1994))

$$\left| \int \eta_{\sigma_j}(x - \epsilon)\phi_{h_x\sigma_j}(\epsilon)dx - \eta(x) \right| \asymp h_x^2.$$

Hence, $\frac{1}{m} \sum_{i=1}^m |\hat{\varphi}_{(-i)}^m(x_i, \sigma_i) - f(x_i|\sigma_i)| = O_p(h_x^2 + h_\sigma^2)$. This establishes Equation (20). Using standard result from density estimation theory (page 21 of Wand and Jones (1994)) we see that variance of ϵ_i is of order h_x^{-1} . Hence, we also have

$$\frac{1}{m} \sum_{i=1}^m \{\hat{\varphi}_{(-i)}^m(x_i, \sigma_i) - f(x_i|\sigma_i)\}^2 = O_p \left(h_x^4 + h_\sigma^4 + \frac{1}{mh_x h_\sigma} \right).$$

By Assumption (A3) this establishes Equation (19) and, hence, Equation (17) follows.

Next, for any $\epsilon > 0$, since $\text{supp}\{g_\mu(\cdot|\sigma)\} \subset [-M, M]$ and $g_\mu(\cdot|\sigma)$ is continuous in σ , by Lemma 1 there exists continuous functions $g_j, j = 1, \dots, S$ such that $g'_\mu(\cdot|\sigma) = \sum_{j=1}^S g_j(\sigma)\delta_{u_j}(\cdot)$ and

$|g'_\mu(\cdot|\sigma) * \eta_\tau(x) - g_\mu(\cdot|\sigma) * \eta_\tau(x)|^2 < \epsilon$ for all x .

Let $\{q_k\}_{k=1}^\infty$ be an orthonormal basis for $L^2[M_1, M_2]$. Since g_j 's are bounded and continuous they all belongs to $L^2[M_1, M_2]$, hence they can be written as $g_j(\sigma) = \sum_{k=1}^\infty w_{jk}q_k(\sigma)$. For each g_j there exists N_j such that we can find \tilde{w}_{jk} with $\|g_j(\cdot) - \sum_{k=1}^{N_j} \tilde{w}_{jk}q_k(\cdot)\|_2^2 < \epsilon/S$. Take $K = \max_j N_j$. Then, there exists $\tilde{w}_{jk}, j = 1, \dots, S, k = 1, \dots, K$, such that $\|g_j(\cdot) - \sum_{k=1}^K \tilde{w}_{jk}q_k(\cdot)\|_2^2 < \epsilon/S$ for all j . Write $\tilde{g}_j(\cdot) = \sum_{k=1}^K \tilde{w}_{jk}q_k(\cdot)$. Let $\tilde{g}_\mu(\cdot|\sigma) = \sum_{j=1}^K \tilde{g}_j(\sigma)\delta_{u_j}(\cdot)$. Then for every $\sigma > 0$ and any fixed $\tau > 0$ we have

$$\|g'_\mu(\cdot|\sigma) * \eta_\tau - \tilde{g}_\mu(\cdot|\sigma) * \eta_\tau\|_2^2 = \left\| \sum_{j=1}^S (\tilde{g}_j(\sigma) - g_j(\sigma))\eta_\tau(\cdot - u_j) \right\|_2^2 = O(\epsilon).$$

Hence, in the feasible region, it is possible to find \tilde{f} such that

$$\frac{1}{m} \sum_{i=1}^m \{\tilde{f}(x_i|\sigma_i) - f(x_i|\sigma_i)\}^2 \leq \epsilon.$$

By Equation (17) we also have with high probability $\frac{1}{m} \sum_{i=1}^m \{\tilde{f}(x_i|\sigma_i) - \hat{\varphi}_{(-i)}^m(x_i, \sigma_i)\}^2 \rightarrow 0$. Hence, with high probability it is possible to find \tilde{f} in the feasible region such that $\frac{1}{m} \sum_{i=1}^m \{\tilde{f}(x_i|\sigma_i) - \hat{\varphi}_{(-i)}^m(x_i, \sigma_i)\}^2 \rightarrow 0$. By definition,

$$\hat{f}^m \in \arg \min_{\tilde{f}} \sum_{i=1}^m \left\{ \hat{\varphi}_{(-i)}^m(x_i, \sigma_i) - \tilde{f}(x_i | \sigma_i) \right\}^2.$$

Thus, we necessarily have $\frac{1}{m} \sum_{i=1}^m \{\hat{f}^m(x_i|\sigma_i) - \hat{\varphi}_{(-i)}^m(x_i, \sigma_i)\}^2 \xrightarrow{P} 0$ and by Equation (17) $\frac{1}{m} \sum_{i=1}^m \{\hat{f}^m(x_i|\sigma_i) - f(x_i|\sigma_i)\}^2 \xrightarrow{P} 0$. The proposition then follows directly from Lemma 2. ■

Remark 1. (Grid Size) Note that

$$\frac{1}{m} \sum_{i=1}^m \{\hat{f}^m(x_i|\sigma_i) - f(x_i|\sigma_i)\}^2 = O(E\|\hat{f}^m - f\|_2^2) = O\{(mh_x h_\sigma)^{-1} + h_x^4 + h_\sigma^4\}.$$

The optimal rate of $(mh_x h_\sigma)^{-1} + h_x^4 + h_\sigma^4$ is $m^{-2/3}$ and is achieved when $h_x \asymp h_\sigma \asymp m^{-1/6}$. Hence, when choosing the grid size we only need

$$\left| \frac{1}{m} \sum_{j=1}^m \eta_\tau(x - \mu_j) - \frac{1}{m} \sum_{j=1}^m \eta_\tau(x - u_{i(j)}) \right|^2 = O(m^{-2/3}),$$

where $u_{i(j)} \in \{u_1, \dots, u_S\}$ is such that $|u_{i(j)} - \mu_j| = O(1/S)$. Since $g_\mu(\cdot|\sigma)$ has bounded support, such $u_{i(j)}$ can always be found. Let $\epsilon = |u_{i(j)} - \mu_j|$, then when $\eta_\tau(\cdot)$ is the density function of $N(0, \tau^2)$

we have

$$|\eta_\tau(x - \mu_j) - \eta_\tau(x - u_{i(j)})|^2 = \frac{1}{2\pi\tau^2} e^{-\frac{x^2}{\tau^2}} \left| 1 - e^{\frac{2x\epsilon - \epsilon^2}{2\tau^2}} \right|^2. \quad (23)$$

We want the above to be of order $O(m^{-2/3})$ uniformly for any x . If x has order greater than $\sqrt{\log m}$ then the RHS of (23) is $O(m^{-2/3})$. When x has order less than $\sqrt{\log m}$, since $e^{-\frac{x^2}{\tau^2}} = O(1)$, we focus on $|1 - e^{\frac{2x\epsilon - \epsilon^2}{2\tau^2}}|^2$. By Taylor expansion,

$$\left| 1 - e^{\frac{2x\epsilon - \epsilon^2}{2\tau^2}} \right|^2 = O \left\{ \left(\frac{2x\epsilon - \epsilon^2}{2\tau^2} \right)^2 \right\}.$$

If $\epsilon = O(m^{-1/3}(\log m)^{-1/2})$ then the above is $O(m^{-2/3})$, and it follows that the grid size of $S(m) \asymp m^{1/3}(\log m)^{1/2}$ is sufficient. ■

Remark 2. In the proof of Proposition 1 we used the fact that for each g_j there exists N_j such that we can find \tilde{w}_{jk} with $\|g_j(\cdot) - \sum_{k=1}^{N_j} \tilde{w}_{jk} q_k(\cdot)\|_2^2 < \epsilon/S$. If we take $\tilde{w}_{ji} = w_{ji}$ then

$$\|g_j(\cdot) - \sum_{k=1}^{N_j} \tilde{w}_{jk} q_k(\cdot)\|_2^2 = \sum_{i=N_j}^{\infty} w_{ji}^2.$$

Since $\{w_{ji}\}_{i=1}^{\infty} \in \Theta(\gamma, c)$ we have

$$\sum_{i=N_j}^{\infty} w_{ji}^2 = o \left(\int_{N_j}^{\infty} x^{-2\gamma-1} dx \right) = O(N_j^{-2\gamma}).$$

Hence, for $\|g_j(\cdot) - \sum_{k=1}^{N_j} w_{jk} q_k(\cdot)\|_2^2 < \epsilon/S$ we only need $N_j^{2\gamma} > S/\epsilon$. Since we have argued that the order of S does not have to be larger than $m^{1/3}(\log m)^{1/2}$, if we take ϵ to be of order $m^{-2/3}$ then the order of $K(m) = \max_j N_j$ does not have to be larger than $m^{1/(2\gamma)}(\log m)^{1/(4\gamma)}$. ■

B.3 Proof of Corollary 1

Note that $f(\cdot|\sigma)$ is continuous, then there exists $K_1 = [-M, M]$ such that $P(x \in K_1^c) \rightarrow 0$ as $M \rightarrow \infty$. Let $\inf_{x \in K_1} f(x|\sigma) = l_0$ and $A_{l_0} = \{x : |\hat{f}^m(x|\sigma) - f(x|\sigma)| \geq l_0/2\}$. Since $E \int |\hat{f}^m(x|\sigma) - f(x|\sigma)|^2 dx \geq (l_0/2)^2 P(A_{l_0})$; it follows that $P(A_{l_0}) \rightarrow 0$. Thus $\hat{f}^m(\cdot|\sigma)$ and $f(\cdot|\sigma)$ are bounded below by a positive number for large m, S, K except for an event that has a low probability. Similar arguments can be applied to the upper bound of $\hat{f}^m(\cdot|\sigma)$ and $f(\cdot|\sigma)$, as well as to the upper and lower bounds for $\hat{f}_0^m(\cdot|\sigma)$ and $f_0(\cdot|\sigma)$. Therefore, we conclude that $\hat{f}_0^m(\cdot|\sigma), \hat{f}^m(\cdot|\sigma), f_0(\cdot|\sigma)$ and $f(\cdot|\sigma)$ are all bounded in the interval $[l_a, l_b], 0 < l_a < l_b < \infty$ for large m, S, K except for an event, say A_ϵ that has low probability. Let $\hat{T}_m(x, \sigma) = \hat{f}_0^m(x|\sigma)/\hat{f}^m(x|\sigma)$ and $T^{\text{OR}}(x, \sigma) = f_0(x|\sigma)/f(x|\sigma)$. We

have

$$\hat{T}_m(x, \sigma) - T^{\text{OR}}(x, \sigma) = (\hat{f}_0^m(x|\sigma)f(x|\sigma) - f_0(x|\sigma)\hat{f}^m(x|\sigma))/(\hat{f}^m(x|\sigma)f(x|\sigma)).$$

It is easy to see that $(\hat{T}_m - T^{\text{OR}})^2$ is bounded by 1. Then

$$E\{\hat{T}_m(x, \sigma) - T^{\text{OR}}(x, \sigma)\}^2 \leq P(A_{l_0}) + c_1 E\{\hat{f}_0^m(x|\sigma) - f_0(x|\sigma)\}^2 + c_2 E\{\hat{f}^m(x|\sigma) - f(x|\sigma)\}^2.$$

Thus, $E\{\hat{T}_m(x, \sigma) - T^{\text{OR}}(x, \sigma)\}^2 \rightarrow 0$. Let $B_\delta = \{x|\sigma : |\hat{T}_m(x, \sigma) - T^{\text{OR}}(x, \sigma)| > \delta\}$. Then $\delta^2 P(B_\delta) \leq E\{\hat{T}_m(x, \sigma) - T^{\text{OR}}(x, \sigma)\}^2 \rightarrow 0$, and the result follows. \blacksquare

B.4 Proof of Theorem 2

We begin with a summary of notation used throughout the proof:

- $Q(t) = m^{-1} \sum_{i=1}^m (T_i^{\text{OR}} - \alpha) I\{T_i^{\text{OR}} < t\}$.
- $\hat{Q}(t) = m^{-1} \sum_{i=1}^m (\hat{T}_{i,m} - \alpha) I\{\hat{T}_{i,m} < t\}$.
- $Q_\infty(t) = E\{(T^{\text{OR}} - \alpha) I\{T^{\text{OR}} < t\}\}$.
- $t_\infty = \sup\{t \in (0, 1) : Q_\infty(t) \leq 0\}$: the ‘‘ideal’’ threshold.

For $\hat{T}_{(k),m} < t < \hat{T}_{(k+1),m}$, define a continuous version of $\hat{Q}(t)$ as

$$\hat{Q}_C(t) = \frac{t - \hat{T}_{(k),m}}{\hat{T}_{(k+1),m} - \hat{T}_{(k),m}} \hat{Q}_k + \frac{\hat{T}_{(k+1),m} - t}{\hat{T}_{(k+1),m} - \hat{T}_{(k),m}} \hat{Q}_{k+1},$$

where $\hat{Q}_k = \hat{Q}(\hat{T}_{(k),m})$. Since $\hat{Q}_C(t)$ is continuous and monotone, its inverse \hat{Q}_C^{-1} is well-defined, continuous and monotone. Next we show the following two results in turn: (i) $\hat{Q}(t) \xrightarrow{P} Q_\infty(t)$ and (ii) $\hat{Q}_C^{-1}(0) \xrightarrow{P} t_\infty$. To show (i), note that $Q(t) \xrightarrow{P} Q_\infty(t)$ by the WLLN, so that we only need to establish that $\hat{Q}(t) - Q(t) \xrightarrow{P} 0$.

We need the following lemma, which is proven in Section B.7.

Lemma 3. *Let $U_i = (T_i - \alpha) I(T_i < t)$ and $\hat{U}_i = (\hat{T}_i - \alpha) I\{\hat{T}_i < t\}$. Then $E(\hat{U}_i - U_i)^2 = o(1)$.*

By Lemma 3 and Cauchy-Schwartz inequality, $E\left\{\left(\hat{U}_i - U_i\right)\left(\hat{U}_j - U_j\right)\right\} = o(1)$. Let $S_m = \sum_{i=1}^m (\hat{U}_i - U_i)$.

It follows that

$$\text{Var}(m^{-1} S_m) \leq m^{-2} \sum_{i=1}^m E\left\{\left(\hat{U}_i - U_i\right)^2\right\} + O\left(\frac{1}{m^2} \sum_{i,j:i \neq j} E\left\{\left(\hat{U}_i - U_i\right)\left(\hat{U}_j - U_j\right)\right\}\right) = o(1).$$

By Corollary 1, $E(m^{-1}S_m) \rightarrow 0$, applying Chebyshev's inequality, we obtain $m^{-1}S_m = \hat{Q}(t) - Q(t) \xrightarrow{p} 0$. Hence (i) is proved. Notice that $Q_\infty(t)$ is continuous by construction, we also have $\hat{Q}(t) \xrightarrow{p} \hat{Q}_C(t)$.

Next we show (ii). Since $\hat{Q}_C(t)$ is continuous, for any $\varepsilon > 0$, we can find $\eta > 0$ such that $\left| \hat{Q}_C^{-1}(0) - \hat{Q}_C^{-1} \left\{ \hat{Q}_C(t_\infty) \right\} \right| < \varepsilon$ if $\left| \hat{Q}_C(t_\infty) \right| < \eta$. It follows that

$$P \left\{ \left| \hat{Q}_C(t_\infty) \right| > \eta \right\} \geq P \left\{ \left| \hat{Q}_C^{-1}(0) - \hat{Q}_C^{-1} \left\{ \hat{Q}_C(t_\infty) \right\} \right| > \varepsilon \right\}.$$

Corollary 1 and the WLLN imply that $\hat{Q}_C(t) \xrightarrow{p} Q_\infty(t)$. Note that $Q_\infty(t_\infty) = 0$. Then $P \left(\left| \hat{Q}_C(t_\infty) \right| > \eta \right) \rightarrow 0$. Hence we have $\hat{Q}_C^{-1}(0) \xrightarrow{p} \hat{Q}_C^{-1} \left\{ \hat{Q}_C(t_\infty) \right\} = t_\infty$, completing the proof of (ii).

To show $\text{FDR}(\delta^{\text{HAMT}}(\hat{t}_m)) = \text{FDR}(\delta^{\text{OR}}(t^*)) + o(1) = \alpha + o(1)$, we only need to show $\text{mFDR}(\delta^{\text{HAMT}}(\hat{t}_m)) = \text{mFDR}(\delta^{\text{OR}}(t^*)) + o(1)$. The result then follows from the asymptotic equivalence of FDR and mFDR, which was proven in Basu et al. (2018).

Define the continuous version of $Q(t)$ as $Q_C(t)$ and the corresponding threshold as $Q_C^{-1}(0)$. Then by construction, we have

$$\delta^{\text{HAMT}}(\hat{t}_m) = \left[I \left\{ \hat{T}_{i,m} \leq \hat{Q}_C^{-1}(0) \right\} : 1 \leq i \leq m \right] \quad \text{and} \quad \delta^{\text{OR}}(t^*) = \left[I \left\{ T_i \leq Q_C^{-1}(0) \right\} : 1 \leq i \leq m \right].$$

Following the previous arguments, we can show that $Q_C^{-1}(0) \xrightarrow{p} t_\infty$. It follows that $\hat{Q}_C^{-1}(0) = Q_C^{-1}(0) + o_p(1)$. By construction $\text{mFDR}(\delta^{\text{OR}}) = \alpha$. The mFDR level of δ^{HAMT} is

$$\text{mFDR}(\delta^{\text{HAMT}}) = \frac{P_{H_0} \left\{ \hat{T}_{i,m} \leq \hat{Q}_C^{-1}(0) \right\}}{P \left\{ \hat{T}_{i,m} \leq \hat{Q}_C^{-1}(0) \right\}}.$$

From Corollary 1, $\hat{T}_{i,m} \xrightarrow{p} T_i^{\text{OR}}$. Using the continuous mapping theorem, $\text{mFDR}(\delta^{\text{HAMT}}) = \text{mFDR}(\delta^{\text{OR}}) + o(1) = \alpha + o(1)$. The desired result follows.

Finally, using the fact that $\hat{T}_{i,m} \xrightarrow{p} T_i^{\text{OR}}$ and $\hat{Q}_C^{-1}(0) \xrightarrow{p} Q_C^{-1}(0)$, we can similarly show that $\text{ETP}(\delta^{\text{HAMT}})/\text{ETP}(\delta^{\text{OR}}) = 1 + o(1)$. ■

B.5 Proof of Lemma 1

Suppose $\mu_i \stackrel{iid}{\sim} g$, for $i = 1, \dots, m$. Let \hat{g} be the empirical density function $\sum_{i=1}^m \delta_{\mu_i}(\cdot)$. Let $f(x|\tau) = g * \eta_\tau(x)$ and $\hat{f}(x|\tau) = \hat{g} * \eta_\tau(x)$. Then

$$E\hat{f}(x|\tau) = E \sum_{i=1}^m \frac{1}{m} \eta_\tau(x - \mu_i) = E\eta_\tau(x - \mu) = \int_{-\infty}^{\infty} \eta_\tau(x - \mu)g(\mu)d\mu = f(x|\tau).$$

Also since η_τ is smooth, thus bounded, it follows that $\text{Var}\{\eta_\tau(x - \mu_i)\} < \infty$ (here we treat μ_i as random). Therefore

$$\begin{aligned}\text{Var}\hat{f}(x|\tau) &= \text{Var}\left\{\int_{-\infty}^{\infty}\eta_\tau(\mu-x)\hat{g}(\mu)d\mu\right\} \\ &= \text{Var}\left\{\frac{1}{m}\sum_{i=1}^m\eta_\tau(x-\mu_i)\right\} \\ &= \frac{1}{m}\text{Var}\{\eta_\tau(x-\mu_i)\} \rightarrow 0.\end{aligned}$$

It follows that $E_{\boldsymbol{\mu}}|f(x|\tau) - \hat{f}(x|\tau)|^2 \rightarrow 0$ as $n \rightarrow \infty$.

The above implies it is possible to find a set $\{\mu_1, \dots, \mu_m\}$ and $\hat{f}(x|\tau) = \frac{1}{m}\sum_{i=1}^m\eta_\tau(x-\mu_i)$ such that for all x , $|f(x|\tau) - \hat{f}(x|\tau)|^2 \rightarrow 0$. Consider the set of functions $\{\sum_{j=1}^k\theta_j\eta_\tau(x-u_j) \mid \sum_{j=1}^k\theta_j = 1, \theta_j \geq 0 \ \forall j\}$. We can make the grid fine enough so that for any $\epsilon' > 0$ and j , there exists $u_{i(j)} \in \{u_1, \dots, u_k\}$ such that $|\mu_j - u_{i(j)}| < \epsilon'$. We can choose ϵ' small enough so that $|\eta_\tau(x-u_j) - \eta_\tau(x-u_{i(j)})|^2 < \epsilon$. Hence,

$$\begin{aligned}\left|\frac{1}{m}\sum_{j=1}^m\eta_\tau(x-\mu_j) - \frac{1}{m}\sum_{j=1}^m\eta_\tau(x-u_{i(j)})\right|^2 &= \frac{1}{m^2}\left|\sum_{j=1}^m\eta_\tau(x-\mu_j) - \sum_{j=1}^m\eta_\tau(x-u_{i(j)})\right|^2 \\ &\leq \frac{1}{m}\sum_{j=1}^m|\eta_\tau(x-\mu_j) - \eta_\tau(x-u_{i(j)})|^2 \leq \epsilon.\end{aligned}$$

By the triangle inequality we have $|f(x|\tau) - \frac{1}{m}\sum_{j=1}^m\eta_\tau(x-u_{i(j)})|^2 \leq \epsilon$, we can let $g'(\cdot) = \frac{1}{m}\sum_{j=1}^m\delta_{u_{i(j)}}(\cdot)$. ■

B.6 Proof of Lemma 2

By Fubini's theorem, we have

$$\begin{aligned}E|\hat{f}(x|\sigma) - f(x|\sigma)|^2 &= E_\sigma E_{\mathbf{x}, \sigma} E_{x|\sigma} |\hat{f}(x|\sigma) - f(x|\sigma)|^2 \\ &= E_\sigma E_{\mathbf{x}, \sigma} \int_{-\infty}^{\infty} |\hat{f}(x|\sigma) - f(x|\sigma)|^2 f(x|\sigma) dx\end{aligned}$$

Hence, if $\tau \sim g_\sigma$ we must have

$$E \int_{-\infty}^{\infty} |\hat{g} * \eta_\tau(x) - g * \eta_\tau(x)|^2 f(x|\tau) dx \rightarrow 0.$$

$E \int_{-\infty}^{\infty} |\hat{g} * \eta_\tau(x) - g * \eta_\tau(x)|^2 dx \rightarrow 0$. Then there exists a sequence of sets \mathcal{X}_m and $\epsilon_1 > 0$ such that $E|\hat{g} * \eta_\tau(x) - g * \eta_\tau(x)| > \epsilon_1$ on \mathcal{X}_m . If $\int_{\mathcal{X}_m} f(x|\tau) dx > 0$ this would imply $E \int_{-\infty}^{\infty} |\hat{g} * \eta_\tau(x) - g * \eta_\tau(x)|^2 dx > \epsilon_1^2 \int_{\mathcal{X}_m} f(x|\tau) dx > 0$.

$\eta_\tau(x)|^2 f(x|\tau) dx \not\rightarrow 0$ a contradiction. If $\int_{\mathcal{X}_m} f(x|\tau) dx \rightarrow 0$, using the definition $f(x|\tau) = g * \eta_\tau(x)$ we have

$$E \int_{\mathcal{X}_m} |\hat{g} * \eta_\tau(x) - g * \eta_\tau(x)|^2 dx \rightarrow E \int_{\mathcal{X}_m} |\hat{g} * \eta_\tau(x)|^2 dx \rightarrow 0$$

Since $\hat{g} * \eta_\tau(x)$ and $g * \eta_\tau(x)$ are both densities there must exist another sequence of sets \mathcal{X}'_m , $\epsilon > 0$ and $\delta > 0$ such that $g * \eta_\tau(x) > \hat{g} * \eta_\tau(x) + \epsilon$ on \mathcal{X}'_m and $\int_{\mathcal{X}'_m} f(x|\tau) dx > \delta$, again contradicting the fact that $E \int_{-\infty}^{\infty} |\hat{g} * \eta_\tau(x) - g * \eta_\tau(x)|^2 f(x|\tau) dx \rightarrow 0$. ■

B.7 Proof of lemma 3

Using the definitions of \hat{U}_i and U_i , we can show that

$$\begin{aligned} (\hat{U}_i - U_i)^2 &= (\hat{T}_{i,m} - T_i^{\text{OR}})^2 I(\hat{T}_{i,m} \leq t, T_i^{\text{OR}} \leq t) + (\hat{T}_{i,m} - \alpha)^2 I(\hat{T}_{i,m} \leq t, T_i^{\text{OR}} > t) \\ &\quad + (T_i^{\text{OR}} - \alpha)^2 I(\hat{T}_{i,m} > t, T_i^{\text{OR}} \leq t). \end{aligned}$$

Denote the three sums on the RHS as I , II , and III respectively. By Corollary 1, $E(I) = o(1)$. Let $\epsilon > 0$. Consider

$$\begin{aligned} P(\hat{T}_{i,m} \leq t, T_i^{\text{OR}} > t) &\leq P(\hat{T}_{i,m} \leq t, T_i^{\text{OR}} \in (t, t + \epsilon)) + P(\hat{T}_{i,m} \leq t, T_i^{\text{OR}} \geq t + \epsilon) \\ &\leq P\{T_i^{\text{OR}} \in (t, t + \epsilon)\} + P(|\hat{T}_{i,m} - T_i^{\text{OR}}| > \epsilon) \end{aligned}$$

The first term on the right hand is vanishingly small as $\epsilon \rightarrow 0$ because T_i^{OR} is a continuous random variable. The second term converges to 0 by Corollary 1. we conclude that $II = o(1)$. In a similar fashion, we can show that $III = o(1)$, thus proving the lemma. ■

C Implementation of HMT, NPMLE B, ASH and ASH 1

C.1 HMT

We use the R interface to MOSEK (MOSEK, 2019) available in the R package `Rmosek` for solving Problem (13). However, note that Problem (13) requires that the KS parameters $\mathcal{W} = (\mathbf{w}_1^T, \dots, \mathbf{w}_S^T)^T$ satisfy Sm inequality constraints $B\mathcal{W} \succeq \mathbf{0}_{Sm}$ and m equality constraints $C\mathcal{W} = \mathbf{1}_m$. Since the number of constraints is much greater than the number of parameters, solvers such as MOSEK may throw an infeasibility certificate if numerical instabilities prohibit the solution from satisfying these constraints, particularly the equality constraints. An alternative strategy is to consider the corresponding dual of Problem (13). This approach has also been advocated by Gu and Koenker (2017), Koenker and Gu (2017), Koenker and Mizera (2014) in the context of empirical Bayes deconvolution using

nonparametric maximum likelihood estimation. The dual of the optimization Problem (13) is

$$\min_{(\boldsymbol{\omega}, \boldsymbol{\rho}) \in \mathbb{R}^{m(S+1)}} \mathbf{1}_m^T \boldsymbol{\rho} + \frac{1}{2} (\mathbf{v} + C^T \boldsymbol{\rho} - B^T \boldsymbol{\omega})^T D^{-1} (\mathbf{v} + C^T \boldsymbol{\rho} - B^T \boldsymbol{\omega}) \quad \text{subject to } \boldsymbol{\omega} \succeq \mathbf{0}_{Sm}, \quad (24)$$

where $\mathbf{v} = -m^{-1} A^T \hat{\boldsymbol{\varphi}}^m$ and $D = m^{-1} A^T A$. Since D is positive semi-definite in our setting, the dual Problem (24) is a standard convex quadratic optimization problem with a non-negativity constraint on the decision variables $\boldsymbol{\omega}$. Moreover, this dual problem always has a solution. For instance, $\boldsymbol{\rho} = \mathbf{0}_m$ and $\boldsymbol{\omega} = \mathbf{0}_{Sm}$ is a feasible solution. Furthermore, if $(\boldsymbol{\rho}^*, \boldsymbol{\omega}^*)$ denotes the optimal solution to Problem (24) then the solution to the primal Problem (13) is $\hat{\mathcal{W}}_m = -D^{-1} (\mathbf{v} + C^T \boldsymbol{\rho}^* - B^T \boldsymbol{\omega}^*)$.

Another practical strategy that works particularly well in our setting is to solve a relaxed version of the primal Problem (13) where the equality constraints $C\mathcal{W} = \mathbf{1}_m$ in Equation (13) are relaxed to the following inequality constraints: $a\mathbf{1}_m \preceq C\mathcal{W} \preceq \mathbf{1}_m$ with a set at 0.9. The corresponding “relaxed primal” problem is often easier to solve than Problem (13). Furthermore, if $\hat{\mathcal{W}}_m = (\hat{\boldsymbol{w}}_1^T, \dots, \hat{\boldsymbol{w}}_S^T)^T$ denotes the optimal solution to this relaxed primal problem then we only require a simple re-scaling of the columns of the $S \times m$ matrix $\mathcal{G} = (\hat{\boldsymbol{g}}_1, \dots, \hat{\boldsymbol{g}}_m)$, where $\hat{\boldsymbol{g}}_i = \{\hat{\boldsymbol{w}}_j^T \boldsymbol{q}(\sigma_i) : 1 \leq j \leq S\}$, to ensure $\sum_{j=1}^S \hat{\boldsymbol{w}}_j^T \boldsymbol{q}(\sigma_i) = 1$ for all $i = 1, \dots, m$. Our implementation in R first attempts to solve the primal Problem (13). In case the solution status from MOSEK’s conic interior-point optimizer throws an infeasibility certificate, it attempts to solve the “relaxed primal” problem. The dual Problem (24) is solved and the corresponding primal solution is recovered if the solution status from solving the relaxed primal is not optimal.

C.2 NPMLE B, ASH and ASH.1

We first describe the construction of NPMLE B and then discuss the implementation of ASH and ASH 1.

For NPMLE B, we continue to take $g_j(\sigma_i) = \boldsymbol{w}_j^T \boldsymbol{q}(\sigma_i)$ but estimate the \boldsymbol{w}_j ’s by solving Problem (9). Denote $\mathcal{W} = (\boldsymbol{w}_1^T, \dots, \boldsymbol{w}_S^T)$, $\boldsymbol{a}_{ij} = \eta_{\sigma_i}(x_i - u_j) \boldsymbol{q}(\sigma_i)$, $\boldsymbol{a}_i = (\boldsymbol{a}_{i1}^T, \dots, \boldsymbol{a}_{iS}^T)^T$ and $A = (\boldsymbol{a}_1, \dots, \boldsymbol{a}_m)^T$. Additionally, let $Q = [\mathbf{1}_S \otimes \boldsymbol{q}(\sigma_1) \dots \mathbf{1}_S \otimes \boldsymbol{q}(\sigma_m)]^T$ where \otimes denotes the usual kronecker product of two matrices, and \boldsymbol{c}_r is an r -dimensional vector with all entries equal to the scalar $c \in \mathbb{R}$. Finally, for $s = 1, \dots, S$, let L_s denote a $m \times KS$ matrix whose entries are 0 except for the $\{K(s-1) + 1\}$ th column which equals $[\boldsymbol{q}(\sigma_1), \dots, \boldsymbol{q}(\sigma_m)]^T$ and denote $L = [L_1^T \dots L_S^T]^T$. With these notations, the primal optimization problem (9) is equivalent to

$$\min_{\boldsymbol{u}, \mathcal{W}} - \sum_{i=1}^m \log u_i \quad \text{subject to } A\mathcal{W} = \boldsymbol{u}, \quad Q\mathcal{W} = \mathbf{1}_m, \quad L\mathcal{W} \succeq \mathbf{0}_{Sm}, \quad (25)$$

where $\boldsymbol{u} = (u_1, \dots, u_m)$. As recommended by [Koenker and Gu \(2017\)](#), [Koenker and Mizera \(2014\)](#), it is often more efficient to solve the dual of Problem (25) and recover the corresponding primal

solution. In our context, the dual problem is given by

$$\min_{\mathbf{v}} - \sum_{i=1}^m \log v_i \text{ subject to } A^T \mathbf{v} \preceq Q^T \mathbf{1}_m, \mathbf{v} \succeq \mathbf{0}_m, \quad (26)$$

where $\mathbf{v} = (v_1, \dots, v_m)$. If \mathbf{v}^* denotes the optimal solution to the dual (26) then the primal solution is $\hat{\mathcal{W}} = (A^T A)^{-1} A^T \mathbf{u}^*$ where $u_i^* = 1/v_i^*$. We use the R interface to MOSEK (MOSEK, 2019) available in the R package `Rmosek` for solving Problem (26) and fix $S = 50$, $K = 10$ for all our numerical experiments.

For implementing the method ASH proposed in Stephens (2017), we use the function `ash` available in the R-package `ashr` and consider two versions of this method: one with $c = 0$ (ASH) and the other with $c = 1$ (ASH 1). For both these versions, we set `mode = "estimate"` and estimate the Clfdr using 3,000 posterior samples. The `ash` function requires specifying the approximate distribution of the components in the mixture used to represent g via the option `mixcompdist` and the `ashr` package provides several choices such as `"uniform"`, `"normal"`, `"halfuniform"`, `"halfnormal"` etc. While this oracle knowledge is not available to HAMT, we provide this information to `ash` depending on the simulation setting at hand and report the choice in the corresponding figure captions. For the real data analysis (Section F), we set `mixcompdist="normal"`.

D Additional numerical experiments

D.1 Experiments involving two-sided composite null hypotheses

Here we assess the numerical performance of HAMT for two-sided composite null hypotheses. We evaluate the following six competing testing procedures from Section 5.2: AdaPTGMM, DECONV, ASH, ASH 1, NPMLE B and OR. We drop GS1 and GS2 from our comparisons since these methods were developed only for testing one sided composite null hypotheses. Additionally, we do not report the performance of BH, CAMT and IHW as these p -value methods exhibited substantially lower power in all our experiments involving two-sided composite nulls.

We fix $m = 10^4$, $\alpha = 0.1$ and evaluate the aforementioned six methods across the following three simulation settings.

- **Setting 1** – presented in Figure 9, is a modification of Setting 2 from Section 5.2. Here $\sigma_i = 0.5, 1$ or 3 with equal probabilities. Conditional on σ_i , $\mu_i = 0$ with probability 0.9 , and $\mu_i = \bar{\sigma}\sigma_i$ or $-\bar{\sigma}\sigma_i$ with probability 0.05 each. We take $\mathcal{A} = [-5, 5]$ for this setting and find that HAMT controls the FDR level at α and dominates all other methods in power.
- **Setting 2** – we sample σ_i independently from $\text{Unif}(0.5, \bar{\sigma})$ but consider a three component mixture distribution for μ_i conditional on σ_i . In particular $\mu_i = 0$ with probability 0.9 and

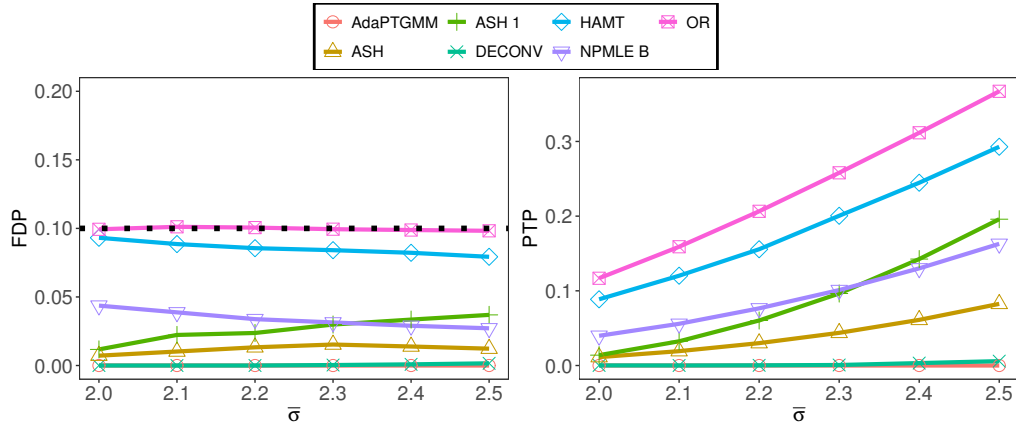


Figure 9: Setting 1: $\sigma_i \stackrel{i.i.d.}{\sim} (1/3)\delta_{(0.5)} + (1/3)\delta_{(1)} + (1/3)\delta_{(3)}$ and conditional on $\sigma_i, \mu_i \sim 0.9\delta_{(0)} + 0.05\delta_{(\bar{\sigma}\sigma_i)} + 0.05\delta_{(-\bar{\sigma}\sigma_i)}$. Here $\mathcal{A} = [-5, 5]$. For ASH and ASH 1, `mixcompdist = "uniform"`.

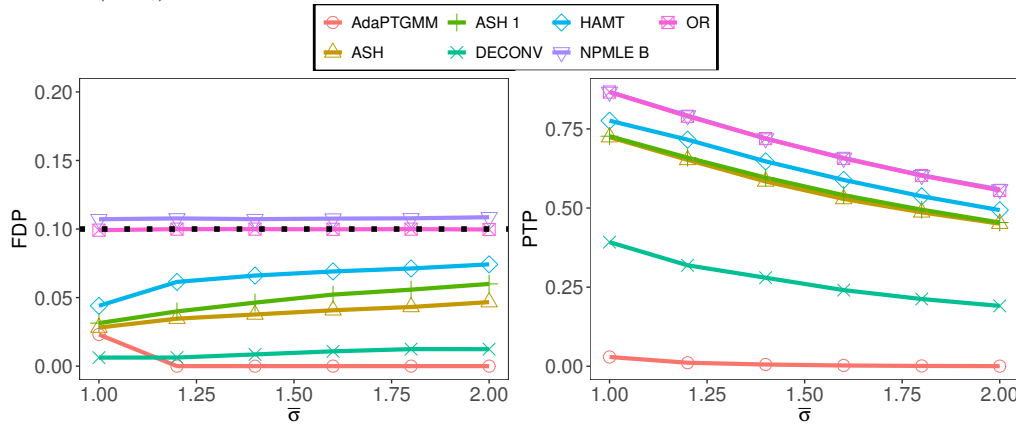


Figure 10: Setting 2: $\sigma_i \stackrel{i.i.d.}{\sim} \text{Unif}(0.5, \bar{\sigma})$. Conditional on $\sigma_i, \mu_i = 0$ with probability 0.9 and $\mu_i \stackrel{ind.}{\sim} N(3, \sigma_i)$ or $N(-3, \sigma_i)$ each with probability 0.05. Here $\mathcal{A} = [-2, 2]$. For ASH and ASH 1, `mixcompdist = "normal"`.

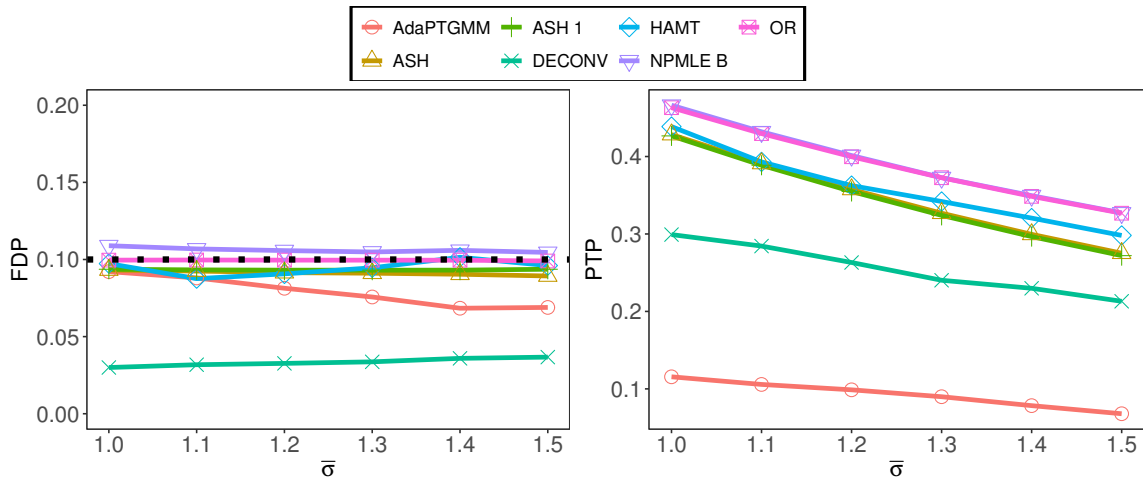


Figure 11: Setting 3: $\sigma_i \stackrel{i.i.d.}{\sim} \text{Unif}(0.5, \bar{\sigma})$. Conditional on $\sigma_i, \mu_i = 0$ with probability 0.8 and $\mu_i \stackrel{ind.}{\sim} N(\sigma_i, 1)$ or $N(\sigma_i, 4)$ each with probability 0.1. Here $\mathcal{A} = [-1, 1]$. For ASH and ASH 1, `mixcompdist = "normal"`.

$\mu_i \stackrel{ind.}{\sim} N(3, \sigma_i)$ or $N(-3, \sigma_i)$ each with probability 0.05. Here we let $\mathcal{A} = [-2, 2]$.

- **Setting 3** – we continue to sample σ_i independently from $\text{Unif}(0.5, \bar{\sigma})$. Conditional on σ_i , $\mu_i = 0$ with probability 0.8 and $\mu_i \stackrel{ind.}{\sim} N(\sigma_i, 1)$ or $N(\sigma_i, 4)$ each with probability 0.1. Here we let $\mathcal{A} = [-1, 1]$.

Figures 10 and 11, respectively, report the performance of the various methods across settings 2 and 3. We find that all methods, with the exception of DECONV and AdaPTGMM, are competitive with respect to their power while NPMLE B marginally fails to control the FDR at 10%.

D.2 Non-Gaussian Likelihood

In this section we assess the performance of HAMT when ϵ_i in Model (1) are not necessarily standard normal random variables. Note that (i) we drop GS1, GS2 and DECONV from our comparisons as these methods rely on a Gaussian likelihood, and (ii) BH, CAMT and IHW are not reported whenever the simulation setting involves testing two-sided composite nulls. The following three simulation settings are considered with $m = 10^4$ and $\alpha = 0.1$.

- **Setting 1** – $\sigma_i \stackrel{i.i.d.}{\sim} (1/3)\delta_{(0.25)} + (1/3)\delta_{(0.75)} + (1/3)\delta_{(1.5)}$, conditional on σ_i , $\mu_i = 0.9\delta_{(0)} + 0.05\delta_{(\bar{\sigma}\sigma_i)} + 0.05\delta_{(-\bar{\sigma}\sigma_i)}$ and, conditional on (μ_i, σ_i) , $X_i = \mu_i + \sigma_i t_\nu$, where t_ν is a central t -distributed random variable with ν degrees of freedom. Here $\mathcal{A} = [-5, 5]$.
- **Setting 2** – same as Setting 1 except that $X_i \stackrel{ind.}{\sim} \text{Logistic}(\mu_i, \sigma_i)$. Here $\mathcal{A} = [-2, 2]$.
- **Setting 3** – $\sigma_i \stackrel{i.i.d.}{\sim} \text{Unif}(0.3, \bar{\sigma})$, $\mu_i = 0.9\delta_{(0)} + 0.1N(3, 1)$ and, conditional on (μ_i, σ_i) , $X_i \stackrel{ind.}{\sim} \text{Laplace}(\mu_i, \sigma_i)$. Here $\mathcal{A} = [-\infty, 2]$.

For settings 2 and 3, ASH and ASH 1 are not included in our comparisons as their corresponding R package `ash` does not provide an implementation when ϵ_i are Logistic or Laplace distributed. Figures 12–14 report the performance of various methods across the three simulation settings. In settings 1 and 2, HAMT dominates all methods in power. In Setting 1, NPMLE B exhibits a relatively high MC error in its FDP distribution for the first three values of $\bar{\sigma}$ and so for each $\bar{\sigma}$ we report its median FDP and PTP across the 200 MC repetitions in Figure 12. In Setting 3, NPMLE B exhibits a marginally higher FDR than 10% for larger values of $\bar{\sigma}$ but is, in general, relatively more powerful than HAMT.

D.3 Unknown variance

Here we investigate the performance of HAMT when the summary statistic X_i are only asymptotically Normal and σ_i are unknown, being approximated by the sample variance S_i^2 . Specifically, conditional on (μ_i, σ_i) and $j = 1, \dots, n$, we let $X_{ij} = \mu_i + \sigma_i c_n \epsilon_{ij}$ where the scaling $c_n = \sqrt{n/\text{Var}(\epsilon_{ij})}$

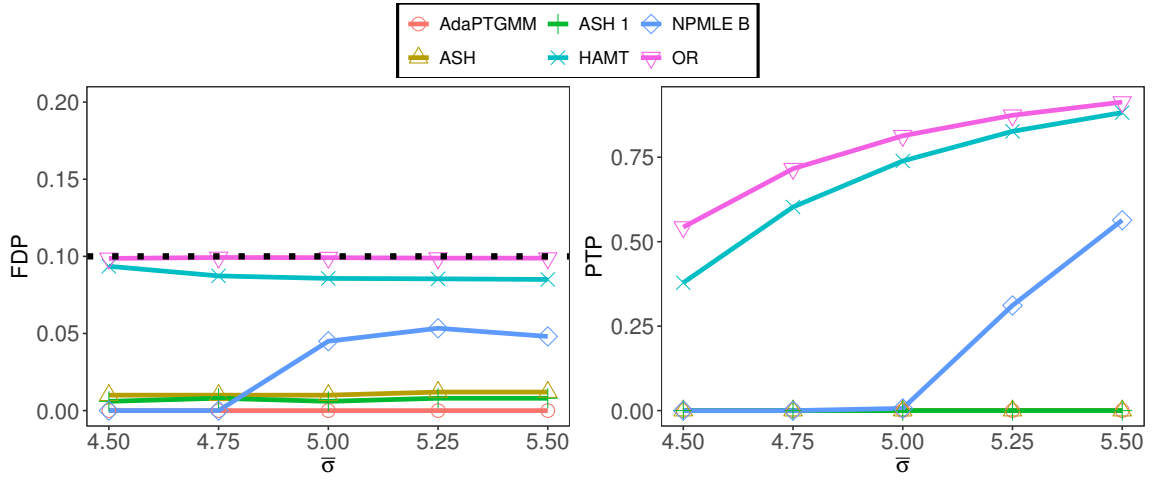


Figure 12: Setting 1: $\sigma_i \stackrel{i.i.d.}{\sim} (1/3)\delta_{(0.25)} + (1/3)\delta_{(0.75)} + (1/3)\delta_{(1.5)}$, conditional on σ_i , $\mu_i = 0.9\delta_{(0)} + 0.05\delta_{(\bar{\sigma}\sigma_i)} + 0.05\delta_{(-\bar{\sigma}\sigma_i)}$ and, conditional on (μ_i, σ_i) , $X_i = \mu_i + \sigma_i t_5$. Here $\mathcal{A} = [-5, 5]$. For ASH and ASH 1, `mixcompdist = "uniform"`

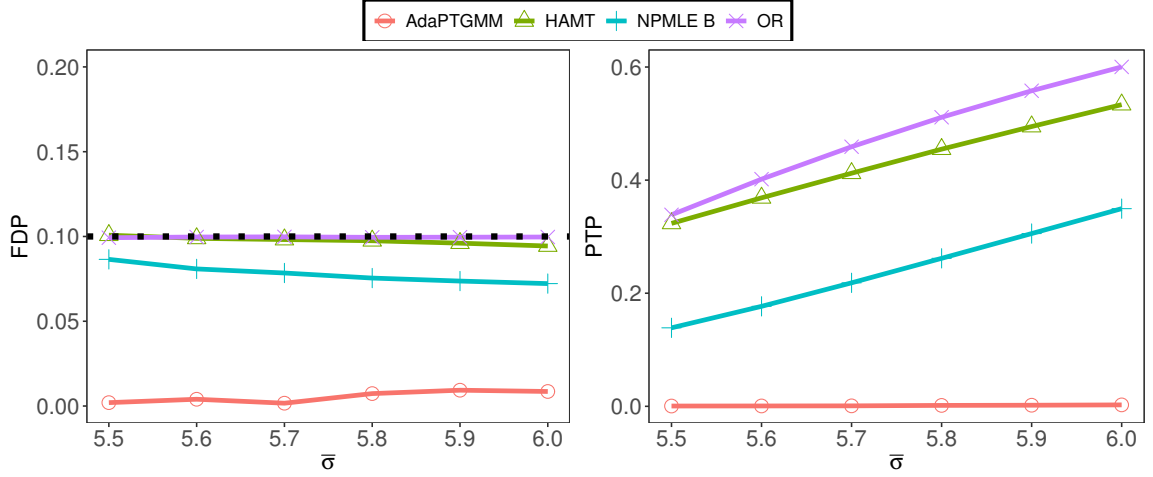


Figure 13: Setting 2: $\sigma_i \stackrel{i.i.d.}{\sim} (1/3)\delta_{(0.25)} + (1/3)\delta_{(0.75)} + (1/3)\delta_{(1.5)}$, conditional on σ_i , $\mu_i = 0.9\delta_{(0)} + 0.05\delta_{(\bar{\sigma}\sigma_i)} + 0.05\delta_{(-\bar{\sigma}\sigma_i)}$ and, conditional on (μ_i, σ_i) , $X_i \stackrel{ind}{\sim} \text{Logistic}(\mu_i, \sigma_i)$. Here $\mathcal{A} = [-2, 2]$.

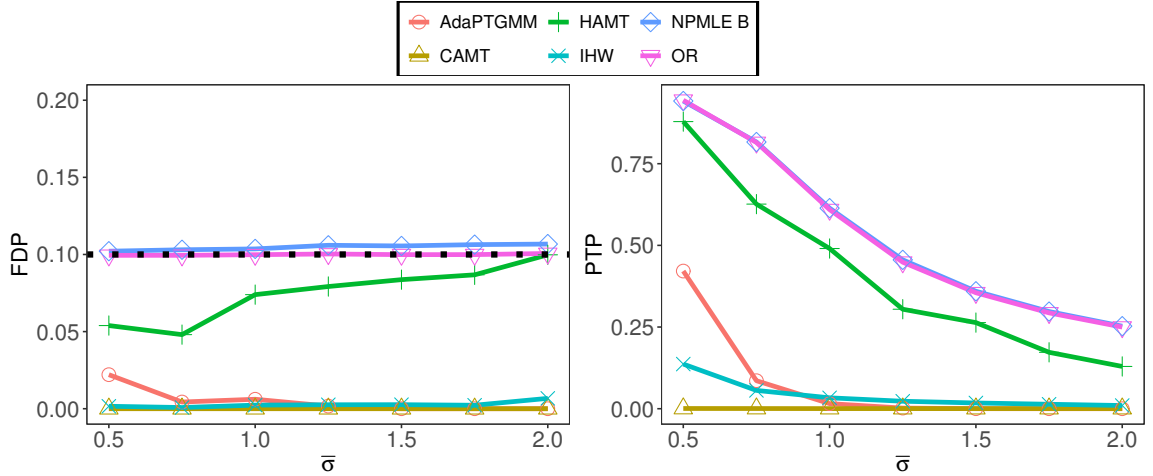


Figure 14: Setting 3: $\sigma_i \stackrel{i.i.d.}{\sim} \text{Unif}(0.3, \bar{\sigma})$, $\mu_i = 0.9\delta_{(0)} + 0.1N(3, 1)$ and, conditional on (μ_i, σ_i) , $X_i \stackrel{ind}{\sim} \text{Laplace}(\mu_i, \sigma_i)$. Here $\mathcal{A} = [-\infty, 2]$.

ensures that $\text{Var}(X_i) = \text{Var}(n^{-1} \sum_{j=1}^n X_{ij}) = \sigma_i^2$. Denote $S_i^2 = n^{-2} \sum_{j=1}^n (X_{ij} - X_i)^2$. In this section we assume that X_i are approximate Gaussian random variables with mean μ_i and variance S_i^2 , and consequently, assess the impact of this assumption on the quality of various testing procedures as n varies. The following four settings are evaluated:

- **Setting 1** - this scenario is borrowed from Setting 3 of Section 5.2 with $\sigma_i \stackrel{i.i.d.}{\sim} \text{Unif}(0.5, 1.5)$ and $\epsilon_{ij} \stackrel{i.i.d.}{\sim} \text{Unif}(-3, 3)$. In Figure 15, we find that as n varies, HAMT, ASH 1 and NPMLE B exhibit similar power while GS1 fails to control the FDR at 10%.
- **Setting 2** - this scenario is borrowed from Setting 4 of Section 5.2 with $\sigma_i \stackrel{i.i.d.}{\sim} 0.9\text{Unif}(0.5, 1) + 0.1\text{Unif}(1, 1.5)$ and ϵ_{ij} are i.i.d central t -distributed random variables with 10 degrees of freedom. In Figure 16, HAMT dominates all other methods in power as n varies while controlling the FDR at 10%.
- **Setting 3** - this scenario is borrowed from Setting 1 of Section 5.2 with $\sigma_i \stackrel{i.i.d.}{\sim} \text{Unif}(0.5, 1)$ and ϵ_{ij} are i.i.d central t -distributed random variables with 10 degrees of freedom. In Figure 17, GS1 and NPMLE B marginally fail to control the FDR at 10%. In terms of power, HAMT and DECONV exhibit similar profiles that are closely followed by ASH and ASH 1.
- **Setting 4** - this scenario is borrowed from Setting 1 of Section D.2 with $\mu_i = 0.9\delta_{(0)} + 0.05\delta_{(4.5\sigma_i)} + 0.05\delta_{(-4.5\sigma_i)}$ and ϵ_{ij} are i.i.d Logistic random variables with location = 0 and scale = 1. In Figure 18, while all methods control the FDR at 10%, HAMT exhibits the best power followed by ASH 1 and NPMLE B.

E Further discussion of the numerical performances of various methods

E.1 HAMT and NPMLE B

We note that the multiple testing procedures underlying HAMT and NPMLE B differ only with respect to how they estimate $g_\mu(\cdot | \sigma)$. Specifically, NPMLE B relies on Problem (9) to estimate \mathcal{W} while HAMT relies on Problem (13). However, as some of the numerical experiments in sections 5.2 and D suggest, this difference can lead to contrasting power and FDR profiles for the two methods. We elaborate on this observation through the lens of the simulation settings for figures 7 and 8. We choose the simulation scenarios accompanying figures 7 and 8 because they represent two out of the four settings where the power of HAMT is substantially higher than that of NPMLE B at the same FDR level. The other settings being figures 12 and 16.

Analysis of Figure 7 - the simulation setting underlying this figure is as follows: $X_i | \mu_i, \sigma_i \stackrel{ind.}{\sim}$

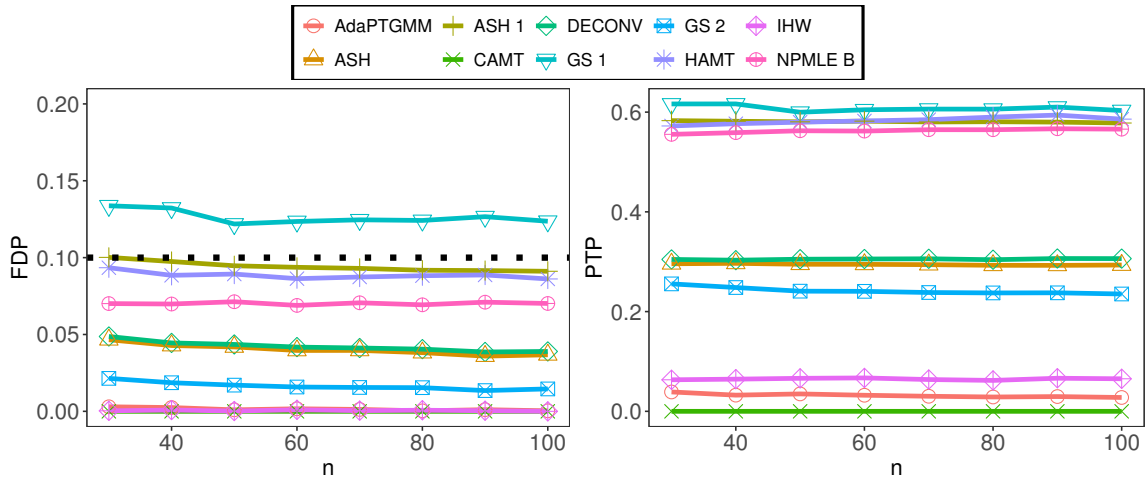


Figure 15: Setting 1: Scenario borrowed from Setting 3 of Section 5.2 with $\sigma_i \stackrel{i.i.d}{\sim} \text{Unif}(0.5, 1.5)$ and $\epsilon_{ij} \stackrel{i.i.d}{\sim} \text{Unif}(-3, 3)$.

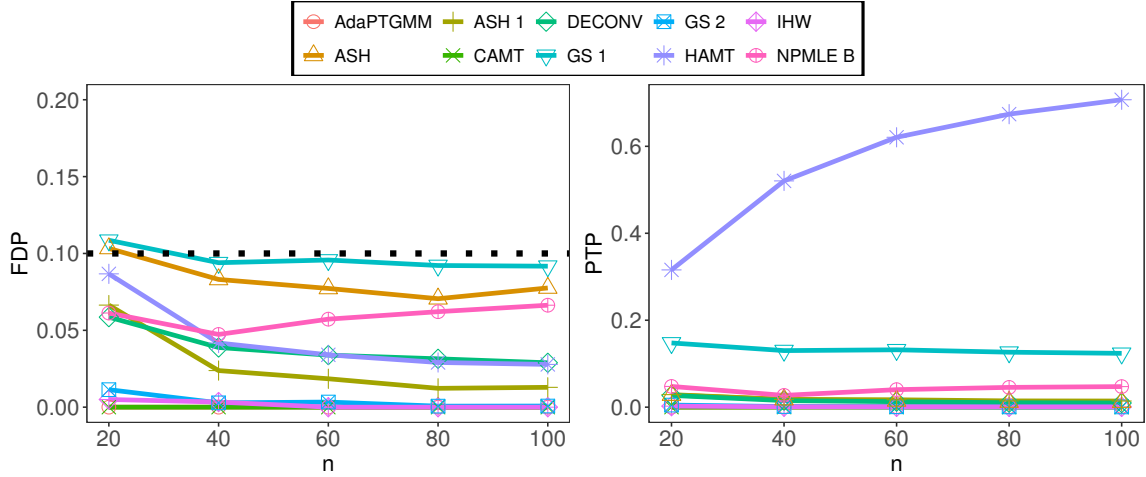


Figure 16: Setting 2: Scenario is borrowed from Setting 4 of Section 5.2 with $\sigma_i \stackrel{i.i.d}{\sim} 0.9\text{Unif}(0.5, 1) + 0.1\text{Unif}(1, 1.5)$ and ϵ_{ij} are i.i.d central t -distributed random variables with 10 degrees of freedom.

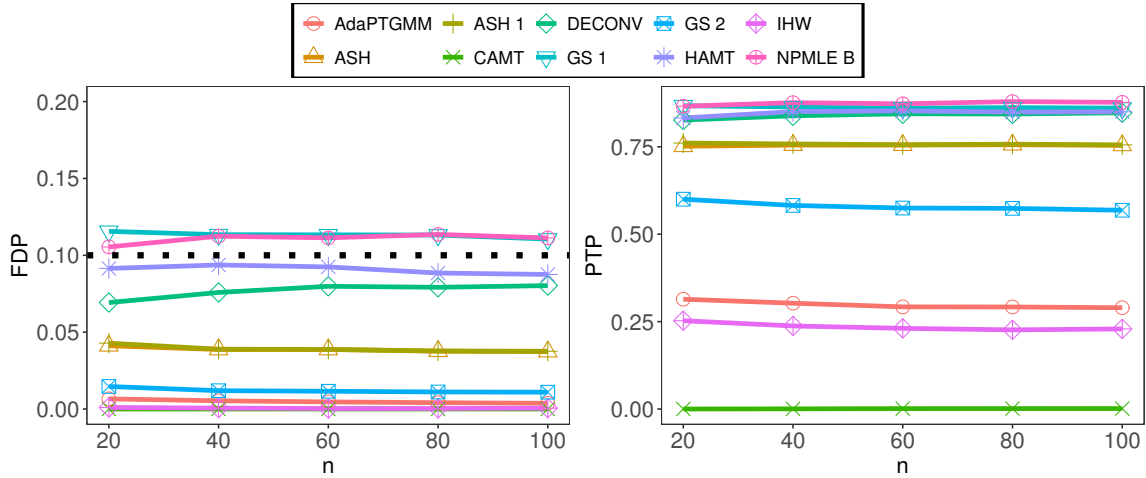


Figure 17: Setting 3: Scenario is borrowed from Setting 1 of Section 5.2 with $\sigma_i \stackrel{i.i.d}{\sim} \text{Unif}(0.5, 1)$ and ϵ_{ij} are i.i.d central t -distributed random variables with 10 degrees of freedom.

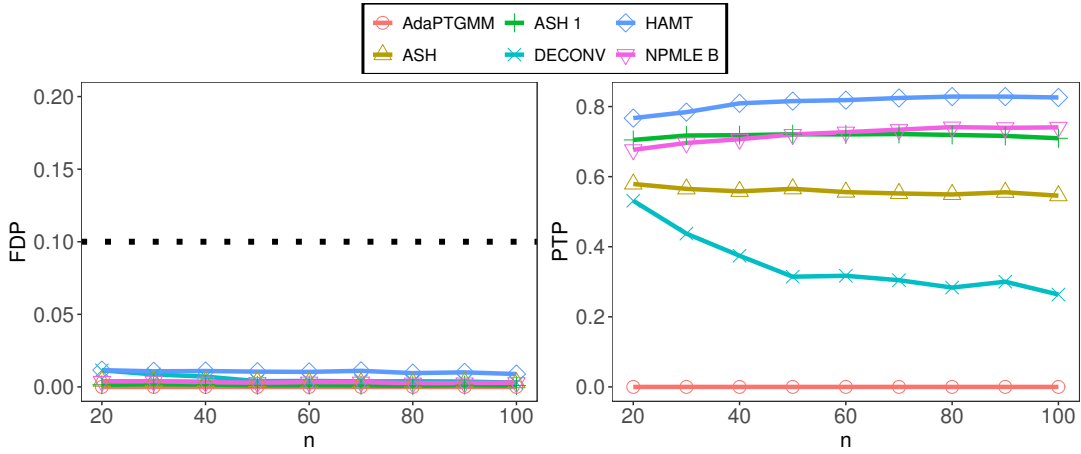


Figure 18: Setting 4: Scenario borrowed from Setting 1 of Section D.2 with $\mu_i = 0.9\delta_{(0)} + 0.05\delta_{(4.5\sigma_i)} + 0.05\delta_{(-4.5\sigma_i)}$ and ϵ_{ij} are i.i.d Logistic random variables with location = 0 and scale = 1.

$N(\mu_i, \sigma_i^2)$, $\sigma_i \stackrel{i.i.d}{\sim} 0.9\text{Unif}(0.5, 1) + 0.1\text{Unif}(1, \bar{\sigma})$ and $\mu_i = 0$, if $\sigma_i \leq 1$ and $2/\sigma_i$, otherwise. Here $\mathcal{A} = (-\infty, 1]$. Thus, in this setting the signal strength, in terms of the magnitude of the non-null μ_i , decreases as $\bar{\sigma}$ increases from 1.2 to 2. For $\bar{\sigma} = 1.2$ and for a random dataset generated from the above hierarchical model, Figure 19 plots the estimate of $f(\cdot | \sigma)$ at $\sigma = 0.7$ (left), $\sigma = 0.95$ (center) and $\sigma = \bar{\sigma} - 0.1$ (right). For NPMLE B, these densities are plotted for four different combinations of (S, K) while HAMT relies on the default choices of $S = 50, K = 10$. We note that while the estimates of $f(\cdot | 0.7)$ obtained from HAMT and the NPMLE B variants are virtually indistinguishable from the ground truth, HAMT appears to be relatively better at estimating $f(\cdot | 0.95)$ and $f(\cdot | \bar{\sigma} - 0.1)$. Furthermore, the four variants of NPMLE B are distinguishable only in the third panel and their respective PTP values, 0.85 ($S = 50, K = 10$), 0.857 ($S = 100, K = 30$), 0.842 ($S = 100, K = 10$) and 0.878 ($S = 50, K = 30$), are marginally less than the PTP of 0.887 returned by HAMT on this random dataset. Figures 20 and 21, respectively, represent the cases $\bar{\sigma} = 1.4$ and $\bar{\sigma} = 1.8$. In both these figures, HAMT is better at estimating $f(\cdot | \bar{\sigma} - 0.1)$ than the NPMLE B variants. This is also evident in the PTP values that HAMT and the NPMLE B variants return. For instance, in Figure 20 HAMT returns a PTP of 0.857 which is substantially better than 0.109 obtained from the NPMLE B variant with $S = 50, K = 30$. Furthermore, in Figure 21 the PTP of HAMT is 0.816 which far exceeds the PTP from the NPMLE B variants. Moreover, the choices of S and K seem to have some impact on the power of NPMLE B when $\bar{\sigma} = 1.4$ but relatively less so when $\bar{\sigma} = 1.8$.

To further understand why the marginal density estimates from HAMT and NPMLE B differ, we examine their respective estimates of $g_\mu(\cdot | \sigma)$. When $\bar{\sigma} = 1.2$, the left panel of Figure 22 presents the $m \times S$ matrix $\mathcal{G} = (\hat{\mathbf{g}}_1, \dots, \hat{\mathbf{g}}_m)^T$ of the estimated prior probabilities obtained from HAMT, where $\hat{\mathbf{g}}_i = \{\hat{\mathbf{w}}_j^T \mathbf{q}(\sigma_i) : 1 \leq j \leq S\}$. The horizontal axis represents the support of μ_i which is given by the grid \mathcal{T} and the vertical axis is σ_i sorted in decreasing order from top to bottom. The black

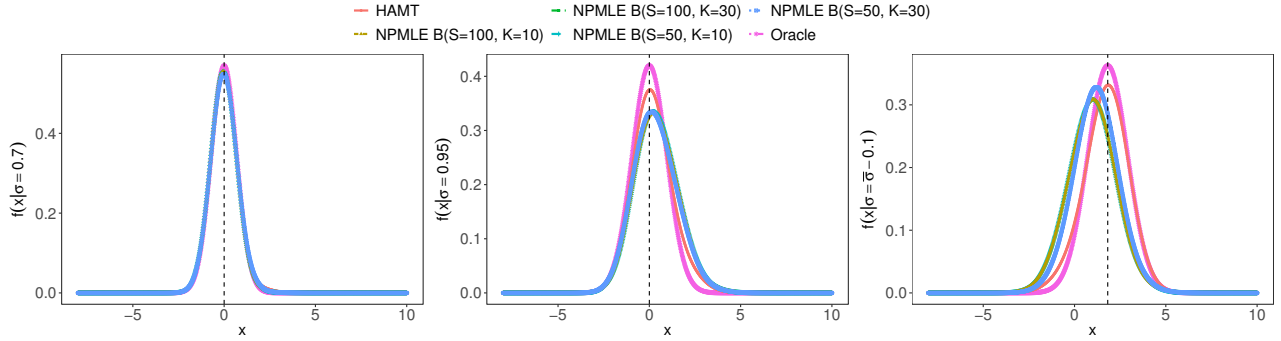


Figure 19: The simulation setting for Figure 7 with $\bar{\sigma} = 1.2$. For a random dataset generated from the underlying hierarchical model, the three panels present the estimate of $f(\cdot | \sigma)$ at $\sigma = 0.7$ (left), $\sigma = 0.95$ (center) and $\sigma = \bar{\sigma} - 0.1$ (right) obtained from HAMT and NPMLE B. The PTP values from the four variants of NPMLE B are: 0.85 ($S = 50, K = 10$), 0.857 ($S = 100, K = 30$), 0.842 ($S = 100, K = 10$) and 0.878 ($S = 50, K = 30$). The PTP from HAMT is 0.887.

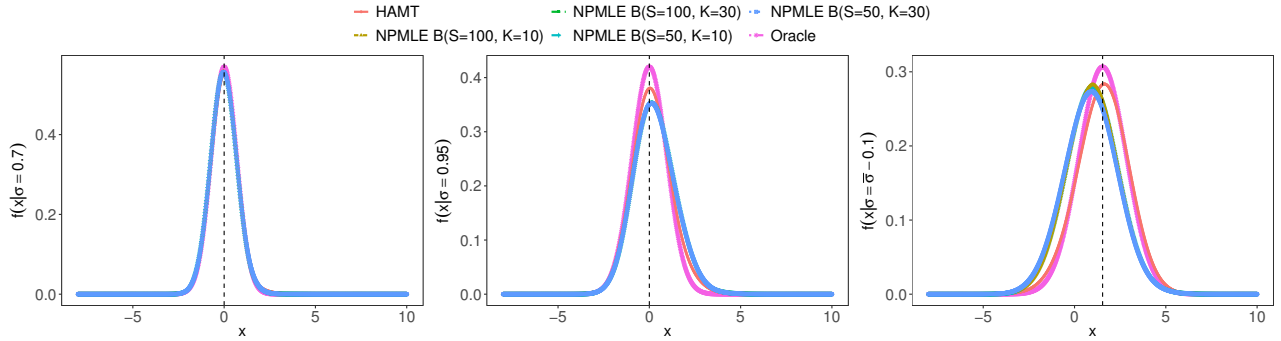


Figure 20: Same as Figure 19 but with $\bar{\sigma} = 1.4$. The PTP values from the four variants of NPMLE B are: 0.089 ($S = 50, K = 10$), 0.103 ($S = 100, K = 30$), 0.073 ($S = 100, K = 10$) and 0.109 ($S = 50, K = 30$). The PTP from HAMT is 0.857.

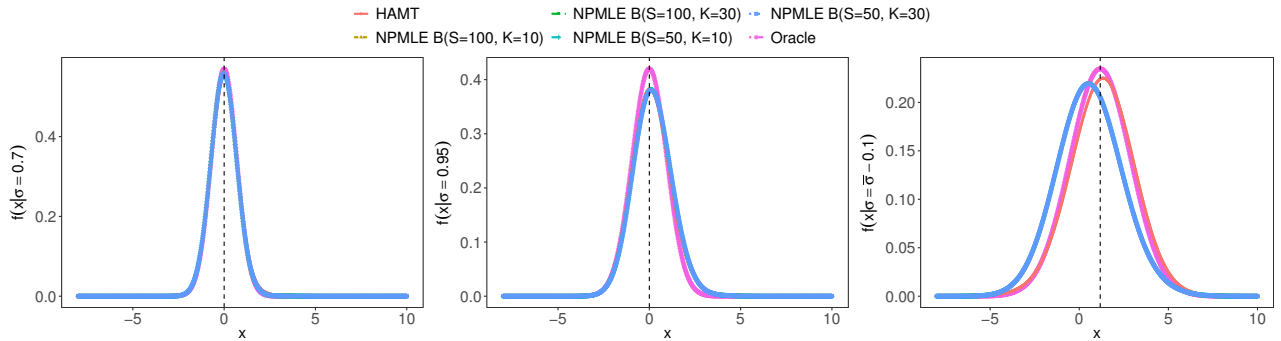


Figure 21: Same as Figure 19 but with $\bar{\sigma} = 1.8$. The PTP values from the four variants of NPMLE B are: 0.018 ($S = 50, K = 10$), 0.01 ($S = 100, K = 30$), 0.01 ($S = 100, K = 10$) and 0.017 ($S = 50, K = 30$). The PTP from HAMT is 0.816.

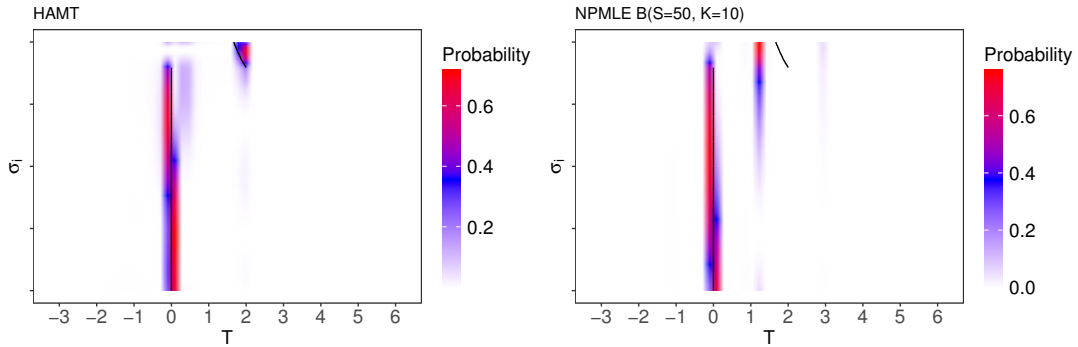


Figure 22: The simulation setting for Figure 7 with $\bar{\sigma} = 1.2$. The left panel presents the $m \times S$ matrix $\mathcal{G} = (\hat{\mathbf{g}}_1, \dots, \hat{\mathbf{g}}_m)^T$ of the estimated prior probabilities obtained from HAMT, where $\hat{\mathbf{g}}_i = \{\hat{w}_j^T \mathbf{q}(\sigma_i) : 1 \leq j \leq S\}$. The black vertical line depicts $\mu_i = 0$ whenever $\sigma_i \leq 1$ and the black oblique line is $\mu_i = 2/\sigma_i$ for $\sigma_i > 1$. The right panel represents the estimated prior probabilities from NPMLE B with $S = 50, K = 10$.

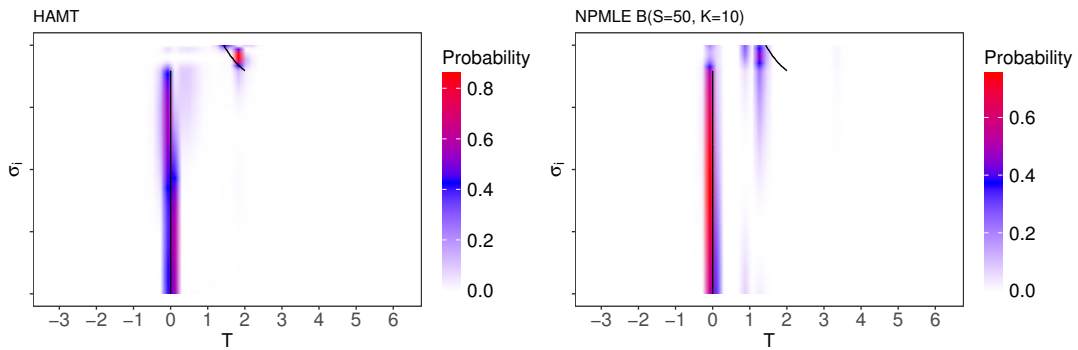


Figure 23: Same as Figure 22 but with $\bar{\sigma} = 1.4$.

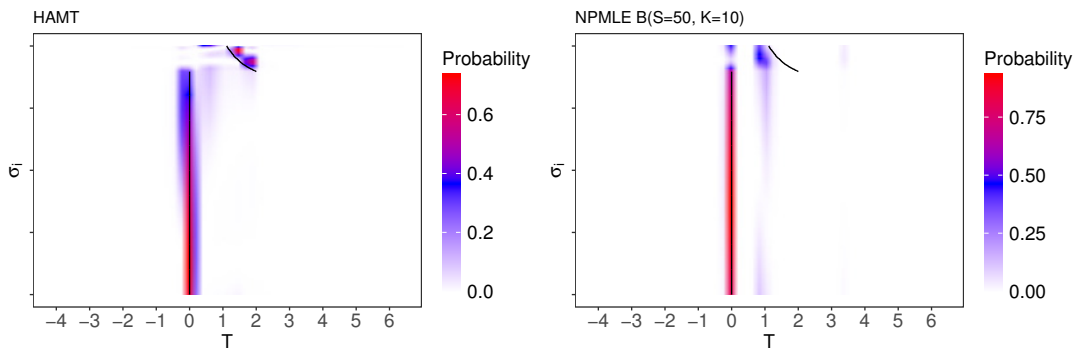


Figure 24: Same as Figure 22 but with $\bar{\sigma} = 1.8$.

vertical line depicts $\mu_i = 0$ whenever $\sigma_i \leq 1$ and the black oblique line is $\mu_i = 2/\sigma_i$ for $\sigma_i > 1$. In the same spirit, the right panel depicts the estimated prior probabilities obtained from NPMLE B with $S = 50, K = 10$.

We make several observations from Figure 22. First, when $\sigma_i \leq 1$ both HAMT and NPMLE B assign probability masses around zero as they should since $\mu_i = 0$ whenever $\sigma_i \leq 1$. However, unlike HAMT, NPMLE B also assigns some mass around 1. Second, when $\sigma_i > 1$ HAMT assigns substantially less mass around 0 than NPMLE B. Finally, while HAMT correctly assigns probability mass around the true non-null μ_i 's, NPMLE B does not and instead assigns a relatively large mass around 1 and 3. The aforementioned differences in the estimated prior probabilities from the two methods manifest themselves in the corresponding conditional marginal density estimates and hence in the respective rankings of the m hypotheses obtained from their Clfdr statistics. Figure 23 represents the case $\bar{\sigma} = 1.4$ and reveals that, unlike HAMT, NPMLE B fails to assign any prior mass around most of the non-null μ_i 's, thus explaining its low power in Figure 7. Furthermore, in contrast to HAMT, NPMLE B assigns relatively more probability mass at 0 even when $\sigma_i > 1$. Finally, Figure 24 represents the case $\bar{\sigma} = 1.8$ where NPMLE B continues to assign zero probability mass around most of the non-null μ_i 's.

Analysis of Figure 8 - the simulation setting underlying this figure provides another opportunity to analyze the differences between HAMT and NPMLE B. Here $X_i | \mu_i, \sigma_i \stackrel{ind.}{\sim} N(\mu_i, \sigma_i^2)$, $\sigma_i \stackrel{i.i.d.}{\sim} \text{Unif}(0.25, \bar{\sigma})$, conditional on σ_i , $\mu_i = 3\sigma_i$ and $\mathcal{A} = (-\infty, 4]$. Thus, as $\bar{\sigma}$ increases from 1.5 to 2, the signal strength increases. With $\bar{\sigma} = 1.5$ and for a random dataset generated from the above hierarchical model, Figure 25 plots the estimates of $f(\cdot | \sigma)$ obtained from HAMT and the four variants of NPMLE B at $\sigma = 0.5$ (left), $\sigma = 1$ (center) and $\sigma = \bar{\sigma} - 0.1$ (right). Figures 26 and 27, respectively, represent the cases $\bar{\sigma} = 1.7$ and $\bar{\sigma} = 1.9$. Overall, the marginal density estimates at $\sigma = 1$ and $\bar{\sigma} - 0.1$ are substantially closer to the ground truth in case of HAMT. Also, the choices of S and K do not seem to generate any visible differences in the marginal density estimates from NPMLE B and this observation is also supported by the relatively similar PTP values that these variants return.

When $\bar{\sigma} = 1.7$, Figure 28 presents the estimated prior probabilities obtained from HAMT (left panel) and NPMLE B (right panel) with $S = 50, K = 10$. The green and black oblique lines depict, respectively, the null and non-null μ_i 's. The disparity in the prior probability estimates from HAMT and NPMLE B in this setting is stark. The probabilities from HAMT, in particular, align closely with the true prior distribution that assigns all probability mass at $3\sigma_i$. For instance, when $\sigma_i = 1$, HAMT assigns virtually no probability mass at 2 and below, and 5 and above. NPMLE B, in contrast, assigns mass around 1 and 5. Furthermore, NPMLE B does not assign any probability mass to the non-null μ_i 's in $(4, 5]$ while HAMT does. These differences manifest themselves in the corresponding marginal density estimates of $f(\cdot | \sigma)$ as seen in Figure 26. Figure 29 presents the same information at $\bar{\sigma} = 1.9$. For the non-null μ_i 's, NPMLE B assigns probability mass only around 5, thus missing a substantial fraction of the non-null μ_i 's. HAMT, in contrast, is relatively better in

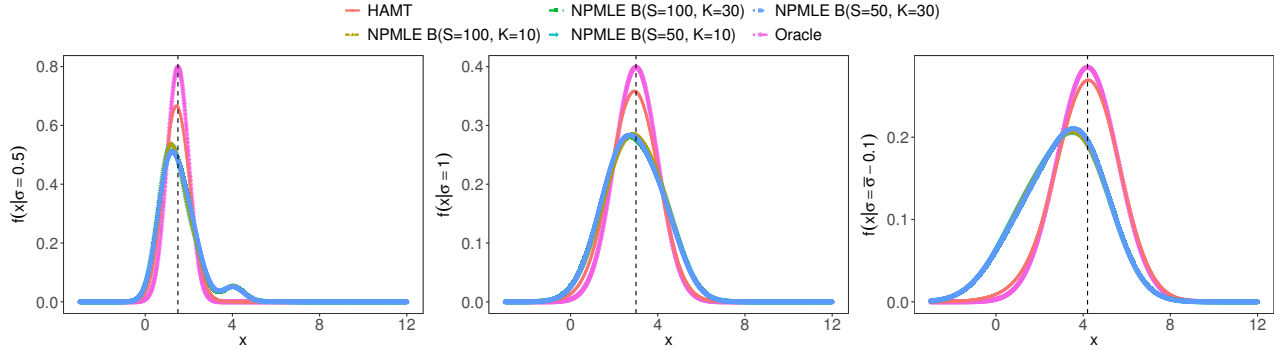


Figure 25: The simulation setting for Figure 8 with $\bar{\sigma} = 1.5$. For a random dataset generated from the underlying hierarchical model, the three panels present the estimate of $f(\cdot | \sigma)$ at $\sigma = 0.5$ (left), $\sigma = 1$ (center) and $\sigma = \bar{\sigma} - 0.1$ (right) obtained from HAMT and NPMLE B. The PTP values from the four variants of NPMLE B are: 0.557 ($S = 50, K = 10$), 0.551 ($S = 100, K = 30$), 0.559 ($S = 100, K = 10$) and 0.538 ($S = 50, K = 30$). The PTP from HAMT is 0.873.

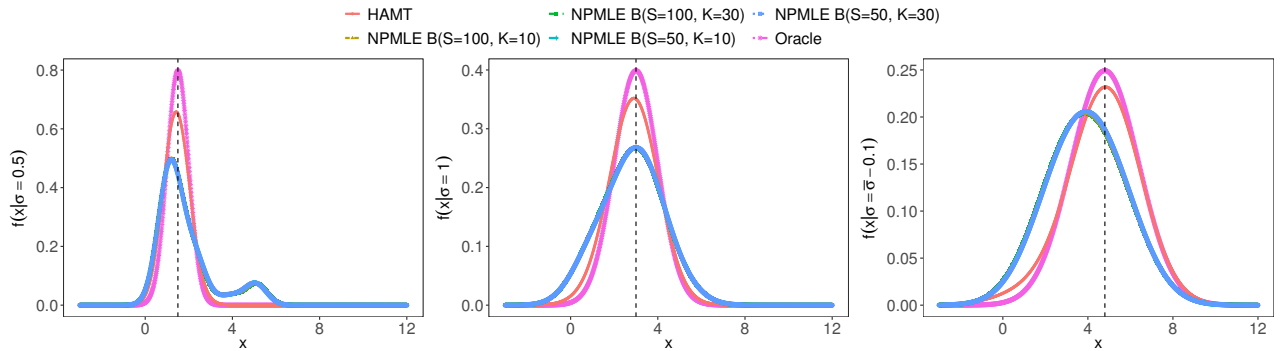


Figure 26: Same as Figure 25 but with $\bar{\sigma} = 1.7$. The PTP values from the four variants of NPMLE B are all approximately 0.024. The PTP from HAMT is 0.797.

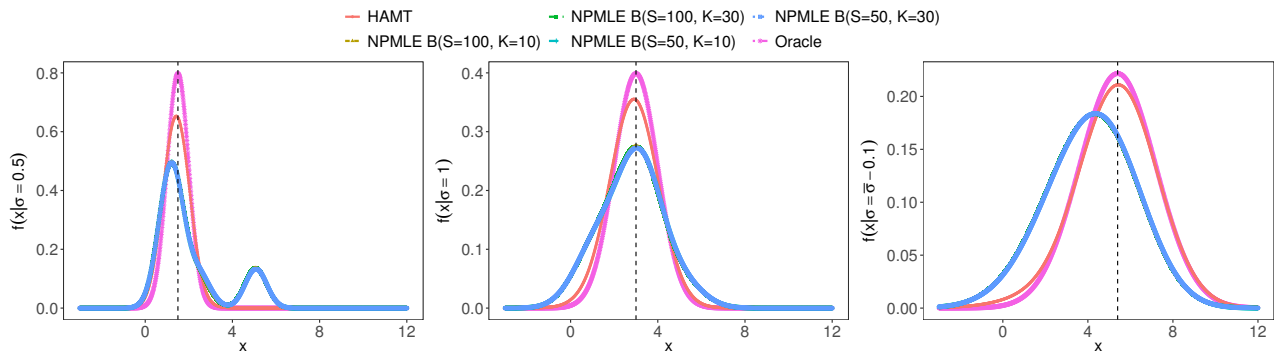


Figure 27: Same as Figure 25 but with $\bar{\sigma} = 1.9$. The PTP values from the four variants of NPMLE B are: 0.468 ($S = 50, K = 10$), 0.488 ($S = 100, K = 30$), 0.489 ($S = 100, K = 10$) and 0.470 ($S = 50, K = 30$). The PTP from HAMT is 0.882.

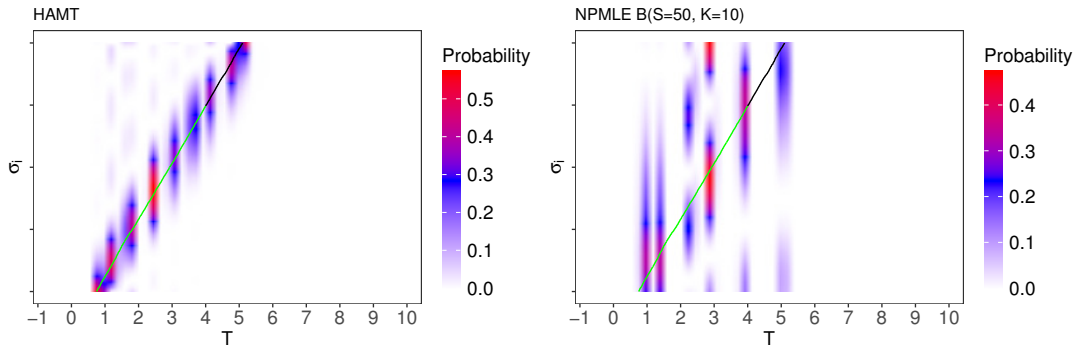


Figure 28: The simulation setting for Figure 8 with $\bar{\sigma} = 1.7$. The left panel presents the $m \times S$ matrix $\mathcal{G} = (\hat{\mathbf{g}}_1, \dots, \hat{\mathbf{g}}_m)^T$ of the estimated prior probabilities obtained from HAMT, where $\hat{\mathbf{g}}_i = \{\hat{w}_j^T \mathbf{q}(\sigma_i) : 1 \leq j \leq S\}$. The green and black oblique lines depict, respectively, the null and non-null μ_i 's. The right panel represents the estimated prior probabilities from NPMLE B with $S = 50, K = 10$.

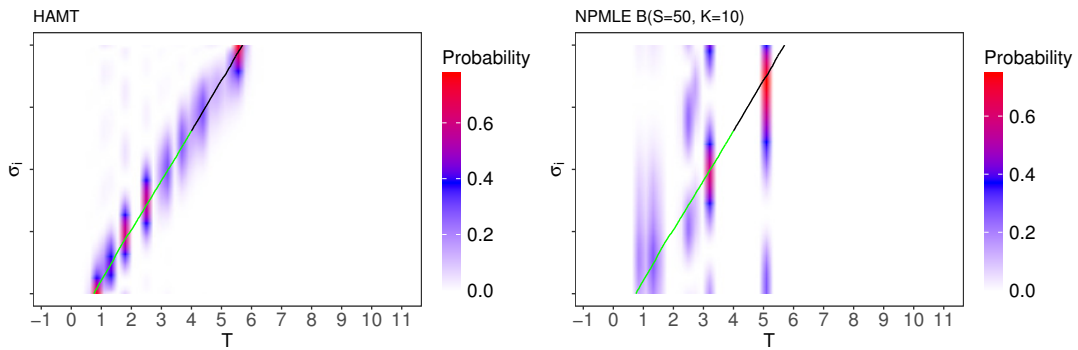


Figure 29: Same as Figure 28 but with $\bar{\sigma} = 1.9$.

estimating $g_\mu(\cdot | \sigma)$ in this setting, which ultimately results in its improved power and FDR profiles compared to NPMLE B.

E.2 Insights on when each method is expected to perform well.

In the simulation studies of sections 5.2 and D, there are six procedures, besides HAMT, that rely on different approaches for estimating $g_\mu(\cdot | \sigma)$. These include two procedures from Gu and Shen (2018) (GS1 and GS2), a procedure based on the deconvolution method of Efron (2016) (DECONV), two procedures from Stephens (2017) (ASH and ASH.1) and NPMLE B. We discuss when each of these methods can be expected to outperform HAMT in power at the same FDR level.

GS1, GS2 and DECONV - GS1 and GS2 are based on the standardized statistic $Z_i = (X_i - \mu_0)/\sigma_i$ and rely on the deconvolution estimate obtained from nonparametric maximum likelihood estimation to construct the LfdR statistic. DECONV, on the other hand, ignores the dependence between μ_i and σ_i . Recall that the discussions in sections 2.3 and 3.3 reveal that these three procedures may exhibit substantial power loss when μ_i and σ_i are correlated. However when μ_i is indeed independent of σ_i , GS1, GS2 and DECONV can be more powerful than HAMT. An example of this scenario is presented in Figure 4 where GS1 and DECONV are competitive to HAMT in power.

NPMLE B - this is the method that is closest to HAMT in its construction. While the simulation experiments in sections 5.2 and D reveal several settings where HAMT is more powerful than NPMLE B, there are also scenarios where NPMLE B is competitive. These include the cases where (i) the distribution of μ_i depends on σ_i , such as Figure 10, and (ii) the distribution of X_i given μ_i, σ_i is non Gaussian, such as Figure 14. A particular setting where NPMLE B can indeed outperform HAMT is when μ_i and σ_i are independent. Figures 30 – 32 represent three such scenarios. Intuitively, when $g_\mu(\cdot | \sigma_i) := g_\mu(\cdot)$ is independent of σ_i , directly maximizing the marginal log-likelihood $\sum_{i=1}^m \log f(x_i | \sigma_i)$ (Problem (9)) is a better approach for learning $g_\mu(\cdot)$ than the density matching approach of HAMT (Problem (13)) because the σ_i 's do not encode any extra information regarding the μ_i 's that the bivariate kernel density estimator $\hat{\varphi}_{(-i)}^m(x_i, \sigma_i)$ (Equation (12)) of $f(x_i | \sigma_i)$ can utilize. However, as discussed in Section 3.1, much research is needed to fully comprehend the conditions under which NPMLE B can guarantee asymptotic FDR control and how the hyper-parameters S and K impact its power.

ASH and ASH.1 - an important assumption underlying these two procedures is that the distribution of the non-null μ_i is unimodal. As Stephens (2017) comment, this unimodal assumption (UA) is naturally satisfied in many practical settings. However, in the simulation studies presented in sections 5.2 and D, the distribution of the non-null μ_i do not satisfy the UA. This is the main reason why ASH and its variant ASH.1 are typically less powerful than HAMT in our numerical experiments. In this section, we borrow three simulation settings from Stephens (2017) and demonstrate that when the

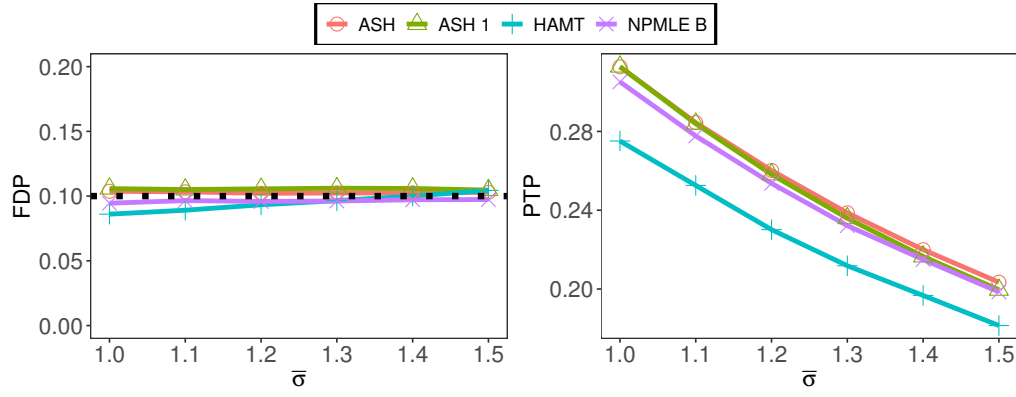


Figure 30: Setting 1: $\sigma_i \stackrel{i.i.d}{\sim} \text{Unif}(0.25, \bar{\sigma})$, $\mu_i \stackrel{i.i.d}{\sim} 0.9\delta_{(0)} + 0.1F_a$, $X_i|\mu_i, \sigma_i \stackrel{ind.}{\sim} N(\mu_i, \sigma_i^2)$. $F_a = 0.4N(0.0.25^2) + 0.2N(0, 0.5^2) + 0.2N(0, 1) + 0.4(0, 2^2)$ and $\mathcal{A} = (-\infty, 1/2]$.

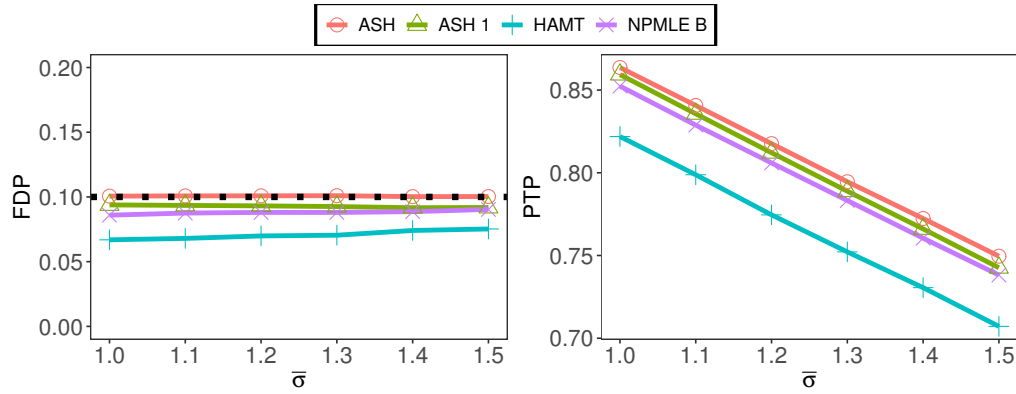


Figure 31: Setting 2: Same as Figure 30 but $F_a = N(0, 4^2)$ and $\mathcal{A} = (-\infty, 1]$.

UA holds, ASH can be more powerful than HAMT.

We let $\sigma_i \stackrel{i.i.d}{\sim} \text{Unif}(0.25, \bar{\sigma})$, $\mu_i \stackrel{i.i.d}{\sim} 0.9\delta_{(0)} + 0.1F_a$, $X_i|\mu_i, \sigma_i \stackrel{ind.}{\sim} N(\mu_i, \sigma_i^2)$, set $\alpha = 0.1$ and vary $\bar{\sigma} \in \{1, 1.1, 1.2, 1.3, 1.4, 1.5\}$. We are interested in testing $m = 10^4$ hypotheses of the form $H_{0i} : \mu_i \in \mathcal{A}$ vs $H_{1i} : \mu_i \notin \mathcal{A}$ where $\mathcal{A} = (-\infty, \mu_0]$. The distributions F_a are borrowed from Table S.3 of [Stephens \(2017\)](#) as follows:

- **Setting 1** - in this scenario $F_a = 0.4N(0.0.25^2) + 0.2N(0, 0.5^2) + 0.2N(0, 1) + 0.4(0, 2^2)$ is a ‘Spiky’ distribution. Here $\mu_0 = 1/2$.
- **Setting 2** - here $F_a = N(0, 4^2)$ is the ‘big-Normal’ and $\mu_0 = 1$.
- **Setting 3** - here $F_a = (2/3)N(0, 1) + (1/3)N(0, 2^2)$ is the ‘near-Normal’ distribution and $\mu_0 = 1/2$.

Figures 30 – 32 report the average FDP and PTP of HAMT, ASH, ASH.1 and NPMLE B across 200 Monte-Carlo repetitions of the data generating process. Unsurprisingly, ASH and ASH.1 are the top two methods in terms of their power, further suggesting that in applications where the UA

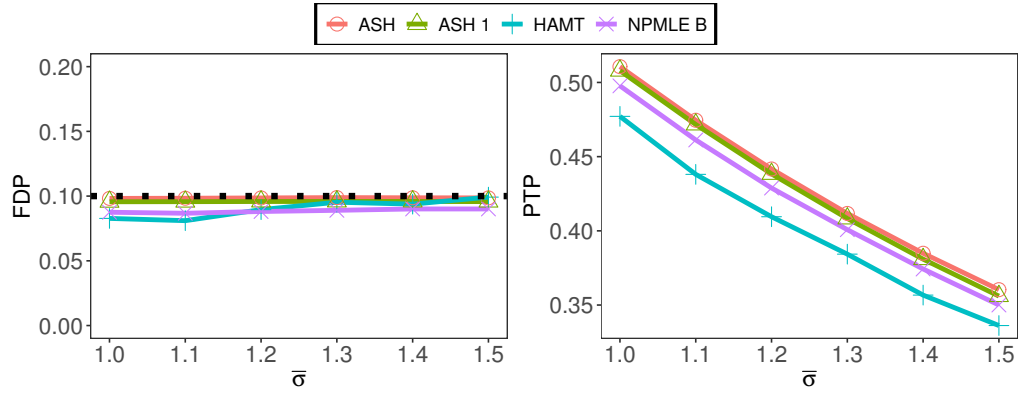


Figure 32: Setting 3: Same as Figure 30 but $F_a = (2/3)N(0, 1) + (1/3)N(0, 2^2)$.

assumption is known to hold, ASH and its variant are indeed powerful alternatives to HAMT. Under these three settings, the distribution of μ_i is independent of σ_i and we find that NPMLE B is also more powerful than HAMT.

F Real data analysis

In this section we analyze a dataset from [Banerjee et al. \(2019\)](#) that hold daily player-level gaming information over 60 days from a mobile app game. For monetization of these games, managers are often interested in identifying a group of players who are most engaged with the game so that personalized promotional offers can be pushed to their devices. While there are several ways of measuring game engagement, such as engagement via purchases or through social media activity, here we use the daily duration of play as a measure of how engaged each player is with the game. However, a positive daily duration of play does not necessarily mean that the player is highly engaged. Rather, from a game manager’s perspective, sustained playing activities translate to high levels of engagement, either through purchases or social media activities. Thus, in this analysis we focus on players who have logged-in to the game for at least 5 days in the 60 day period and the goal is to select those players whose mean daily duration of play exceeds 30 minutes.

Formally, let $Y_{ij} > 0$ denote the duration of play in minutes for player i on day j where $j = 1, \dots, n_i$ and $i = 1, \dots, m$. Here $n_i \in [5, 60]$ denotes the number days that player i has logged-in to the game and there are $m = 10,336$ such players in our data. Following [Banerjee et al. \(2019\)](#), we work with the log duration of play $X_{ij} = \log Y_{ij}$ and denote $X_i = n_i^{-1} \sum_{j=1}^{n_i} \log Y_{ij}$. We assume that $X_i \mid (n_i, \mu_i, \sigma_i) \stackrel{\text{ind.}}{\sim} N(\mu_i, \sigma_i^2)$, and test $H_{0,i} : \mu_i \leq \log(30)$ vs $H_{1,i} : \mu_i > \log(30)$. Since σ_i are unknown in this example, we calculate the sample standard deviation S_i and consider the m pairs (X_i, σ_i) for the testing problem, where we set $\sigma_i = S_i / \sqrt{n_i}$ with some abuse of notation.

We first discuss the estimate of prior probabilities arising from the deconvolution estimator that HAMT relies on. The heatmap in Figure 33 presents the $m \times S$ matrix $\mathcal{G} = (\hat{g}_1, \dots, \hat{g}_m)^T$ of the

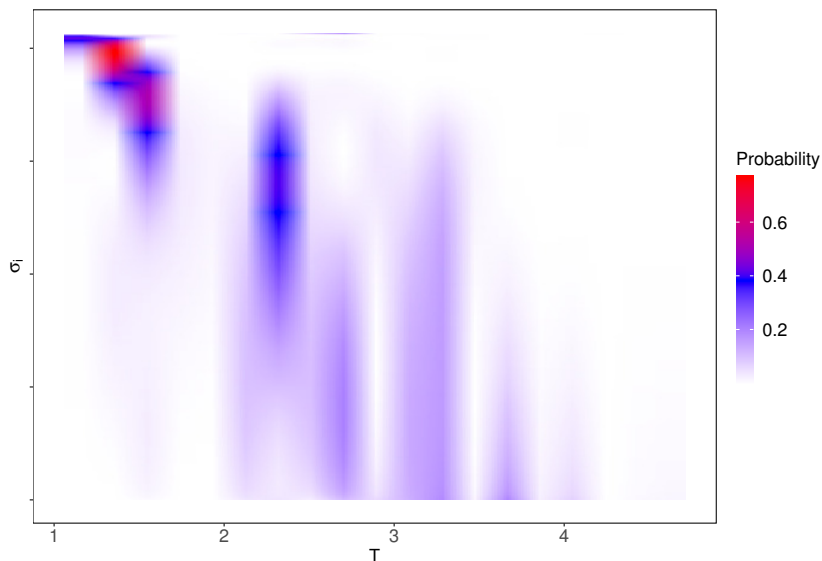


Figure 33: The heatmap representing the $m \times S$ matrix $\mathcal{G} = (\hat{\mathbf{g}}_1, \dots, \hat{\mathbf{g}}_m)^T$ where $\hat{\mathbf{g}}_i = \{\hat{\mathbf{w}}_j^T \mathbf{q}(\sigma_i) : 1 \leq j \leq S\}$. The horizontal axis represents the support of μ_i which is give by the grid \mathcal{T} , truncated to $[1, 4.6]$, and the vertical axis is the standard error σ_i .

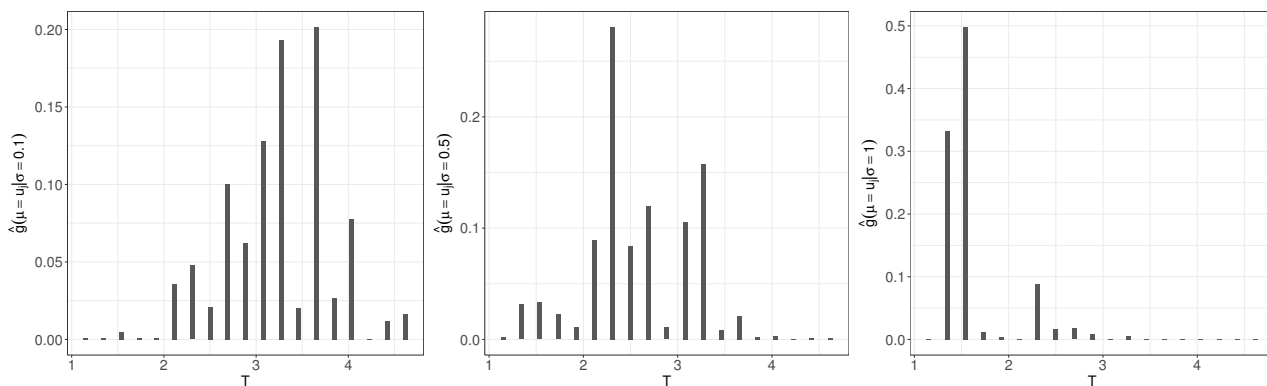


Figure 34: Plot of the estimated prior masses $\hat{\mathbf{g}}_i$ for $\sigma_i = \sigma \in \{0.1, 0.5, 1\}$. The horizontal axis is truncated to $[1, 4.6]$ as the estimated probability mass is negligible outside this interval.

estimated prior probabilities where $\hat{\mathbf{g}}_i = \{\hat{\mathbf{w}}_j^T \mathbf{q}(\sigma_i) : 1 \leq j \leq S\}$. The horizontal axis represents the support of μ_i which is give by the grid \mathcal{T} , truncated to $[1, 4.6]$ for ease of presentation, and the vertical axis is σ_i arranged in an increasing order from bottom to top. It is interesting to note that when σ_i are small, most of the prior mass is concentrated in $[2, 4]$. As σ_i increases, the deconvolution estimator adjusts and assigns more mass in the interval $[1, 3]$. This is further elucidated in Figure 34 where we plot $\hat{\mathbf{g}}_i$ for $\sigma_i = \sigma \in \{0.1, 0.5, 1\}$, and notice a change in the spread of the estimated prior density as σ increases from left to right. Deconvolution estimators that ignore the dependence between μ_i and σ_i are incapable of demonstrating such patterns in the estimated prior density.

For the multiple testing problem described earlier, HAMT relies on the deconvolution estimates $\hat{\mathbf{g}}_i$ to estimate the oracle Clfdr statistic T_i^{OR} . Table 1 reports the percentage of hypotheses rejected by

Table 1: Percentage of hypotheses rejected by each method.

α	GS 1	GS 2	DECONV	NPMLE B	ASH	ASH 1	HAMT
0.05	2.38%	1.34%	3.40%	3.98%	3.51%	4.54%	3.37%
0.1	3.30%	1.75%	4.76%	5.49%	4.88%	6.57%	4.44%
0.15	4.04%	2.11%	6.07%	6.86%	6.18%	8.52%	5.38%

each method for different choices of the FDR level α and we find that HAMT rejects more hypotheses than GS 1 and GS 2 while ASH 1 rejects the most. The red dots in the bottom right panel of Figure 35 indicate the hypotheses rejected by HAMT at $\alpha = 0.1$. In the remaining three panels of Figure 35, we compare the rejections of GS 1 versus GS 2 (top left), ASH versus ASH 1 (top right) and DECONV versus NPMLE B (bottom left). In these three panels, the red dots indicate hypotheses rejected by both method 1, such as GS 1, and method 2, such as GS 2. Similarly, the blue dots represent hypotheses rejected by method 1 but not by method 2 and the green dots depict hypotheses rejected by method 2 but not by method 1. We note that the rejection regions of GS 1 and GS2 depend only on $Z_i = (X_i - \mu_0)/\sigma_i$ and ASH 1 rejects relatively more hypotheses than ASH, particularly when σ_i is large and Z_i is small. In contrast, the rejection regions of HAMT and NPMLE B depend on both Z_i and σ_i . Moreover, in comparison to the other methods, HAMT rejects more hypotheses when σ_i is small and does not reject any hypotheses when σ_i is bigger than 0.5. The rejection regions of DECONV, ASH and ASH 1 give the impression that they depend on both Z_i and σ_i , however as seen in our simulation experiments, these methods may fail to control the FDR at the desired level in case μ_i and σ_i are correlated as their deconvolution estimator is not designed to capture this dependence.

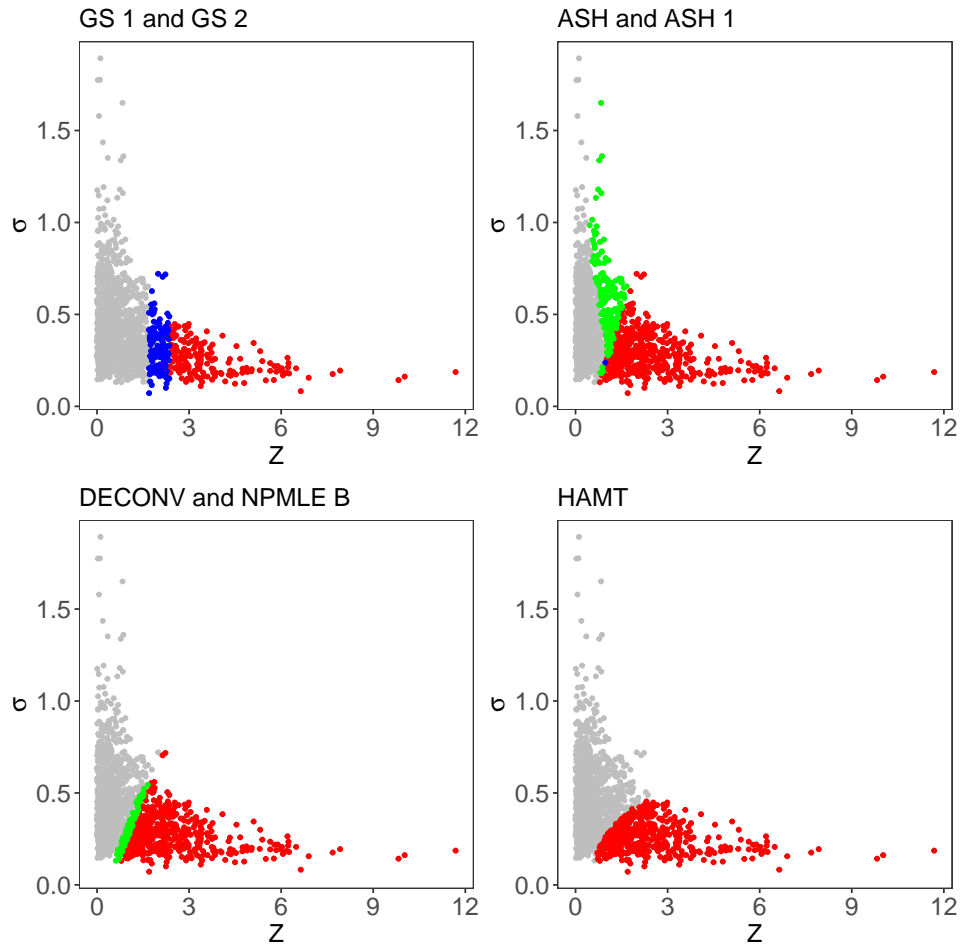


Figure 35: Scatter plot of (Z_i, σ_i) , $i = 1, \dots, m$ where $Z_i = (X_i - \mu_0)/\sigma_i$. The red dots in the bottom right panel indicate the hypotheses rejected by HAMT at $\alpha = 0.1$. In the remaining three panels, we compare the rejections of GS 1 versus GS 2 (top left), ASH versus ASH 1 (top right) and DECONV versus NPMLE B (bottom left). In these three panels, the red dots indicate hypotheses rejected by both method 1, such as GS 1, and method 2, such as GS 2. Similarly, the blue dots represent hypotheses rejected by method 1 but not by method 2 and the green dots depict hypotheses rejected by method 2 but not by method 1. The horizontal axis is truncated below 0 as all rejections are made when $Z_i > 0$.

References

- Banerjee, T., L. J. Fu, G. M. James, G. Mukherjee, and W. Sun (2023). Nonparametric empirical bayes estimation on heterogeneous data. *arXiv preprint arXiv:2002.12586*.
- Banerjee, T., G. Mukherjee, S. Dutta, and P. Ghosh (2019). A large-scale constrained joint modeling approach for predicting user activity, engagement, and churn with application to freemium mobile games. *Journal of the American Statistical Association*.
- Barber, R. F. and E. J. Candès (2015). Controlling the false discovery rate via knockoffs. *The Annals of Statistics* 43(5), 2055–2085.
- Basu, P., T. T. Cai, K. Das, and W. Sun (2018). Weighted false discovery rate control in large-scale multiple testing. *Journal of the American Statistical Association* 113(523), 1172–1183.
- Bates, S., E. Candès, L. Lei, Y. Romano, and M. Sesia (2021). Testing for outliers with conformal p-values. *arXiv:2104.08279*, Preprint.
- Benjamini, Y. and Y. Hochberg (1995). Controlling the false discovery rate: a practical and powerful approach to multiple testing. *Journal of the Royal statistical society: series B (Methodological)* 57(1), 289–300.
- Benjamini, Y., A. M. Krieger, and D. Yekutieli (2006). Adaptive linear step-up procedures that control the false discovery rate. *Biometrika* 93(3), 491–507.
- Boca, S. M. and J. T. Leek (2018). A direct approach to estimating false discovery rates conditional on covariates. *PeerJ* 6, e6035.
- Cai, T. T. and W. Sun (2009). Simultaneous testing of grouped hypotheses: Finding needles in multiple haystacks. *Journal of the American Statistical Association* 104(488), 1467–1481.
- Cao, H., J. Chen, and X. Zhang (2022). Optimal false discovery rate control for large scale multiple testing with auxiliary information. *The Annals of Statistics* 50(2), 807–857.
- Chao, P. and W. Fithian (2021). Adapt-gmm: Powerful and robust covariate-assisted multiple testing. *arXiv preprint arXiv:2106.15812*.
- Chen, J. (2024). Empirical bayes when estimation precision predicts parameters. *arXiv preprint arXiv:2212.14444*.
- Dicker, L. H. and S. D. Zhao (2016, 02). High-dimensional classification via nonparametric empirical Bayes and maximum likelihood inference. *Biometrika* 103(1), 21–34.

- Efron, B. (2004). Large-scale simultaneous hypothesis testing: the choice of a null hypothesis. *Journal of the American Statistical Association* 99(465), 96–104.
- Efron, B. (2008). Microarrays, empirical bayes and the two-groups model. *Statistical science* 23(1), 1–22.
- Efron, B. (2012). *Large-scale inference: empirical Bayes methods for estimation, testing, and prediction*, Volume 1. Cambridge University Press.
- Efron, B. (2014). Two modeling strategies for empirical bayes estimation. *Statistical science: a review journal of the Institute of Mathematical Statistics* 29(2), 285.
- Efron, B. (2016). Empirical bayes deconvolution estimates. *Biometrika* 103(1), 1–20.
- Efron, B. and R. Tibshirani (2007). On testing the significance of sets of genes. *The annals of applied statistics* 1(1), 107–129.
- Fu, L., B. Gang, G. M. James, and W. Sun (2022). Heteroscedasticity-adjusted ranking and thresholding for large-scale multiple testing. *Journal of the American Statistical Association* 117(538), 1028–1040.
- Genovese, C. and L. Wasserman (2002). Operating characteristics and extensions of the false discovery rate procedure. *Journal of the Royal Statistical Society: Series B (Statistical Methodology)* 64(3), 499–517.
- G’Sell, M. G., S. Wager, A. Chouldechova, and R. Tibshirani (2016). Sequential selection procedures and false discovery rate control. *Journal of the royal statistical society: series B (statistical methodology)* 78(2), 423–444.
- Gu, J. and R. Koenker (2017). Empirical bayesball remixed: Empirical bayes methods for longitudinal data. *Journal of Applied Econometrics* 32(3), 575–599.
- Gu, J. and S. Shen (2018). Oracle and adaptive false discovery rate controlling methods for one-sided testing: theory and application in treatment effect evaluation. *The Econometrics Journal* 21(1), 11–35.
- Guan, L. and R. Tibshirani (2022). Prediction and outlier detection in classification problems. *Journal of the Royal Statistical Society. Series B, Statistical Methodology* 84(2), 524.
- Hu, J. X., H. Zhao, and H. H. Zhou (2010). False discovery rate control with groups. *Journal of the American Statistical Association* 105(491), 1215–1227.

- Ignatiadis, N. and W. Huber (2021). Covariate powered cross-weighted multiple testing. *Journal of the Royal Statistical Society: Series B (Statistical Methodology)* 83(4), 720–751.
- Jin, J. and T. T. Cai (2007). Estimating the null and the proportion of nonnull effects in large-scale multiple comparisons. *Journal of the American Statistical Association* 102(478), 495–506.
- Kiefer, J. and J. Wolfowitz (1956). Consistency of the maximum likelihood estimator in the presence of infinitely many incidental parameters. *The Annals of Mathematical Statistics*, 887–906.
- Koenker, R. and J. Gu (2017). Rebayes: An r package for empirical bayes mixture methods. *Journal of Statistical Software* 82(1), 1–26.
- Koenker, R. and I. Mizera (2014). Convex optimization, shape constraints, compound decisions, and empirical bayes rules. *Journal of the American Statistical Association* 109(506), 674–685.
- Laird, N. (1978). Nonparametric maximum likelihood estimation of a mixing distribution. *Journal of the American Statistical Association* 73(364), 805–811.
- Lei, L. and W. Fithian (2016). Power of ordered hypothesis testing. In *International conference on machine learning*, pp. 2924–2932. PMLR.
- Lei, L. and W. Fithian (2018). Adapt: an interactive procedure for multiple testing with side information. *Journal of the Royal Statistical Society: Series B (Statistical Methodology)* 80(4), 649–679.
- Leung, D. and W. Sun (2021). Zap: z -value adaptive procedures for false discovery rate control with side information. *arXiv preprint arXiv:2108.12623*.
- Li, A. and R. F. Barber (2017). Accumulation tests for fdr control in ordered hypothesis testing. *Journal of the American Statistical Association* 112(518), 837–849.
- Li, A. and R. F. Barber (2019). Multiple testing with the structure-adaptive benjamini–hochberg algorithm. *Journal of the Royal Statistical Society: Series B (Statistical Methodology)* 81(1), 45–74.
- Liu, Y., S. K. Sarkar, and Z. Zhao (2016). A new approach to multiple testing of grouped hypotheses. *Journal of Statistical Planning and Inference* 179, 1–14.
- Love, M. I., W. Huber, and S. Anders (2014). Moderated estimation of fold change and dispersion for rna-seq data with `deseq2`. *Genome biology* 15(12), 1–21.
- Lu, M. and M. Stephens (2019). Empirical bayes estimation of normal means, accounting for uncertainty in estimated standard errors. *arXiv preprint arXiv:1901.10679*.
- MOSEK, A. (2019). *MOSEK Rmosek package 10.0.34*.

- Pop-Eleches, C. and M. Urquiola (2013). Going to a better school: Effects and behavioral responses. *American Economic Review* 103(4), 1289–1324.
- Scott, J. G., R. C. Kelly, M. A. Smith, P. Zhou, and R. E. Kass (2015). False discovery rate regression: an application to neural synchrony detection in primary visual cortex. *Journal of the American Statistical Association* 110(510), 459–471.
- Silverman, B. W. (1986). *Density estimation for statistics and data analysis*, Volume 6. CRC press.
- Stephens, M. (2017). False discovery rates: a new deal. *Biostatistics* 18(2), 275–294.
- Sun, W. and T. T. Cai (2007). Oracle and adaptive compound decision rules for false discovery rate control. *Journal of the American Statistical Association* 102(479), 901–912.
- Sun, W. and A. C. McLain (2012). Multiple testing of composite null hypotheses in heteroscedastic models. *Journal of the American Statistical Association* 107(498), 673–687.
- Tansey, W., Y. Wang, D. Blei, and R. Rabadan (2018). Black box fdr. In *International conference on machine learning*, pp. 4867–4876. PMLR.
- Uffelmann, E., Q. Q. Huang, N. S. Munung, J. De Vries, Y. Okada, A. R. Martin, H. C. Martin, T. Lappalainen, and D. Posthuma (2021). Genome-wide association studies. *Nature Reviews Methods Primers* 1(1), 1–21.
- Wand, M. P. and M. C. Jones (1994). *Kernel smoothing*, Volume 60. CRC press.
- Wasserman, L. (2006). *All of nonparametric statistics*. Springer Science & Business Media.
- Weinstein, A., Z. Ma, L. D. Brown, and C.-H. Zhang (2018). Group-linear empirical bayes estimates for a heteroscedastic normal mean. *Journal of the American Statistical Association*, 1–13.
- Xie, X., S. Kou, and L. D. Brown (2012). Sure estimates for a heteroscedastic hierarchical model. *Journal of the American Statistical Association* 107(500), 1465–1479.
- Zhang, M. J., F. Xia, and J. Zou (2019). Fast and covariate-adaptive method amplifies detection power in large-scale multiple hypothesis testing. *Nature communications* 10(1), 1–11.
- Zhang, X. and J. Chen (2022). Covariate adaptive false discovery rate control with applications to omics-wide multiple testing. *Journal of the American Statistical Association* 117(537), 411–427.